Journal of
Civil
Engineering
Researchers

Chief Editorial:
Morteza Jamshidi

Managing Editor:
Kamyar Bagherineghad

J-Researchers

Contents

Sustainable Neighborhood Waste Management: Hybrid Digestion Approaches for Organic Waste Processing

Seyed Mohammad Hosseini, [ID] [a,*] Zahra Gholami, [ID] [b] Meysam Seyfi Kafshgari, [ID] [c]

[a] *PhD of Environmental engineering, Member of Mazndaran Science Technology Park, Sari, Iran*

[b] *PhD of chemical engineering, ORLEN UniCRE, a.s., Revoluční 1521/84, 400 01 Ústí nad Labem, Czech Republic*

[c] *Nanotechnology Research Institute, Departement of Chemical Engineering, Babol Noshirvani University of Technology, Babol, Iran*

ABSTRACT

Effective waste management is crucial for urban sustainability and environmental conservation. This study evaluates the efficiency and quality of compost produced through normal and thermophilic in-vessel composting and anaerobic digestion within a neighborhood waste management model. By analyzing physicochemical properties, process temperatures, carbon to nitrogen ratios, germination index, and biogas production rates, the study highlights the advantages of integrating these methods. Results indicate that thermophilic in-vessel composting accelerates the composting process, achieving rapid temperature increases and enhanced microbial activity. Anaerobic digestion complements this by producing biogas and yielding high-quality compost with low phytotoxicity. The combined approach not only optimizes compost production and quality but also contributes to renewable energy generation and reduced greenhouse gas emissions. These findings provide a framework for implementing sustainable, localized waste management systems, offering significant insights for policy and operational decisions in municipal waste management.

1. Introduction

Effective waste management is critical for environmental sustainability and urban efficiency. Composting stands out as a particularly viable option among the various methods available for processing organic waste. Composting can be conducted through two primary methods: in-vessel and open aeration. Studies have shown that in-vessel composting not only yields higher-quality compost but also significantly reduces processing time, particularly when utilizing thermophilic conditions [1-3].

The contemporary world is grappling with an energy crisis and escalating greenhouse gas (GHG) emissions. According to the International Energy Agency [4], approximately 78% of the global energy supply comes

---

* Corresponding author. Tel.: +989123111147; e-mail: envhosseini@gmail.com.

from oil, coal, and natural gas, while around 62% of electricity generation is still reliant on non-renewable sources. Transitioning to renewable energy sources is crucial to mitigate these issues and reduce GHG emissions [5-6]. Municipal solid waste (MSW) management plays a vital role in this context. Optimizing economic costs and minimizing GHG emissions are essential goals in MSW management [7]. For instance, optimizing transportation routes can reduce GHG emissions by approximately 47.43% [7].

Implementing in-situ processing of the organic fraction of MSW (OFMSW), such as in-vessel composting reactors, is increasingly necessary for both economic and environmental reasons [2]. These reactors are often installed in various neighborhoods, transforming waste management from a large-scale urban model to a more localized neighborhood approach [8].

Neighborhood-based waste management systems offer several advantages. By processing waste closer to its source, transportation costs, and related emissions are significantly reduced. Additionally, localized systems can be tailored to the specific needs and capacities of individual communities, enhancing overall efficiency and engagement. This decentralized approach also promotes community responsibility and awareness regarding waste management practices.

Furthermore, the integration of anaerobic digestion with composting processes presents a promising avenue for improving waste management outcomes. Anaerobic digestion not only reduces the volume of waste but also produces biogas, a valuable source of renewable energy. This biogas can be harnessed to generate electricity or heat, further contributing to the reduction of reliance on fossil fuels and decreasing the carbon footprint of waste management operations [9].

The quality of compost produced through different methods is critical for determining the best approach to organic waste management. Thermophilic in-vessel composting, for instance, accelerates the decomposition process through higher temperatures, resulting in faster stabilization of organic matter and the elimination of pathogens. This method is particularly effective in producing high-quality compost that is rich in nutrients and free from harmful microorganisms [2].

In contrast, anaerobic digestion primarily focuses on biogas production while also generating a digestate that can be further composted. The synergy between anaerobic digestion and subsequent composting can optimize the overall process, leading to better resource recovery and improved compost quality. The integration of these processes can be particularly beneficial in neighborhood waste management models, where space and resources might be limited, but the demand for efficient and sustainable waste processing solutions is high.

This study aims to compare the quality of compost produced from normal and thermophilic in-vessel composting pilot plants with compost generated from anaerobically digested organic compounds. This comparison highlights the benefits and efficiency of different composting methods within neighborhood waste management models. By focusing on localized waste management systems, this research contributes to the broader goals of reducing energy consumption, minimizing GHG emissions, and enhancing the overall sustainability of urban environments.

The outcomes of this research have the potential to inform policy and operational decisions in municipal waste management, providing a framework for the implementation of more sustainable and community-centric waste processing technologies. As cities continue to grow and the demand for effective waste management solutions increases, the findings of this study could play a crucial role in shaping the future of urban sustainability.

2. Material and method

Results from research conducted over the past decade have been compiled and analyzed to determine an appropriate reactor for processing the organic fraction of municipal solid waste (OFMSW) within a neighborhood waste management model.

2.1. Step 1: Bench-Scale Study

Previous research demonstrated that thermochemical pretreatment and thermophilic conditions could significantly reduce the duration of the composting process. Specifically, the average composting time for rice straw was reduced to 9 days under these conditions [3].

2.2. Step 2: Full-Scale In-Vessel Composting Pilot Plant (IVCP) Operation

Building on the findings from 2013 [3], a thermophilic in-vessel composting pilot plant was designed and constructed in 2020 (Figure 1). The IVCP comprises several components:
- In-vessel composter
- Screw mixer
- Bottom aeration system
- Leachate collection tank and recirculation system
- Hot water jacket
- Control panel

The composting process time was evaluated under both the thermophilic composting process (TCP) and the normal composting process (NCP). Approximately 500 kg of source-separated OFMSW was composted over 60 days

under both TCP and NCP conditions by the pilot plant. The TCP condition was maintained using a hot water jacket around the IVCP, while the NCP was created by discontinuing the hot water flow. Parameters such as pH, electrical conductivity (EC), moisture content (MC), total organic carbon (TOC), total Kjeldahl nitrogen (TKN), and germination index (GI) were measured based on standard methods [3].

2.3. Step 3: Full-Scale Garage Dry Anaerobic Digester (GDAD) Operation

In 2022, to investigate biogas production from urban organic waste and the effect of anaerobic digestion on accelerating the composting process, a garage dry anaerobic digester (GDAD) was constructed. This step utilized a GDAD with a capacity of approximately 3 cubic

meters as a pilot plant (Figures 3 and 4). The pilot unit included:

- GDAD equipped with a hot water jacket
- Leachate collection tank and recirculation system
- Programmable logic controllers (PLC)
- Electrical heater
- Pressure valve
- Gas flowmeter
- Moisture removal column
- Gas flare

Cow manure was mixed with organic waste to optimize the carbon-nitrogen (C:N) ratio and alkalinity of the substrate [10]. Approximately 800 kg of OFMSW from the Tehran MSW processing center was used as the raw substrate. Additionally, 20 kg of cow manure mixed with 100 liters of water was added as an inoculant to the leachate collection tank. Biogas production was monitored over 30 days.

Figure 1. Dimension of In-vessel composting reactor.

Figure 2. In-vessel composting reactor pilot plant.
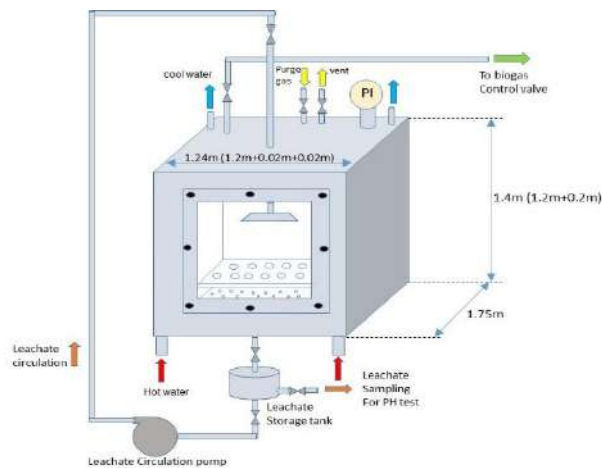
Figure 3. Garage Dry Anaerobic Digester used in this study.

Figure 4. The pilot plant used in this study.

After five days, biogas production began and was sufficient to ignite the flare, with the maximum production rate observed on the 14th day (Figure 5). At the end of the 30-day period, when biogas production ended, the digested organic matter was discharged from the reactor for compost production. The reactor door was left open for two days to minimize odor emissions, after which the digested materials were piled to a height of 80 cm for further composting. Parameters such as temperature, C:N ratio, and GI were monitored over a 45-day period.

Figure 5. Biogas produced on the 14th day.

3. Results and discussion

3.1. Physiochemical properties of feedstock in step 2

The physicochemical properties of feedstock play a crucial role in determining the efficiency and effectiveness of the composting process. One of the most significant indicators is the carbon to nitrogen ratio (C:N), which is essential for evaluating the composting potential of organic materials [3]. A balanced C:N ratio ensures that the composting process proceeds efficiently, with optimal microbial activity and minimal emissions of greenhouse gases such as methane and ammonia.

As shown in Table 1, the initial C:N ratio for the OFMSW is remarkably high at 50.52. This elevated ratio indicates a carbon-rich feedstock, which can impede the composting process by slowing down the microbial activity necessary for organic matter decomposition. In contrast, cow manure has a much lower C:N ratio of 13.87, which is more conducive to composting as it provides a balanced nutrient profile that supports microbial growth and activity. Recent literature supports the importance of optimizing the C:N ratio. The ratio significantly influences the decomposition of organic waste during composting. Organisms maintain a specific C:N ratio at the tissue level, which is vital for determining the microbial decomposition pathways of organic matter. Carbon provides energy and serves as the fundamental building block of life, while nitrogen is essential for the formation of proteins, nucleic

acids, and other cellular components. Therefore, a balanced supply of carbon-rich and nitrogenous materials is necessary for effective composting. The ideal C:N ratio for efficient composting ranges from 25–35:1. Excess carbon can slow down the decomposition process, whereas too much nitrogen can cause unpleasant odors. Regular turning of compost piles helps maintain the C:N ratio by releasing excess nitrogen in the form of ammonia [11].

Table 1.

Physiochemical properties of feedstocks in step2.

No	Parameters	OFMSW	Cow manure
1	MC (%)	82	63
2	TOC (%)	48	43
3	TKN (%)	0.95	3.1
4	C:N	50.52	13.87
5	pH	6.92	7.14
6	EC (µS/cm)	2542	1252

By mixing OFMSW with cow manure, the overall properties of the feedstock become more suitable for the composting process. This adjustment not only enhances the C:N ratio but also improves other critical parameters. For instance, the moisture content (MC) of OFMSW is 82%, which is higher than the 63% found in cow manure. A high moisture content can lead to anaerobic conditions, negatively impacting the composting process. By blending these materials, the moisture content can be balanced to create an optimal environment for aerobic decomposition. A study by Tang et al. [12] corroborates these findings, indicating that maintaining moisture content between 50-60% is crucial for effective aerobic composting. Excessive moisture can create anaerobic pockets, slowing down the composting process and potentially leading to the production of malodorous compounds.

The total organic carbon (TOC) content is 48% for OFMSW and 43% for cow manure. While both materials are rich in organic carbon, the presence of cow manure helps to moderate the overall carbon levels, making the substrate more favorable for composting microorganisms. The total Kjeldahl nitrogen (TKN) content also shows a significant difference, with OFMSW having 0.95% and cow manure having 3.1%. This difference further highlights the importance of blending these feedstocks to achieve a balanced nutrient profile that supports effective composting. This result aligns with findings by Yatoo et al. [13], who highlighted the necessity of a balanced TOC and TKN for microbial growth and efficient composting. They noted that integrating nutrient-rich materials like cow manure can significantly enhance compost quality by providing essential nutrients for microbial communities.

The pH values of the feedstocks are relatively close, with OFMSW at 6.92 and cow manure at 7.14, indicating

that both materials are within the optimal range for composting. However, the electrical conductivity (EC) values differ significantly, with OFMSW having an EC of 2542 µS/cm and cow manure at 1252 µS/cm. High EC levels can indicate the presence of soluble salts, which can inhibit microbial activity if not properly managed. Mixing the two feedstocks can help to dilute these salts, reducing potential inhibitory effects and promoting a healthier composting process.

It can be concluded that the adjustment of the C:N ratio and other physiochemical properties through the combination of OFMSW and cow manure is essential for optimizing the composting process. This blend ensures a balanced nutrient supply, appropriate moisture content, and a conducive pH environment, all of which are critical for efficient microbial activity and effective composting. Such strategic management of feedstock properties is fundamental to improving compost quality and process efficiency, ultimately contributing to more sustainable waste management practices.

3.2. Comparison of changes in compost production index

This section compares key parameters across two distinct periods, including the process temperature, C:N ratio, and GI. The comparison aims to identify any significant changes or trends in these parameters over time, providing valuable insights into the dynamics of the process.

3.2.1. Temperature

Temperature is a critical parameter in the composting process as it influences the rate of microbial activity and the overall efficiency of organic matter decomposition. The temperature variations observed in the NCP, IVCP, and GDAD provide valuable insights into the effectiveness of each method. As depicted in Figure 6, the temperature in the IVCP increases more rapidly compared to NCP and GDAD. This rapid temperature rise in the IVCP indicates a more accelerated composting process. The thermophilic conditions maintained within the IVCP, coupled with effective agitation and adequate moisture content, create an optimal environment for thermophilic microorganisms. These microorganisms thrive at higher temperatures, leading to faster decomposition of organic wastes and a more efficient composting process.

The NCP, on the other hand, exhibits a slower temperature increase. This slower rise can be attributed to the lack of controlled conditions that are present in the IVCP. In open composting processes, such as NCP, temperature regulation is more challenging, leading to less consistent microbial activity and prolonged composting times.

GDAD, which operates under anaerobic conditions, shows a different temperature profile compared to both NCP and IVCP. The anaerobic digestion process does not rely on high temperatures to the same extent as aerobic composting. Instead, it focuses on biogas production through microbial activity in the absence of oxygen. The temperature in GDAD tends to stabilize at a moderate level, sufficient to support the anaerobic microbes responsible for breaking down organic matter. While GDAD may not achieve the high temperatures seen in IVCP, it effectively converts organic waste into biogas and digestate. The higher process rate in the IVCP can be attributed to the thermophilic conditions, which significantly enhance the microbial degradation of organic materials. The effective agitation and moisture control further support this accelerated decomposition. As a result, the IVCP can achieve complete composting more quickly than NCP and GDAD.
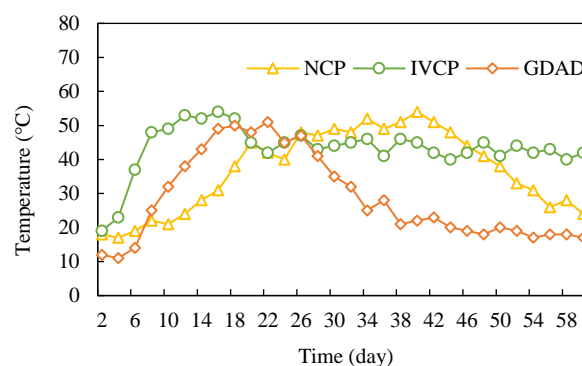
Figure 6. Variations in the temperature of NCP, IVCP and GDAD.

The temperature variations observed in the different composting methods highlight the superior efficiency of the IVCP in processing organic waste. The controlled thermophilic conditions in the IVCP lead to a faster and more effective composting process, producing high-quality compost in a shorter time frame. In contrast, the NCP and GDAD, while effective in their own right, do not achieve the same level of temperature control and process efficiency as the IVCP. These findings highlight the importance of temperature management in composting and the benefits of in-vessel systems for rapid and efficient organic waste processing.

3.2.2. C:N ratio

The C:N ratio is a key indicator in composting, reflecting the balance of carbon-rich and nitrogen-rich materials. While it is not an absolute measure of compost maturity, it is highly correlated with the rate of composting and the quality of the final product [3]. The changes in C:N ratio during composting can provide valuable insights into the effectiveness of different composting processes. As shown in Figure 7, the C:N ratio for the IVCP decreases

more rapidly compared to the GDAD and the NCP. This rapid decline in the C:N ratio for IVCP indicates a faster decomposition of organic materials facilitated by the controlled thermophilic conditions and effective agitation within the reactor. These conditions enhance microbial activity, accelerating the breakdown of carbon-rich compounds and converting them into more stable forms.

In contrast, the GDAD shows a slower decrease in the C:N ratio initially, but it eventually reaches the lowest level after 26 days. This slower initial reduction can be attributed to the anaerobic conditions in GDAD, where the breakdown of organic matter is driven by different microbial communities compared to aerobic composting. However, once the anaerobic microbes become fully active, the process accelerates, resulting in a significant reduction in the C:N ratio.
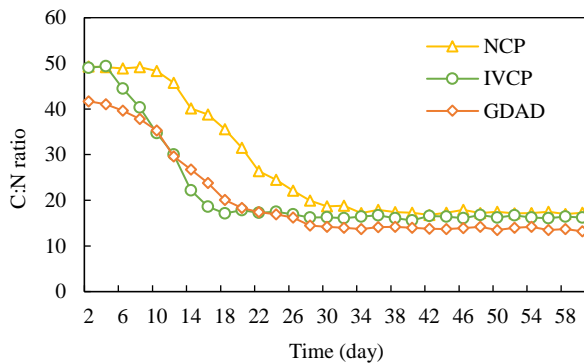

Figure 7. C:N ratio variation in NCP, IVCP, and GDAD.

The lower C:N ratio at the end of the GDAD process suggests a more complete degradation of organic matter, potentially leading to higher-quality compost. This is supported by the observation that the quality of compost produced from GDAD is better than that from IVCP, despite the faster process rate in IVCP. The higher quality of GDAD compost may be due to the comprehensive breakdown of complex organic compounds under anaerobic conditions, producing a more stable and nutrient-rich product.

In the case of NCP, the C:N ratio decreases at a slower rate compared to both IVCP and GDAD. This can be attributed to the less controlled environmental conditions in NCP, which result in less efficient microbial activity and slower decomposition of organic matter. The lower efficiency of NCP indicates the advantages of controlled composting environments, such as those provided by IVCP and GDAD, in achieving faster and more effective composting.

While the C:N ratio alone cannot fully determine compost maturity, its variation during the composting process provides critical insights into the efficiency and quality of different composting methods. The rapid reduction in IVCP highlights its efficiency, while the low

final C:N ratio in GDAD points to its potential for producing high-quality compost. These findings suggest that a combination of these methods could optimize both the speed and quality of compost production, contributing to more sustainable and effective waste management practices.

3.2.3. Germination index (GI)

The Germination Index is a valuable tool for assessing compost maturity and phytotoxicity due to its shorter measurement time and lower cost [14]. This index serves as a reliable indicator, reflecting the presence and reduction of phytotoxic substances produced during the initial stages of the composting process. As compost matures, the concentration of these toxic substances decreases, resulting in higher GI values, indicative of a non-toxic, mature compost [14]. Kong et al. [14] emphasized that a GI above 80% indicates mature and non-phytotoxic compost.

Figure 8 illustrates the variation in GI values across the NCP, IVCP, and GDAD. The GI values for GDAD increase at a faster rate compared to NCP and IVCP, highlighting the effectiveness of the anaerobic digestion process in reducing phytotoxicity and enhancing compost maturity. By the 18th day, the GI value for GDAD surpasses 90%, signifying that the compost has reached full maturity. In contrast, the GI values for IVCP and NCP achieve similar maturity levels at later stages, specifically on the 24th and 36th days, respectively. The rapid increase in GI for GDAD can be attributed to the anaerobic conditions, which effectively facilitate the breakdown of organic matter and the stabilization of compost. The anaerobic digestion process promotes the degradation of complex organic compounds and the reduction of phytotoxic substances, resulting in a compost product that is safe for plant growth in a shorter period.
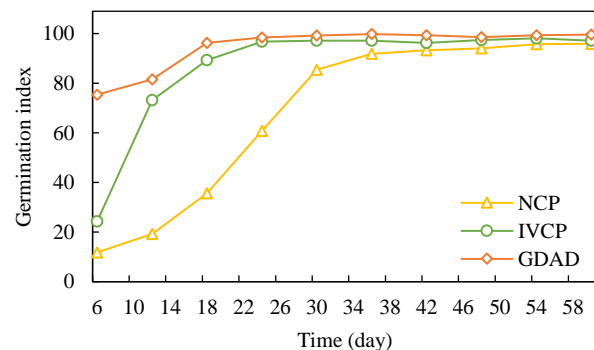

Figure 8. GI variation in NCP, IVCP, and GDAD.

In the case of IVCP, the controlled thermophilic conditions and mechanical agitation contribute to a steady increase in GI values. Although the maturation process in IVCP is slightly slower than GDAD, the in-vessel system ensures a consistent and efficient composting environment.

This controlled setting helps maintain optimal temperatures and moisture levels, which are critical for microbial activity and the decomposition of organic matter. By the 24th day, the GI values in IVCP indicate mature compost suitable for agricultural and horticultural applications.

The NCP exhibits the slowest increase in GI values, reaching maturity on the 36th day. The slower progression in NCP can be attributed to the less controlled environmental conditions resulting in variable temperatures and moisture levels. These fluctuations can hinder microbial activity and slow down the decomposition process, thereby delaying the reduction of phytotoxic substances and the maturation of compost.

Overall, the GI data highlights the efficiency and effectiveness of different composting methods. rapid increase of high GI values in GDAD indicates its potential for producing mature compost quickly, making it a valuable option for waste management strategies prioritizing speed and efficiency. IVCP, while slightly slower, offers the benefits of a controlled environment, ensuring consistent and high-quality compost production. NCP, although effective, requires a longer time frame to achieve similar results. These findings emphasize the importance of selecting appropriate composting methods based on specific requirements and constraints. The rapid maturation in GDAD and the controlled efficiency in IVCP present compelling options for enhancing compost production processes, ultimately contributing to more sustainable and effective waste management practices.

3.3. Biogas generation rate

The production of biogas is a vital component of the anaerobic digestion process, particularly in the context of municipal solid waste (MSW) management. Biogas, primarily composed of methane, can be harnessed as a renewable energy source, thereby reducing reliance on fossil fuels and contributing to sustainable energy solutions. As noted by Avinash and Mishra [9] incorporating leachate or sludge from wastewater treatment can significantly enhance the biogas production rate in an anaerobic digestion process. Specifically, increasing the moisture content to greater than 75% of field capacity (FC) can boost biogas production by approximately 30%. This increase is due to the improved microbial activity facilitated by the higher moisture content, which creates an optimal environment for the anaerobic bacteria responsible for biogas generation.

In the current study, biogas production was monitored over a specified period to evaluate the effectiveness of the GDAD in converting organic waste into biogas. The results indicate that biogas production commenced on the fifth day and peaked on the 14th day. This peak production highlights the efficiency of the GDAD system in rapidly initiating and maintaining the anaerobic digestion process.

The addition of leachate or sludge likely played a crucial role in this enhanced biogas generation. The higher moisture content provided by these additives ensures that the anaerobic bacteria have sufficient water for their metabolic processes, essential for breaking down organic matter and producing methane. Additionally, the presence of leachate or sludge may introduce additional nutrients and microbial consortia that further aid in the digestion process. The sustained biogas production observed over the 30-day period demonstrates the stability and effectiveness of the GDAD system. The gradual decline in biogas generation towards the end of the period is typical of anaerobic digestion processes as the readily digestible organic matter is depleted. At this stage, the residual digested material can be further processed into compost, contributing to a circular waste management approach.
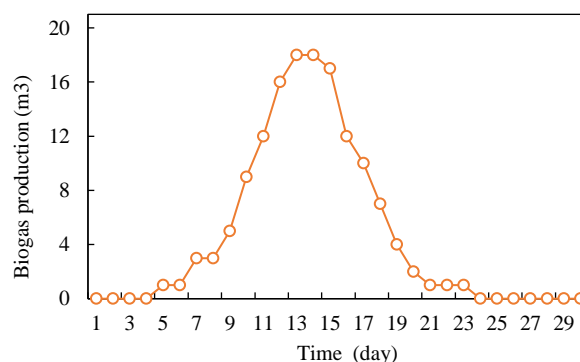
Figure 9. Biogas production in Garage Dry Anaerobic Digester.

The practical implications of these findings are significant. By optimizing the moisture content and incorporating wastewater sludge, it is possible to enhance biogas production rates, thereby improving the overall efficiency of anaerobic digestion systems. This approach not only maximizes energy recovery from organic waste but also supports waste reduction and resource recycling objectives. In conclusion, the addition of leachate or wastewater sludge to anaerobic digestion processes markedly improves biogas production. The results from the GDAD system underscore the potential of such enhancements in municipal solid waste management, providing a pathway towards more sustainable and efficient waste-to-energy solutions.

The reported results in the current study align well with recent literature on composting and anaerobic digestion. The integration of thermophilic in-vessel composting and anaerobic digestion presents a promising approach for efficient waste management, combining rapid composting processes with renewable energy production. Future research and practical implementations should focus on

optimizing these processes to enhance sustainability and resource recovery in urban waste management systems.

4. Conclusion

This study underscores the potential of integrating thermophilic in-vessel composting and anaerobic digestion in neighborhood waste management models to achieve superior efficiency and sustainability. Thermophilic in-vessel composting, with its controlled high-temperature environment, significantly enhances the decomposition rate and compost quality by promoting optimal microbial activity. In contrast, anaerobic digestion not only reduces waste volume and produces renewable biogas but also generates a nutrient-rich digestate that can be further composted to yield high-quality compost.

The findings demonstrate that a balanced C:N ratio, achieved by combining OFMSW with cow manure, is critical for efficient composting. Additionally, the rapid attainment of high GI values in anaerobic digestion highlights its efficacy in swiftly producing mature, non-phytotoxic compost. The synergy between these processes offers a robust solution for localized waste management, addressing the dual goals of waste reduction and renewable energy production.

The results of this study align with contemporary research, reinforcing the importance of controlled composting environments and the benefits of integrating composting with anaerobic digestion. This integrated approach supports the broader objectives of urban sustainability by reducing energy consumption, minimizing greenhouse gas emissions, and enhancing resource recovery. Future research should focus on optimizing these processes further to enhance their applicability and efficiency in diverse urban settings, contributing to the global efforts towards sustainable waste management and renewable energy utilization.

References

[1]   Devendra, R., et al. "Quality control and assessment of compost obtained from open and In-Vessel composting methods." Materials Today: Proceedings (2023). https://doi.org/10.1016/J.MATPR.2023.06.350

[2]   Yang, Mingchao, et al. "Operational performance of organic fraction of municipal solid waste discarded from communities, using an in-vessel hyperthermophilic composting technology." Journal of Cleaner Production 427 (2023): 139059. https://doi.org/10.1016/J.JCLEPRO.2023.139059

[3]   Hosseini, Seyed Mohammad, and Hamidi Abdul Aziz. "Evaluation of thermochemical pretreatment and continuous thermophilic condition in rice straw composting process enhancement." Bioresource technology 133 (2013): 240-247. https://doi.org/10.1016/J.BIORTECH.2013.01.098

[4]   International Energy Agency. (2020). World Energy Statistics 2020. International Energy Agency. Retrieved from [IEA Website] (https://www.iea.org/reports/world-energy-statistics-2020)

[5]   Mohsin, Muhammad, et al. "Assessing the impact of transition from nonrenewable to renewable energy consumption on economic growth-environmental nexus from developing Asian economies." Journal of environmental management 284 (2021): 111999. https://doi.org/10.1016/j.jenvman.2021.111999

[6]   Sanz-Cobena, Alberto, et al. "Strategies for greenhouse gas emissions mitigation in Mediterranean agriculture: A review." Agriculture, ecosystems & environment 238 (2017): 5-24. https://doi.org/10.1016/j.agee.2016.09.038

[7]   Pamukçu, Hale, Pelin Soyertaş Yapıcıoğlu, and Mehmet İrfan Yeşilnacar. "Investigating the mitigation of greenhouse gas emissions from municipal solid waste management using ant colony algorithm, Monte Carlo simulation and LCA approach in terms of EU Green Deal." Waste Management Bulletin 1.2 (2023): 6-14. https://doi.org/10.1016/j.wmb.2023.05.001

[8]   Pasang, Haskarlianus, Graham A. Moore, and Guntur Sitorus. "Neighbourhood-based waste management: a solution for solid waste problems in Jakarta, Indonesia." Waste management 27.12 (2007): 1924-1938. https://doi.org/10.1016/j.wasman.2006.09.010

[9]   Avinash, Lagudu S., and Anumita Mishra. "Enhancing biogas production in anaerobic digestion of MSW with addition of bio-solids and various moisture sources." Fuel 354 (2023): 129414. https://doi.org/10.1016/J.FUEL.2023.129414

[10]   DeCola, Amy C., et al. "Microbiome assembly and stability during start-up of a full-scale, two-phase anaerobic digester fed cow manure and mixed organic feedstocks." Bioresource Technology 394 (2024): 130247. https://doi.org/10.1016/J.BIORTECH.2023.130247

[11]   Ahmed, Temoor, et al. "Fertilization of Microbial Composts: A Technology for Improving Stress Resilience in Plants." Plants 12.20 (2023): 3550. https://doi.org/10.3390/plants12203550

[12]   Tang, Ruolan, et al. "Effect of moisture content, aeration rate, and C/N on maturity and gaseous emissions during kitchen waste rapid composting." Journal of Environmental Management 326 (2023): 116662. https://doi.org/10.1016/j.jenvman.2022.116662

[13]   Yatoo, Ali Mohd, et al. "Production of nutrient-enriched vermicompost from aquatic macrophytes supplemented with kitchen waste: Assessment of nutrient changes, phytotoxicity, and earthworm biodynamics." Agronomy 12.6 (2022): 1303. https://doi.org/10.3390/agronomy12061303

[14]   Kong, Yilin, et al. "Determining the extraction conditions and phytotoxicity threshold for compost maturity evaluation using the seed germination index method." Waste Management 171 (2023): 502-511. https://doi.org/10.1016/J.WASMAN.2023.09.040

Journal of Civil Engineering Researchers

Journal homepage: www.journals-researchers.com

J-Researchers

Analyzing the nonlinear dynamics of the three degree of freedom frame structure based on the NewMark-β method and the effect of stiffness on the displacement of the structure

Hosein Sarkoyeh, [iD] [a,*] Mohammad Ali Hajarizadeh, [iD] [a] Saeed Alaie, [iD] [a]

[a] *Structural engineering PhD student, Faculty of Civil Engineering, Islamic Azad University, Chalous branch, Tehran, Iran*

[a] *Structural engineering PhD student, Faculty of Civil Engineering, Islamic Azad University, Bushehr branch, Bushehr, Iran*

[a] *Structural engineering PhD student, Faculty of Civil Engineering, Islamic Azad University, Ahvaz branch, Ahvaz, Iran*

ABSTRACT

The analytical method of the simplified model of a structure has provided a basis for the analysis under the effect of earthquake (dynamic) load, which has an important importance in the seismic analysis of the structure. In this article, three degree of freedom steel frame structure is simulated and analyzed in MATLAB based on the NewMark-β method, taking into account the effect of harmonic loads. The vibration response of the steel frame structure has been analyzed considering the stiffness. The results show that the NewMark-β method is a new idea for earthquake response. The construction of the steel frame according to the range of changes of its elastic modulus through dynamic analysis makes the seismic analysis of the frame structures more practical, as well as the analysis of the SS model, which provides a basis for the size of the stiffness coefficient. By applying force on the top and bottom floors, different structural responses are observed according to the stiffness of the structure. The structure of the SS frame and the effect of the force on it when the force is applied to its floors, according to the height of the floors and the position of applying the force with the change of time, the binding stiffness of the amount of displacement will also change and the stability of the structure will be greatly reduced.

1. Introduction

The ever-increasing progress in the construction industry is particularly prominent. So that every day we see a general change in building frames, especially in tall buildings, which in addition to increasing the height, the vertical design and shape which is more and more complex, the structural system also becomes increasingly diverse, which causes more prerequisites for The design of the vibrations of building structures. The purpose of seismic design is to make the building have the corresponding resistance ability to earthquakes of different frequencies

---

* Corresponding author. Tel.: +989111944420; e-mail: hosein.sarkoyeh@gmail.com.

and intensity during the service life [1]. The distribution of structural stiffness is accompanied by certain unevenness. Therefore, to a large extent, it will lead to the overall deformation of the building, and in serious cases, it can cause local cracking of the building. Therefore, the bottom frame structure is difficult to be used effectively in some areas with high fortification intensity. To further improve the seismic design value of building structures, the influence of structural stiffness must be considered [2].

Unlike linear analysis, incremental iterative formulas for structural nonlinear analysis have not been developed to the extent that every researcher follows the same logical steps [3]. In most cases, only the Newton-Raphson method or other algorithms are used as tools for incremental iterative analysis [4]. In structural dynamics, a multi degree of freedom (MDOF) structure is often equalized by a single degree of freedom (SDOF) model [30]. Such a SDOF system is based on the dynamic properties adopted from the MDOF system. Structural responses of this SDOF model to earthquake is determined by conducting a nonlinear time history analysis of the model, subjected to a set of ground motion records. Accordingly, the numerical analysis of SDOF systems is of high importance in this field of structural engineering. [31]. However, there are many varieties in each stage of the calculation structure, especially in the calculation of the element node forces (referred to as the correction stage), which will affect the accuracy of the calculation results and the convergence of the iterative process [5]. For the NewMark-β method, when the control parameters $\alpha = 1/2$ and $\beta = 1/4$, the mean constant acceleration method has second-order accuracy (to meet the engineering requirements). NewMark-β is unconditionally stable and is widely used. By controlling the NewMark-β, the results can be more accurate and converging, and the velocity and acceleration responses can be calculated more easily than other methods. used the nonstationary Kanai Tajimi model to record the ground acceleration in MATLAB, simulating the idealized model of the frame structure. investigated the seismic input single-degree of freedom (SDOF) structure and found that the acceleration changed linearly with the step. The response spectrum is used to analyze the response of the structure linear system and seismic input, without considering the nonlinear factors. Three constitutive models for nonlinear analysis of structures were proposed, as follows: linear elastic-elasticity, complete plasticity, and Armstrong Frederick cyclic hardening plasticity. calculated the dynamic response multi-degree-of-freedom nonclassical damping linear system by (MDOF) based on idealized shear stiffness matrix construction and assuming that all floors have the quality. It provides the seismic acceleration time history of the shock response spectrum program, which can be used to calculate peak ground acceleration and velocity based on the known shock

response spectrum of the acceleration time history of the earthquake [6]. investigated the response of linear SDOF earthquakes to ground motion through the NewMark method. The response of linear single degree of freedom to seismic ground motion provides a simplified calculation method, which is easy to implement by MATLAB program. The non-linear (or linear) response of a single degree of freedom damped mass-spring system under external forces was predicted. The dynamic analysis of multi-structure underground excitation was presented. However, the idealized model based on the foregoing does not consider the effect of structural stiffness reduction and it is not used by considering the RCS structure. Geometrical nonlinearity of materials is an important characteristic of RCS structures. The design of (RCS) structures is generally based on elastic theory. However, the stiffness coefficient of RCS structure was not constant due to the plastic development of RCS. Due to the effect of seismic force, the response of structural stiffness reduction became more and more obvious [7]. investigated the influence of nanomaterials on reinforcement plasticity, which provided a reference for the research on structural stiffness [8]. investigated the influence of nano-strengthening on the properties and microstructure of recycled concrete, providing another idea for the study of concrete stiffness. The review of the existing literature showed that the scholars have provided different assumptions on the seismic modes and structural mode shapes. He conducted reasonable numerical simulations based on these assumptions and proposed different ideas for structural seismic modal analysis. However, none of the above researches considered time factors caused by reinforced concrete (RCS) structural stiffness reduction. Therefore, the objective of this study is to introduce the stiffness reduction according to the empirical formula, compare the displacement, velocity, and acceleration responses before and after the stiffness reduction is applied at different positions, and obtain the functional relationship between the stiffness reduction factor and the acceleration of the third floor of the RCS frame structure.

Only when the constitutive models of RCS structures of different materials are well-mastered can the stiffness coefficient be analyzed effectively. It is of great significance for different scholars to study the material characteristics through experiments [9,10]. According to the different theoretical basis of mechanics, the existing constitutive models can be roughly divided into the following types: linear elastic and nonlinear elastic constitutive models based on elastic theory; elastoplastic and elastoplastic hardening constitutive models based on the classical plasticity theory; and the constitutive model of concrete described by inner time theory. Later Ni et al. also established a series of constitutive models under different conditions through numerical simulation and experiments

[11,12]. analyzed the stiffness and deflection of RCS members after cracking and established constitutive models at different stages [13]. conducted shear and tension compression experiments on RCS plates and obtained the stress-strain relationship of the corresponding RCS plates [14]. used the hypothesis of strain coordination and strength equivalence to construct the RCS structure plastic damage model. This model can be used in the ABAQUS finite element damage plasticity numerical analysis of RCS walls structures and provides another way of thinking for the analysis of the RCS wall structure seismic damage model [15]. used ABAQUS to conduct finite element simulation in mass concrete and obtained the nonlinear constitutive relation and failure criterion for concrete. proposed a three-dimensional constitutive model for concrete and obtained good failure characteristics of RCS structures by the model through experiments [16]. used the William Wanke plastic constitutive model to describe the nonlinear behavior of concrete, taking into account the interaction between steel bars and concrete and verifying it through experiments [17,18]. classified the RCS structure constitutive models, applying the elastoplastic model of the flow law, considered the softening behavior, and used the damage model to correct it. Zhang et al. conducted a numerical simulation on RCS beams, taking into account the influence of stiffness degradation during the loading and unloading of RCS structures, and verified its constitutive model. simulated the hysteretic relationship of RCS columns based on the uniaxial tension and compression of concrete provided by the China Code for Design of Concrete Structures [19]. These constitutive relations can well reflect the variation trend of elastic modulus in the loading process so that the change rate of stiffness can be analyzed. The analysis of the constitutive model provides a reasonable idea for the reduction of the stiffness coefficient and a reference for the reasonable value of the stiffness coefficient. The process of flowchart is shown in the graphical abstract.

2. NewMark-β method

The newMark-β method is a method to unify the linear acceleration method, being widely used in finite element analysis. Acceleration is modified by the NewMark-β method, as:

$$\dot{y}(t + \Delta t) = \dot{y}(t) + [(1 - a)\ddot{y}(t) + a\ddot{y}(t + \Delta t)]\Delta t \quad (1)$$

$$y(t+\Delta t)=y(t) +\dot{y}(t)\Delta t +[(\tfrac{1}{2} - \beta)\ddot{y}(t) + \beta\ddot{y}(t + \Delta t)]\Delta t^2 \quad (2)$$

If $\alpha = 1/2$, only keep β, which is the NewMark-β method. If $\alpha = 1/2$, $\beta = 1/6$, that is equivalent to the acceleration varying linearly over Δt, which is the Wilson-θ method with θ = 1; if the acceleration is constant in Δt, it is the average acceleration method.

It can be obtained from Equations (1) and (2) [6]:

$$\ddot{y}(t + \Delta t) = \frac{1}{\beta\Delta t^2}[y(t + \Delta t) - y(t)] - \frac{1}{\beta\Delta t}\dot{y}(t) \quad (3)$$
$$- (\frac{1}{2\beta} - 1)\ddot{y}(t)$$

$$\dot{y}(t + \Delta t) = \frac{1}{\beta\Delta t}[y(t + \Delta t) - y(t)] - (\frac{\alpha}{\beta} - 1)\dot{y}(t) \quad (4)$$
$$- (\frac{1}{2\beta} - 1)\Delta t\ddot{y}(t)$$

Substitute the Equations (3) and (4) into the dynamic equation at t + Δt:

$$\bar{K}(t + \Delta t)y(t + \Delta t) = \bar{F}(t + \Delta t) \quad (5)$$

Now we paste:

$$\bar{K}(t + \Delta t) = \frac{1}{\beta\Delta t^2}M + \frac{\alpha}{\beta\Delta t}C(t + \Delta t) + K(t + \Delta t) \quad (6)$$

$$\bar{F}(t + \Delta t) = M[\frac{1}{\beta\Delta t^2}y(t) + \frac{1}{\beta\Delta t}\dot{y}(t) \quad (7)$$
$$+ \left(\frac{1}{2\beta} - 1\right)\ddot{y}(t)]$$

The accuracy of the NewMark-β calculation results is mainly determined by the time step Δt. The determination of Δt needs to consider the load change and the length of the natural vibration period T. In general, it is required that Δt be less than 1/7 of the natural vibration period of the minimum structure that has an important effect on the response. When $\beta \geq 0.25$, the NewMark-β method is unconditionally stable; when $\beta < 0.25$, it is conditionally stable [20].

$$\{\ddot{u}\}_{t+\Delta t} = \frac{1}{\gamma\Delta t^2}(\{u\}_{t+\Delta t} - \{u\}_t) - \frac{1}{\gamma\Delta t}\{\dot{u}\}_t \quad (8)$$
$$- (\frac{1}{2\gamma} - 1)\{\ddot{u}\}_t$$

$$\{\dot{u}\}_{t+\Delta t} = \frac{\beta}{\gamma\Delta t}(\{u\}_{t+\Delta t} - \{u\}_t) - (1 - \frac{\beta}{\gamma})\{\dot{u}\}_t \quad (9)$$
$$- (1 - \frac{\beta}{2\gamma})\Delta t\{\ddot{u}\}_t$$

Considering the vibration differential equation at time t + Δt, it can be obtained as:

$$[M]\{\ddot{u}\}_{t+\Delta t} + [C]\{\dot{U}\}_{t+\Delta t} + [K]\{u\}_{t+\Delta t} = \{R\}_{t+\Delta t} \quad (10)$$

Solve for available {u}t+Δt and {u̇}t+Δt first, then solve {ü}t+Δt

The calculation steps of NewMark-β method are as follows [21]:

2.1. Initial calculation:

Forming stiffness matrix [K], Mass matrix [M], and the damping matrix [C];

Setting initial value $\{u\}0$, $\{\dot{u}\}0$, and $\{\ddot{u}\}0$;

Select the integral step size t, parameter α and β, and calculate the integral constant:

$$\alpha_0 \qquad \alpha_1 \qquad \alpha_2 = \frac{1}{\gamma\Delta t} \quad \alpha_3 \qquad (11)$$
$$= \frac{1}{\gamma\Delta t^2} \quad = \frac{\beta}{\gamma\Delta t} \qquad\qquad = \frac{1}{2\gamma} - 1$$

$$\alpha_4 \qquad \alpha_5 \qquad \alpha_6 \qquad \alpha_7$$
$$= \frac{\beta}{\gamma} - 1 \quad = \frac{\Delta t}{2}(\frac{\beta}{\beta} \quad = \Delta t(1 \quad = \beta\Delta t$$
$$\qquad\qquad - 2) \qquad - \beta)$$

Forming effective stiffness matrix:

$$[\bar{K}] = [K] + \alpha_0[M] + \alpha_1[C] \qquad\qquad (12)$$

2.2. Calculating the time step:

Calculating the effective load at time t + Δt:
$$\{\bar{F}\}_{t+\Delta t} = \{F\}_{t+\Delta t} + [M](\alpha_0\{u\}_t + \alpha_2\{\dot{u}\}_t$$
$$+ \alpha_3\{\ddot{u}\}_t) + [C](\alpha_1\{u\}_t \qquad (13)$$
$$+ \alpha_4\{\dot{u}\}_t + \alpha_5\{\ddot{u}\}_t)$$
Getting the displacement at time t + Δt:
$$[\bar{K}]\{u\}_{t+\Delta t} = \{\bar{F}\}_{t+\Delta t} \qquad\qquad (14)$$
Calculating the velocity and acceleration at time t + Δt [9]:
$$\{\ddot{u}\}_{t+\Delta t} = \alpha_0(\{u\}_{t+\Delta t} - \{u\}_t) - \alpha_2\{\dot{u}\}_t - \alpha_3\{\ddot{u}\}_t \quad (15)$$
$$\{\dot{u}\}_{t+\Delta t} = \{\dot{u}\}_t + \alpha_6\{\ddot{u}\}_t + \alpha_7\{\ddot{u}\}_{t+\Delta t} \qquad (16)$$

3. Analysis and discussion

Taking the multilayer frame structures as an analysis example, the structural calculation model is shown in Figure1 and the stiffness information of each floor is shown in Table 1and 2.

3.1. Structural stiffness reduction of RCS structure

Structure and affect the resistance and dynamic characteristics of the structure, resulting in local or overall, per-performance loss [22]. The experiment of high-strength steel provides an idea of reinforcing steel, and the combination effect with concrete is more obvious [23]. Scholars have proposed some models, that well-reflected the force characteristics of stiffness degrading components, and obtained some hysteretic cycle rules, such as the IMK hysteretic cycle rule. The MODLMK bending moment Angle model proposed through the OpenSees simulation experiment well-reflected the relationship between column top force and displacement, which validates the effectiveness and stability of the model [6].
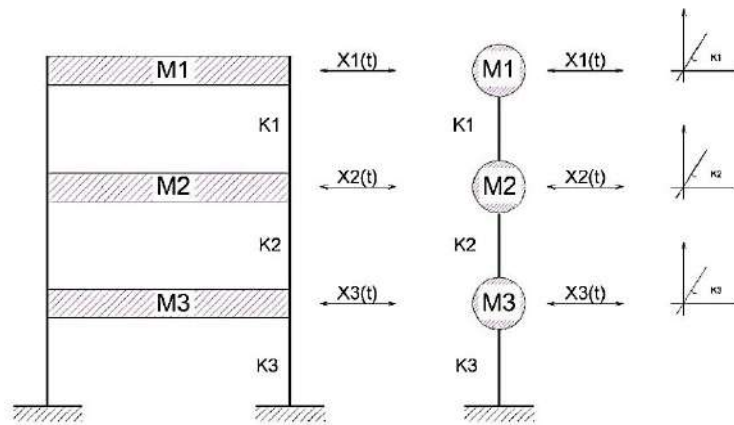
Figure 1: The structure of the computational model of the three-story frame

Table 1:

Characteristics of the mass and stiffness of the structure with a floor height of 3 meters

Floor	Mass (Ton)	Column cross-section	Section moment of inertia (mm4)	Hardness (N.mm)
1	200	IPB 200	$5.7*10^7$	$1.06 * 10^9$
2	0	IPB 240	$1126*10^5$	$2.1 * 10^{10}$
3	0	IPB 280	$1927*10^5$	$3.6 * 10^{10}$

Table 2:

Characteristics of the mass and stiffness of the structure with a floor height of 6 meters

Floor	Mass (Ton)	Column cross-section	Section moment of inertia (mm4)	Hardness (N.mm)
1	200	IPB 200	$5.7*10^7$	$1.33 * 10^8$
2	0	IPB 240	$1126*10^5$	$2.63 * 10^9$
3	0	IPB 280	$1927*10^5$	$4.5 * 10^9$

The stiffness reduction coefficient of the scaffold column took into account an overall comprehensive stiffness reduction coefficient. In the elastic second-order analysis, the overall displacement of the structure and the horizontal displacement between layers were approximately the same as the Stiffness degradation that occurs in plastic hinge areas of RCS frame structures under repeated loads. The accumulation of structural fatigue will increase the plastic zone of the results of the nonlinear analysis [24]. In the American (ACI 318-14) code [25], the structural effect was calculated, the reduction coefficient of the beam member was 0.35, and the column member was 0.7. The cracked wall was 0.35 and the plate was 0.25 In the New Zealand (NZS3101) code, the reduction coefficient of beam members was different due to different sections. The rectangular section was 0.4, and the T-type and L-type components were 0.35. Column components are valued according to different axial compression ratios. China Code for Design of Concrete Structures GB50010-2010 [26] also considered the influence of stiffness reduction, and the reduction coefficient of beam members was 0.4, column members were 0.6, and wall members were 0.45. In this paper, a harmonic load calculation example was applied. The calculation example is considered as the stiffness coefficient is 0.75. During the nonlinear analysis, a stiffness reduction coefficient of 0.75 was introduced to reduce the elastic stiffness K0 to K0 * 0.75, so that under the original load level of the structure, the elastic analysis and nonlinear analysis could produce approximately the same structural response [6]. The internal forces and deformations of the structure under nonlinear conditions were simulated by a unified stiffness reduction factor, rather than giving different reduction factors for different stiffness degradation sections. The unified reduction factor was called the comprehensive stiffness reduction factor. The analysis of the constitutive model provides a reasonable way to reduce the stiffness coefficient [27]. The stiffness reduction coefficient was introduced to analyze the structural acceleration response with different reduction coefficients of stiffness α in the ranges of (0.5, 1). By analyzing the experimental results made by Zhan et al [15]. the constitutive relation of RCS is derived, and the variation trend of elastic modulus in the loading process is obtained by fitting the constitutive relation of the RCS beam, as shown in Figures 2 and 3. It is found that the variation of the stiffness coefficient keeps the descending section and has obvious polynomial characteristics with the gradient of variation at 0.05 So under the original load level of the structure, the elastic analysis and nonlinear analysis produced approximately the same structural response.

Using this principle, the same nonlinear constitutive model S in the structure of different input levels corresponded to different reduction factors, but with the

engineering practicability, through a universally applicable reduction factor. However, given engineering practicability, through a universally applicable reduction factor, it was used in the elastic second-order analysis method. The elastic second-order method and the nonlinear finite element method are used to calculate the interlayer displacement Angle and interlayer displacement. The results were equivalent, instead of just constraining the stiffness reduction coefficient α of a certain state [28]. In addition, carbon nanotube cement mortar also improves the workability of concrete and has important research value in mitigating stiffness degradation response [29].
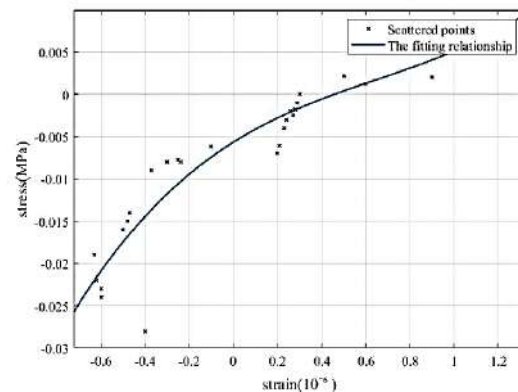
Figure 2: Stress–strain relationship fitting made [18]
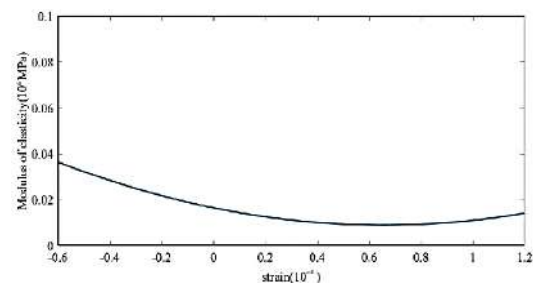
Figure 3: Variation of elastic modulus

3.2. Analysis results

The three degree of freedom frame structure is three-story exposed to a harmonic load once at the top or bottom of the structure for 0.2 seconds, and the response time is 3 seconds with time steps of 0.01 seconds and damping at the value of k * 0.005 is formed The steps of the damping matrix are made based on the Rayleigh method. Damping is used to compare the loads applied in different positions before and after reducing the stiffness, for vibration analysis, MATLAB simulation is used. The forms in different conditions of the stiffness matrix of the structure and the three-story frame element are made according to Figure 1 and analyzed in the local coordinate system.

Material parameters including elastic modulus Mpa E = $2.1*10^5$, frame height in structure "A" H = 3 @ 3 meters, frame height in structure "B" H = 6 @ 3 meters, and other specifications based on tables 1 and 2 were made and the stiffness matrix of the frame element is formed in the local coordinate system as shown in Figure 1 so that the weight force is located only in the M1 level.

The mass matrix of the three-story frame:

$$M = \begin{bmatrix} m_1 & 0 & 0 \\ 0 & m_2 & 0 \\ 0 & 0 & m_3 \end{bmatrix} \Rightarrow M = 2*10^6 \begin{bmatrix} 1 & 0 & 0 \\ 0 & 0 & 0 \\ 0 & 0 & 0 \end{bmatrix}$$

The stiffness matrix of the three-story frame A:

$$K = \begin{bmatrix} k_1 & -k_1 & 0 \\ -k_1 & k_1+k_2 & -k_2 \\ 0 & -k_2 & k_2+k_3 \end{bmatrix} \Rightarrow$$

$$K = 10^{10} \begin{bmatrix} 0.106 & -0.106 & 0 \\ -0.106 & 2.21 & -2.1 \\ 0 & -2.1 & 5.7 \end{bmatrix}$$

The stiffness matrix of the three-story frame B:

$$K = \begin{bmatrix} k_1 & -k_1 & 0 \\ -k_1 & k_1+k_2 & -k_2 \\ 0 & -k_2 & k_2+k_3 \end{bmatrix} \Rightarrow$$

$$K = 10^9 \begin{bmatrix} 0.133 & -0.133 & 0 \\ -0.133 & 2.67 & -2.63 \\ 0 & -2.63 & 7.12 \end{bmatrix}$$

Harmonic load F = 500 sin ($20 * \pi * t$) at the top or bottom of the structure, with a force action time of 0.2 seconds, a response time of 3 seconds, and a step size of 0.01 was made based on Rayleigh damping matrix method.

A harmonic load F = 500 sin ($20*\pi*t$) is applied to the top of the frame structure, and the structural response is shown in Figure 4.

As can be seen in Figures 4 and 5, the displacement responses were compared before and after reducing the stiffness under the applied harmonic load conditions. In Figure 4, the top change of the three-story frame structure is in the range of m1 alignment, which in case A was in the time limit of about 0.25 seconds, around $-2.8 * 10^{-7}$ to $2.5*10^{-7}$. These displacements in the level of m2 and m3 are very small and they move again and it was approximately with the change of the harmonic function. It reached its peak in the change of about 0.2 seconds and then its displacement fluctuation was gradually leveled with the stop of load application in the change of about 4 seconds. In case B, by changing the case that can be applied in changing the stiffness reduction factor of 0.875 due to the increase in the height of each floor of the structure from 3 meters to 6 meters, the displacement range that can be changed and expands with time and in changing the range ($-6.4 * 10^{-7}$ to $5.7 * 10^{-7}$), and the maximum absolute displacement value was lower than before. So that it can

reach its peak in the change of about 0.5 seconds and then its displacement fluctuation is gradually leveled by stopping the application of load in the change of about 11 seconds. The reduction of displacement difference between different classes also increased.

(2) The harmonic load F = 500 sin ($20*\pi*t$) is applied to the bottom of the frame structure, and the structural response is shown in Figure 5.
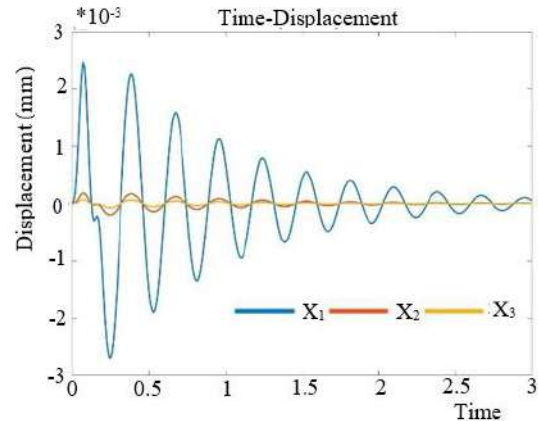
(a)
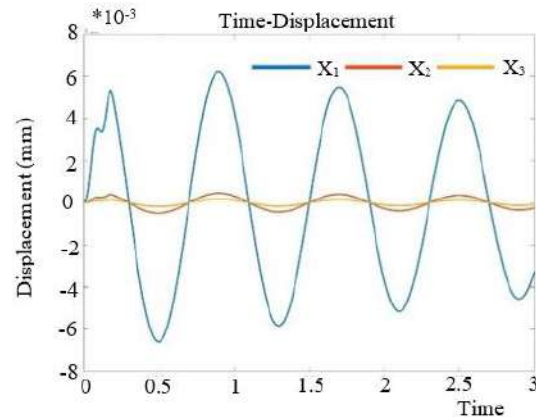
(b)

Figure 4 - The amount of displacement of the structure when the force is applied to the maximum level of the floor - (A, the height of the structure is 3 meters - B, the height of the structure is 6 meters)

When downward load was applied, displacement images were compared before and after reduction. The curve was very different from the harmonic curve. In case A, the displacement process of m2 and m3 floors were the same and close to each other before the reduction. After reduction, the displacement difference of each layer increased and the absolute value of its maximum displacement has changed a lot. The displacement responses, before and after reduction, were compared under the applied harmonic load conditions. At the top of the three-story frame structure, the range of displacement change before reduction with time was in the range

$(-1.33 * 10^{-8}\ To\ 1.3 * 10^{-8})$ The displacement of the first, second and third floors act in different directions and move with time, and it is approximately with the change of the harmonic function and reached its peak in about 0.1 second, and then its displacement fluctuation gradually leveled off with the stop of applying the load in about 4.4 seconds. became. In case B, by changing the case that can be applied in the reduction factor, the stiffness of 0.875 due to the increase in the height of each floor of the structure from 3 meters to 6 meters, the range of displacement that can be expanded with time and in the range of $(-1.04 * 10^{-7}\ to\ 1.02 * 10^{-7})$ and the maximum absolute value of displacement was higher than before. So that it can reach its peak in the change of about 0.1 second, and then its displacement fluctuation is gradually leveled by stopping the application of load in about 12 seconds. The decrease, the difference in displacement between different classes also increased.
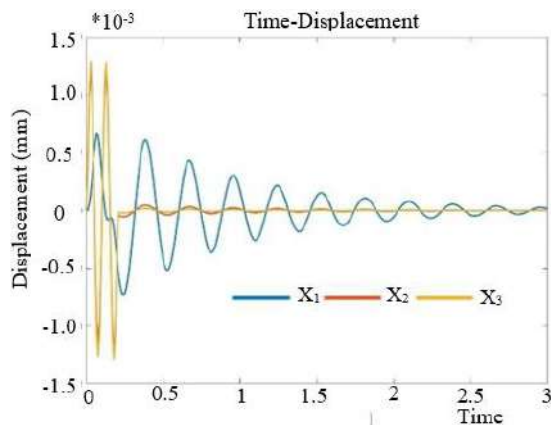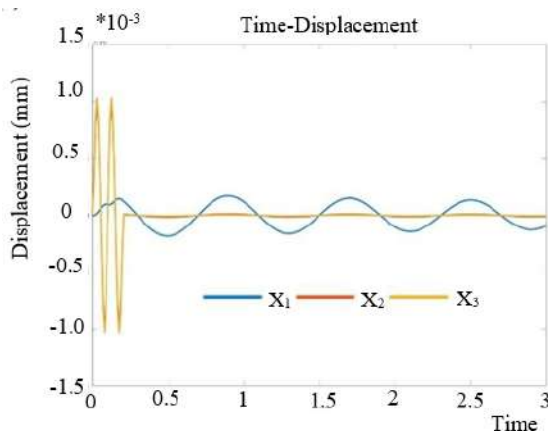

(a)

(b)

Figure 5- The amount of displacement of the structure when the force is applied to the lowest level of the floor - (A, the height of the structure is 3 meters - B, the height of the structure is 6 meters)

In summary, under low load operators, the displacement and velocity over time had a large change due to the reduction in stiffness, it is clear that while it can be in the process of changing the acceleration, it almost keeps the original shape. Reducing the stiffness also has an obvious effect on the stability of the structure.

3.3. Effects of reducing stiffness in the structure

At the top level of the frame structure, the force $F = 500 \sin(20* \pi * t)$ harmonic load, once at the top level of the frame structure and once at the bottom level of the frame structure and comparing the displacement of the structure according to the stiffness coefficient, in diagrams A of Figures 4 and 5 It is clear. The more rigid the structure is and the shorter the height, the more regular the height of the floors will be, compared to situations where the structure has more height and less stiffness. Once again, once at the top level of the frame structure and once at the bottom level of the frame structure, the comparison of the displacement of the structure according to the stiffness coefficient is clear in diagrams B of Figures 4 and 5. When the force is applied at the highest level, the more rigid the structure is, and the shorter its height (Figure A), the shorter the period compared to the case where the structure is less rigid and higher (Figure B) Meanwhile, the main mass is at the level of m1 and its value is zero at the levels of m2 and m3, and if the force is applied at the lower level, the value of the period is almost equal. Considering that the mass is in the m1 level and the m2 and m3 levels have no mass, the maximum displacement is in the m1 position when the force is in the upper level, and the maximum displacement is in the m2 and m3 level when the force is in the lower level.

4. Conclusion

- The NewMark-β method provides a new idea for seismography and the response of the steel frame structure is more practical for the analysis and analysis of the frame structures caused by harmonic load vibrations.
- Through the analysis of the built pattern of the steel frame structure, the range of changes of the elastic modulus is obtained, which can be provided as a basis for the value of the stiffness coefficient.
- The application of top load and bottom load have different structural responses to the steel frame structure, and the effect of the load on the structure is less favorable when it can act on the load at the bottom.

- The higher the height of the structure and the lower its stiffness, the displacement of the upper floor in the case where the force can be applied to the lowest level has a lower displacement than the case where the height of the structure is lower and its stiffness is higher.

References

[1] Bazaz, HamidReza Bolouri, Ali Akhtarpour, and Abbas Karamodin. "The influence of nailing on the seismic response of a superstructure with underground stories." Modern Applications of Geotechnical Engineering and Construction: Geotechnical Engineering and Construction. Springer Singapore, 2021.

[2] Chang, Jin-Hae. "Equibiaxially stretchable colorless and transparent polyimides for flexible display substrates." Reviews on Advanced Materials Science 59.1 (2020): 1-9. https://doi.org/10.1515/rams-2020-0003

[3] Bikçe, Murat, and Tahir Burak Çelik. "Failure analysis of newly constructed RC buildings designed according to 2007 Turkish Seismic Code during the October 23, 2011 Van earthquake." Engineering Failure Analysis 64 (2016): 67-84. https://doi.org/10.1016/j.engfailanal.2016.03.008

[4] Georgoussis, George K. "Modified seismic analysis of multistory asymmetric elastic buildings and suggestions for minimizing the rotational response." Earthquakes and Structures 7.1 (2014): 39-55. https://doi.org/10.12989/eas.2014.7.1.039

[5] Xiao, Jianzhuang, Thi Loan Pham, and Tao Ding. "Shake table test on seismic response of a precast frame with recycled aggregate concrete." Advances in Structural Engineering 18.9 (2015): 1517-1534. https://doi.org/10.1260/1369-4332.18.9.1517

[6] Liu, Yizhe, et al. "Dynamic analysis of multilayer-reinforced concrete frame structures based on NewMark-β method." Reviews on Advanced Materials Science 60.1 (2021): 567-577. https://doi.org/10.1515/rams-2021-0042

[7] Hu, Yusheng, et al. "Simultaneous enhancement of strength and ductility with nano dispersoids in nano and ultrafine grain metals: a brief review." Reviews on Advanced Materials Science 59.1 (2020): 352-360. https://doi.org/10.1515/rams-2020-0028

[8] Meng, Tao, et al. "Effect of nano-strengthening on the properties and microstructure of recycled concrete." Nanotechnology Reviews 9.1 (2020): 79-92. https://doi.org/10.1515/ntrev-2020-0008

[9] Alsalama, Manal M., et al. "Enhancement of thermoelectric properties of layered chalcogenide materials." Reviews on Advanced Materials Science 59.1 (2020): 371-378. https://doi.org/10.1515/rams-2020-0023

[10] Reiterman, Pavel, et al. "Freeze-thaw resistance of cement screed with various supplementary cementitious materials." Reviews on advanced materials science 58.1 (2019): 66-74. https://doi.org/10.1515/rams-2019-0006

[11] Ni, Haitao, et al. "Grain orientation induced softening in electrodeposited gradient nanostructured nickel during cold rolling deformation." Reviews on Advanced Materials Science 59.1 (2020): 144-150. https://doi.org/10.1515/rams-2020-0105

[12] ZHAN, Ting-bian, et al. "The equivalent constitutive relationship for reinforced concrete based on tension-stiffening." Transactions of Beijing institute of Technology 37.9 (2017): 881-887. https://doi.org/10.15918/j.tbit1001-0645.2017.09.001

[13] Vecchio, Frank. "The response of reinforced concrete to in-plane shear and normal stresses." Publication 82 (1982). https://doi.org/10.3130/aijs.62.89_2

[14] Xin-pu, S. H. E. N., W. A. N. G. Chen-yuan, and Zhou Lin. "A damage plastic constitutive model for reinforced concrete and its engineering application." 工程力学 24.9 (2007): 122-128.

[15] Zhang, Wei, Hegao Wu, and Kai Su. "Review for application of ABAQUS in nonlinear FEM analysis of mass reinforced concrete." Shuili Fadian Xuebao(Journal of Hydroelectric Engineering) 24.5 (2005): 70-74.

[16] Zhan, Ting Bian, et al. "Elastoplastic model with damage for reinforced concrete." Zhongbei Daxue Xuebao (Ziran Kexue Ban)/Journal of North University of China (Natural Science Edition) 38.3 (2017): 380-390.

[17] Desai, C. S., S. Somasundaram, and Gv Frantziskonis. "A hierarchical approach for constitutive modelling of geologic materials." International Journal for Numerical and Analytical Methods in Geomechanics 10.3 (1986): 225-257. https://doi.org/10.1002/nag.1610100302

[18] Desai, Chandrakant S. Mechanics of materials and interfaces: The disturbed state concept. CRC press, 2000. https://doi.org/10.1201/9781420041910

[19] Sun, Yafei, et al. "Study of the mechanical-electrical-magnetic properties and the microstructure of three-layered cement-based absorbing boards." Reviews on Advanced Materials Science 59.1 (2020): 160-169. https://doi.org/10.1515/rams-2020-0014

[20] Hou, Ling, Ren-qing Zhu, and Quan Wang. "The two-dimensional study of the interaction between liquid loshing and elastic structures." Journal of marine science and application 9.2 (2010): 192-199.

[21] Dong, Yao-Rong, et al. "Experimental study on viscoelastic dampers for structural seismic response control using a user-programmable hybrid simulation platform." Engineering Structures 216 (2020): 110710. https://doi.org/10.1016/j.engstruct.2020.110710

[22] Shi, Weixing, et al. "Experimental and numerical study on adaptive-passive variable mass tuned mass damper." Journal of Sound and Vibration 452 (2019): 97-111. https://doi.org/10.1016/j.jsv.2019.04.008

[23] Bayock, Francois Njock, et al. "Experimental review of thermal analysis of dissimilar welds of High-Strength Steel." Reviews on Advanced Materials Science 58.1 (2019): 38-49. https://doi.org/10.1515/rams-2019-0004

[24] Liu, Y., et al. "The application of elastic second-order method with considering stiffness reduction to two-span bent structure." Journal of Chongqing University 40.9 (2017): 1-7.

[25] ACI Committee, 318. "Building code requirements for structural concrete (ACI 318-08) and commentary." American Concrete Institute, 2008.

[26] Pei, Junjie, and Guangxiu Fang. "Experimental Study on Mechanical Properties of New Recycled Concrete Composite Beams." IOP Conference Series: Earth and Environmental Science. Vol. 330. No. 2. IOP Publishing, 2019. https://doi.org/10.1088/1755-1315/330/2/022107

[27] Nie, Jian-guo, and Yu-hang Wang. "Comparison study of constitutive model of concrete in ABAQUS for static analysis of structures." 工程力学 30.4 (2013): 59-67. https://doi.org/10.6052/j.issn.1000-4750.2011.07.0420

[28] Liu, Y., et al. "Discussion of the stiffness reduction factor of bent-columns." Journal of Chongqing University 4 (2007): 61-66.

[29] Gao, Song, et al. "Preparation and piezoresistivity of carbon nanotube-coated sand reinforced cement mortar." Nanotechnology Reviews 9.1 (2020): 1445-1455. https://doi.org/10.1515/ntrev-2020-0112

[30] Vamvatsikos, Dimitrios, and C. Allin Cornell. "Direct estimation of seismic demand and capacity of multidegree-of-freedom systems through incremental dynamic analysis of single degree of freedom approximation." Journal of Structural Engineering 131.4 (2005):

589-599. https://doi.org/10.1061/(ASCE)0733-9445(2005)131:4(589)

[31] Babaei, Mehdi, et al. "New methods for dynamic analysis of structural systems under earthquake loads." Journal of Rehabilitation in Civil Engineering 10.3 (2022): 81-99.

J-Researchers

Shallow Foundations and Deep Foundations; Drilled Piers, Aggregate Piers and Stone Columns; Design Recommendations, Construction Considerations, and Performance

Hossein Alimohammadi, [iD] [a,*]

ª Terracon Consultants, Inc., Nashville, TN, USA 37217

ABSTRACT

This paper presents a comprehensive review of shallow foundations, floor slabs, and deep foundations, focusing on drilled piers, micropiles, aggregate piers, and stone columns. The study aims to consolidate definitions, design methodologies, and construction recommendations pertinent to these foundation types. Shallow foundations, including mat and spread footings, and floor slabs are reviewed with respect to their design considerations and construction techniques, emphasizing their role in efficiently supporting superstructures. Deep foundations such as drilled piers and micropiles are evaluated for their capacity to transfer loads to deeper, more stable layers of soil. The review includes discussions on their design principles, installation methods, and performance in different geotechnical contexts. Additionally, aggregate piers and stone columns are explored as ground improvement techniques, offering insights into their design parameters and construction practices to enhance soil bearing capacity and mitigate settlement issues. By synthesizing current literature and engineering practices, this review aims to provide engineers, researchers, and practitioners with a comprehensive resource for understanding the complexities of foundation design and construction. Key recommendations are offered to guide future research and practical applications in the field of geotechnical engineering.

1. Introduction: Shallow foundations definitions, design and construction recommendations

Shallow foundations, also known as footings, are a common type of foundation system used in construction. These foundations are employed where the bearing strata are close to the ground surface, and the loads imposed by the structure are relatively light. Shallow foundations are cost-effective and simpler to construct compared to deep foundations. The primary types of shallow foundations include strip footings, spread footings, mat or raft foundations, and combined footings. Each type has specific applications and design considerations. Shallow foundation systems are a vital component of construction, offering cost-effective and efficient solutions for a variety of structures. Understanding the different types of shallow

* Corresponding author. Tel.: +12254853307; e-mail: Hossein.Alimohammadi@terracon.com.

foundations, their applications, and key design and construction considerations is essential for ensuring their successful implementation. Continued research and development in geotechnical engineering will further enhance the performance and reliability of shallow foundations in future construction projects.

Strip footings are continuous strips of concrete that support walls. They are commonly used in residential construction and low-rise buildings where the load distribution is linear. Strip footings are advantageous in terms of ease of construction and cost-efficiency, especially in cohesive soils where differential settlement is less of a concern. Spread footings, also known as isolated footings, support individual columns or piers. They are typically square or rectangular and distribute the load over a larger area to prevent excessive settlement. This type of footing is suitable for structures with relatively uniform load distributions and can be designed to accommodate varying soil conditions. Mat or raft foundations consist of a large slab of concrete that supports multiple columns and walls. These foundations are used when soil conditions are poor, and the load needs to be distributed over a wide area to reduce settlement. Mat foundations are common in high-rise buildings and structures with heavy loads, as they provide stability and uniform settlement characteristics. Combined footings support more than one column and are used when columns are close to each other, making individual footings impractical. They are designed to balance the load distribution and are typically employed in scenarios where the spacing between columns is too small for isolated footings.

Shallow foundations are utilized in a wide range of construction projects. Their applications span residential buildings, commercial structures, and light industrial buildings. Shallow foundations are extensively used in residential construction due to their simplicity and cost-effectiveness. Strip footings and spread footings are common choices for supporting walls and individual columns in houses and low-rise apartments. In commercial buildings, such as office buildings and shopping centers, mat foundations are often used to support the higher loads and ensure uniform settlement. Combined footings may also be employed to optimize space and load distribution in tightly spaced column layouts. Light industrial buildings, which may have varying load requirements and soil conditions, benefit from the versatility of shallow foundations. Spread footings and mat foundations are commonly used to support machinery, storage areas, and structural components.

The design of shallow foundations involves several critical considerations to ensure stability, durability, and performance under load. Understanding soil properties is fundamental in the design of shallow foundations. Soil bearing capacity, compressibility, and permeability

influence the selection and design of the foundation type. Geotechnical investigations are essential to assess these properties and ensure the foundation can adequately support the imposed loads. Accurate load calculations are crucial for designing shallow foundations. The load includes the weight of the structure, live loads, and environmental loads such as wind and seismic forces. The foundation must be designed to distribute these loads evenly to prevent excessive settlement and potential failure. Settlement is a critical factor in the performance of shallow foundations. Differential settlement can cause structural damage and must be minimized. Design strategies, such as increasing the foundation area or using reinforced concrete, help control settlement and ensure long-term stability. Proper construction practices are essential to the success of shallow foundations. This includes ensuring accurate excavation, proper placement of reinforcement, and quality control of concrete. Adherence to design specifications and standards is crucial to avoid issues such as uneven settlement and structural failure.

The foundation settlement will depend upon the variations within the subsurface soil profile, the structural loading conditions, the embedment depth of the footings, the thickness of the compacted fill, and the quality of the earthwork operations. It should be noted that the sides of the excavation for spread footings must be nearly vertical, and the concrete should be placed neat against these vertical faces for the passive earth pressure value to be valid. If the loaded side is sloped or benched and then backfilled, the allowable passive pressure will be significantly reduced. It is recommended that the passive resistance in the upper 2 feet of the soil profile should be neglected. Lateral resistance due to friction at the base of the footing should be ignored where uplift also occurs. For bedrock-supported foundations, a probe hole for scratch testing of the bedrock should be performed by the contractor at the bottom of the footing for the Geotechnical Engineer's use. The hole should be a minimum of 2 inches in diameter and extend to a depth equal to at least two times the foundation width but not less than 6 feet. The contractor should provide safe entry for the inspection, including air monitoring. Use of passive earth pressures requires the sides of the excavation for the spread footing foundation to be nearly vertical and the concrete placed neat against these vertical faces or that the footing forms be removed and compacted structural fill be placed against the vertical footing face. Embedment is necessary to minimize the effects of frost and/or seasonal water content variations. For sloping ground, maintain depth below the lowest adjacent exterior grade within 5 horizontal feet of the structure. Differential settlements are noted for equivalent-loaded foundations and bearing elevation as measured over a span of 50 feet. For bedrock-supported foundations, a probe hole for scratch testing of the bedrock should be

installed by the contractor at the bottom of the footing for the Geotechnical Engineer's use. The hole should be a minimum of 2 inches in diameter and extend to a depth equal to at least two times the foundation width and not less than 6 feet. The contractor should provide safe entry for the inspection, including air monitoring.

Shallow foundations subjected to overturning loads should be proportioned such that the resultant eccentricity is maintained in the center third of the foundation (e.g., e < b/6, where b is the foundation width). This requirement is intended to keep the entire foundation area in compression during the extreme lateral/overturning load event. Foundation oversizing may be required to satisfy this condition. Uplift resistance of spread footings can be developed from the effective weight of the footing and the overlying soils with consideration to the IBC basic load combinations and recommendations illustrated in Table 1.

Table 1.

Uplift resistance of spread footings recommendations

Item	Description
Soil Moist Unit Weight	100 pcf
Soil Effective Unit Weight[1]	40 pcf
Soil weight included in uplift resistance	Soil included within the prism extending up from the top perimeter of the footing at an angle of 20 degrees from vertical to ground surface

1. Effective (or buoyant) unit weight should be used for soil above the foundation level and below a water level. The high groundwater level should be used in uplift design as applicable.

Similar construction consisting of bedrock-supported foundations has utilized rock anchors as a feasible and cost-effective option to resist uplift forces both in footings and crane pads. Prior to any rock anchor and foundation construction, the base of all foundation excavations should be essentially horizontal and free of water, soil, and loose or detached rocks before placing concrete. In addition, rock surfaces beneath foundations that are exposed after overburden removal and that are to be filled with lean concrete should be horizontal. Lateral and uplift loads can also be resisted using rock anchors. If foundations are designed with rock anchors, they should be installed in relatively intact bedrock with no clayey seams and weathered rock lenses. Intact bedrock for the purposes of this report is any rock that cannot be excavated with a large-size trackhoe or other heavy-duty excavator having REC/RQD values at least 90/75 or better. Rock anchors should extend into competent bedrock to provide ample resisting forces for upward movements and to obtain adequate bond length with the grout and rock, and grout and anchor rod. Uplift capacity of individual rock anchors should be calculated based on the weight of a cone of rock as shown in the adjacent diagram. Additional resistance will be provided by the friction across the fractures, which

can be taken as an angle (ϕ) equal to 45 degrees. The apex of the cone should be placed from 0 to 1/4 of the way up from the bottom tip, depending on the anchor type. It is recommended that a unit weight (γ) of 150 pounds per cubic foot (pcf) be used for intact bedrock. An allowable bond strength of 200 pounds per square inch (psi) should be adequate for the limestone-grout interface when 3,000 psi strength grout is used. A factor of safety of 2.0 has been used for calculating the allowable grout-rock bond strength. Bond strength between the grout and anchor will be dependent on the anchor type and grout strength. It is recommended that the structural engineer and/or rock anchor designers determine rock anchor embedment to address potential failure modes (i.e., rock mass, grout/rock, and grout/rebar), but will require additional input from the design team. Based on the weathered and fractured condition of the anticipated bearing rock, it is recommended that a cone failure test setup be applied to the proof test as illustrated in Figure 1.
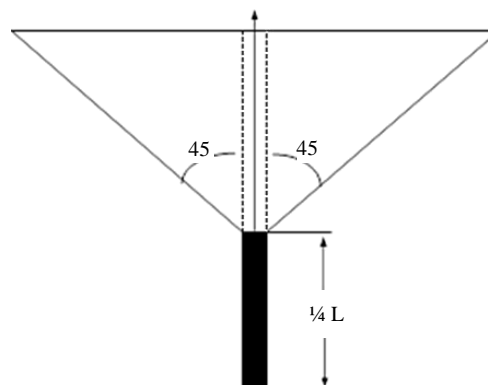
Figure 1. The cone failure test

When developing the appropriate tests and verification methods for construction, designers and contractors should review both FHWA-IF-99-015 and ASTM D3689-07 (Reapproved 2013) for testing apparatuses, setups, and loading guidelines. Given the REC and RQD values of the bedrock, it is suggested that only the bond of the anchor to the bedrock requires testing, not the bedrock failure cone. At a minimum, a proof load test should be conducted on each anchor installed. For proof testing, the anchor is initially loaded with a seating load of 10 percent of the design load. Subsequently, the anchor is stressed in increments of 25 percent of the design load with elongation measurements recorded at each increment. Proof loading is applied in sequential increments in one cycle and is generally carried to 125 percent of the design load. A reasonable period of time is allowed between load increments so that the anchor elongation has stabilized before starting the next load increment. The maximum proof load is held for a period of between 5 minutes and one hour. In no case should an anchor be loaded to more

than 80 percent of the ultimate tensile capacity of the steel tendon.

Uplift resistance of spread footings can be developed from the effective weight of the footing and the overlying soils. As illustrated in Figure 2, the effective weight of the soil prism defined by diagonal planes extending up from the top of the perimeter of the foundation to the ground surface at an angle, θ, of 20 degrees from the vertical can be included in uplift resistance. The maximum allowable uplift capacity should be taken as the sum of the effective weight of soil plus the dead weight of the foundation, divided by an appropriate factor of safety. A maximum total unit weight of 100 pcf should be used for the backfill. This unit weight should be reduced to 40 pcf for portions of the backfill or natural soils below the groundwater elevation.
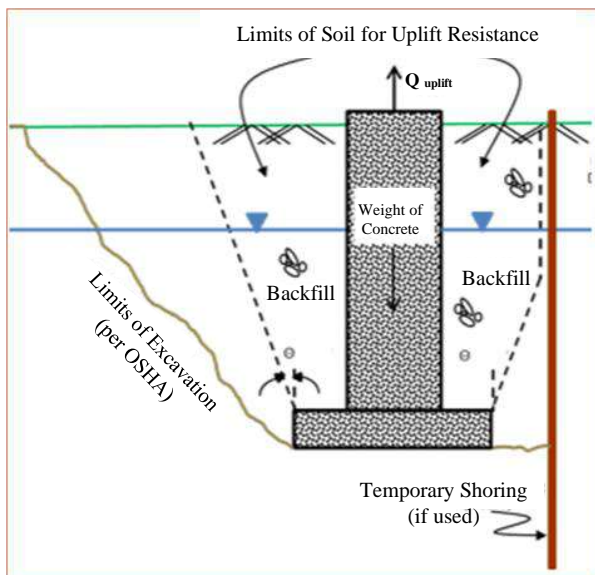
Figure 2. The diagonal planes extending up from the top of the perimeter of the foundation to the ground surface

To ensure the successful implementation of shallow foundations, the following construction recommendations should be considered: Proper site preparation is vital. This includes clearing the site of debris, ensuring a level base, and compacting the soil to the required density. Any unsuitable soil should be removed and replaced with appropriate fill material. Excavation must be carried out according to design specifications. The depth and dimensions of the excavation should match the foundation plans. Shoring or bracing may be necessary in loose or unstable soils to prevent collapse during excavation. Placing reinforcement accurately is essential for the structural integrity of the foundation. Reinforcement should be positioned according to the design drawings, with proper spacing and cover to protect against corrosion and ensure load transfer. The quality of concrete and proper curing practices significantly impact the foundation's

performance. Concrete should be mixed to the specified strength and poured without interruptions. Adequate curing methods, such as keeping the concrete moist, are necessary to achieve the desired strength and durability. Implementing a robust quality control process ensures that the foundation construction meets the design standards. Regular inspections, material testing, and adherence to construction protocols help identify and rectify issues promptly.

The footing excavations should be evaluated under the observation of the Geotechnical Engineer. The base of all foundation excavations should be free of water and loose soil/rock prior to placing concrete. Concrete should be placed soon after excavating to reduce bearing soil disturbance. Care should be taken to prevent wetting or drying of the bearing materials during construction. Excessively wet or dry material or any loose/disturbed material in the bottom of the footing excavations should be removed or reconditioned before foundation concrete is placed.

If the expected cuts for the lowest level of the structure and where the site's perimeter and cuts transition will likely result in some foundations bearing on weathered bedrock or other softer-than-rock materials, then this will result in different bearing materials over a short distance. Experience indicates that this condition could result in differential settlement and cracking within masonry walls where the material transition occurs or between ancillary and main structure foundations. To minimize this condition, it is recommended that where weathered or unsuitable bedrock is exposed in isolated areas, overexcavate the bedrock to competent bedrock and backfill with lean concrete, or bear the entire wall length between expansion joints on similar materials, either rock or suitable structural fills.

Since it is impractical to determine exactly where this condition will occur within the structures, adjustments will have to be performed in the field under the direction of the geotechnical engineer. A liberal number of expansion joints should be incorporated into the structure design to accommodate differential movement.

If unsuitable bearing soils are observed at the base of the planned footing excavation, the excavation should be extended deeper to suitable soils, and the footings could bear directly on these soils at the lower level or on lean concrete backfill placed in the excavations. The lean concrete replacement zone is illustrated in the sketch in Figure 3.

Overexcavation for structural fill placement below footings should be conducted as shown below. The overexcavation should be backfilled up to the footing base elevation, with well graded aggregates placed. Experience has indicated that rock formations which can be penetrated with geotechnical drill flight augers can sometimes be

excavated using heavy-duty construction equipment such as large backhoes with rock teeth or ripper-equipped dozers. Excavation in rock formations which cannot be penetrated with geotechnical drill flight augers is usually much more difficult and often requires the use of other techniques such as pneumatic breakers or blasting. The contractors should anticipate and plan that excavations will extend into bedrock. Rippability of the bedrock will vary, and the use of jackhammers and other rock excavation equipment and/or methods is anticipated to be required to reach the anticipated excavation depths. Furthermore, if blasting methods are used that may disturb the bedrock below the desired depth, then any loosened bedrock pieces should be recompacted as outlined for "shot rock" fill, or removed and replaced with suitable engineered fill or lean concrete. Heaved or dislodged fragments of bedrock should not remain in place as they pose a risk for unpredictable settlement and potential void collapse.

2. Floor slab definitions, design and construction recommendations

Floor slabs are crucial structural elements in building construction, serving as horizontal platforms that transfer loads to supporting structures. They are primarily categorized into solid, hollow-core, ribbed, and waffle slabs. Solid slabs are often employed in residential and commercial buildings due to their simplicity and ease of construction. Hollow-core slabs, characterized by longitudinal voids, are used in multi-story buildings for their efficiency in material usage and weight reduction. Applications of floor slabs extend to various structures, including residential, commercial, and industrial buildings, each demanding specific design considerations. In high-rise buildings, post-tensioned slabs are preferred for their enhanced load-bearing capacity and reduced deflection. In industrial settings, reinforced concrete slabs are chosen for their durability and ability to withstand heavy loads.
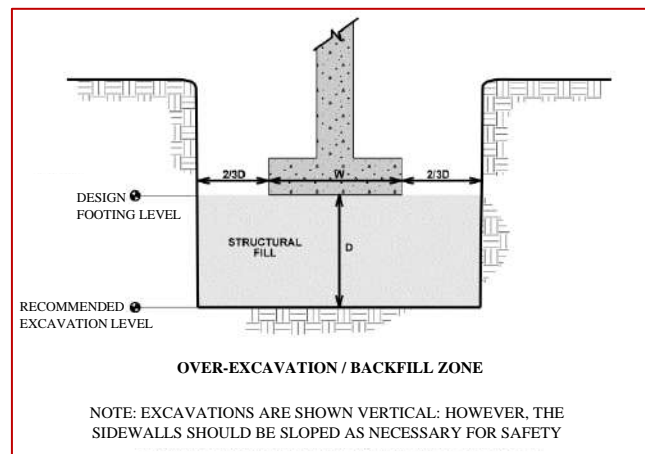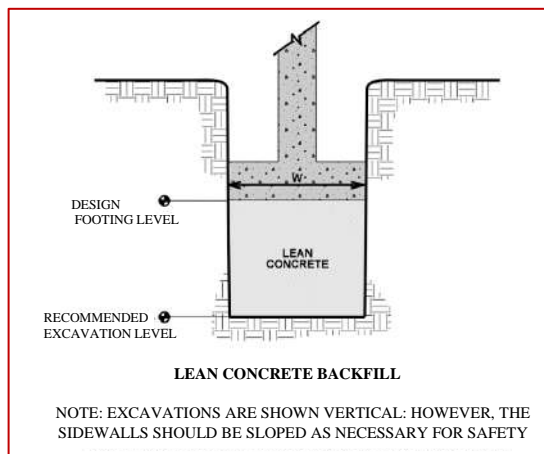
(a)   (b)

Figure 3. a) and b) Overexcavation for structural fill placement

Table 2.

Floor slab design parameters

Item	Description
Floor Slab Support [1]	Minimum 6 inches of free-draining (less than 5% passing the U.S. No. 200 sieve) crushed aggregate compacted to at least 95% of ASTM D 698 or #57 stone [2, 3]
Estimated Modulus of Subgrade Reaction [2]	100 pounds per square inch per inch (psi/in) for point loads

1. Floor slabs should be structurally independent of building footings or walls to reduce the possibility of floor slab cracking caused by differential movements between the slab and foundation.

2. Modulus of subgrade reaction is an estimated value based upon our experience with the subgrade condition, and the floor slab support as noted in this table. It is provided for point loads. For large area loads the modulus of subgrade reaction would be lower.

3. Free-draining granular material should have less than 5% fines (material passing the No. 200 sieve). Other design considerations such as cold temperatures and condensation development could warrant more extensive design provisions.

Design recommendations emphasize the importance of load calculations, material selection, and adherence to building codes. Modern design approaches incorporate finite element analysis (FEA) to accurately predict slab behavior under various loading conditions. Construction recommendations stress proper curing, reinforcement placement, and quality control to ensure structural integrity and longevity. Design parameters for floor slabs are provided in Table 2. Specific attention should be given to positive drainage away from the structures and the positive drainage of the aggregate base beneath the floor slab.

Advancements in construction technologies, such as precast and prefabricated slabs, have streamlined the construction process, reducing time and labor costs. Sustainable practices, including the use of recycled materials and energy-efficient designs, are increasingly integrated into floor slab construction, aligning with global trends toward environmentally responsible building practices.

The use of a vapor retarder should be considered beneath concrete slabs on grade covered with wood, tile, carpet, or other moisture-sensitive or impervious coverings, or when the slab will support equipment sensitive to moisture. When conditions warrant the use of a vapor retarder, the slab designer should refer to ACI 302 and/or ACI 360 for procedures and cautions regarding the use and placement of a vapor retarder.

Saw-cut control joints should be placed in the slab to help control the location and extent of cracking. For additional recommendations, refer to the ACI Design Manual. Joints or cracks should be sealed with a waterproof, non-extruding compressible compound specifically recommended for heavy-duty concrete pavement and wet environments.

Where floor slabs are tied to perimeter walls or turn-down slabs to meet structural or other construction objectives, our experience indicates differential movement between the walls and slabs will likely be observed in adjacent slab expansion joints or floor slab cracks beyond the length of the structural dowels. The Structural Engineer should account for potential differential settlement through the use of sufficient control joints, appropriate reinforcing, or other means. In addition to the mitigation measures, the floor slab can be stiffened by adding steel reinforcement, grade beams, and/or post-tensioned elements.

Regarding floor slab construction considerations, finished subgrade within and for at least 10 feet beyond the floor slabs should be protected from traffic, rutting, or other disturbances and maintained in a relatively moist condition until floor slabs are constructed. If the subgrade becomes damaged or desiccated before the construction of floor slabs, the affected material should be removed, and structural fill should be added to replace the resulting excavation. Final conditioning of the finished subgrade should be performed immediately before the placement of the floor slab support course.

The Geotechnical Engineer should approve the condition of the floor slab subgrades immediately before the placement of the floor slab support course, reinforcing steel, and concrete. Attention should be paid to high-traffic areas that were rutted and disturbed earlier, and to areas where backfilled trenches are located.

Before the construction of grade-supported slabs, varying levels of remediation may be required to reestablish stable subgrades within slab areas due to construction traffic, rainfall, disturbance, desiccation, etc. As a minimum, confirm that interior trench backfill placed beneath slabs is compacted in accordance with recommendations outlined in this report. All floor slab subgrade areas should be moisture-conditioned and properly compacted to the recommendations in this report immediately before the placement of the stone base and concrete.

3. Deep foundation including drilled piers and micropiles, aggregate piers and stone columns definitions, design and construction recommendations

Deep foundation systems are integral components in constructing structures where surface soils cannot support the load. This review covers three primary types of deep foundations: drilled piers and micropiles, aggregate piers, and stone columns. These systems offer various applications, advantages, and construction methods tailored to specific geotechnical conditions.

As an alternative to a shallow foundation support system, buildings should be supported on a deep foundation system (drilled piers or micropiles) extending to intact bedrock. When the building location is finalized and footing locations are precisely staked in the field by the surveyor, considerations should be given to perform air track probings at each footing location before construction. This will confirm the depth to intact bedrock, finalize pier or pile locations and depths, and ensure all piers or piles are embedded within intact bedrock below any voids and/or thick clayey seams encountered in borings. Additional borings are recommended to confirm boring data and the preliminary foundation recommendations outlined herein when the building location, structural loadings, and grading configuration are available.

The allowable skin friction and passive resistances have a factor of safety of about 2. To mobilize the rock strength parameters, the piers or piles should be socketed at least 3 feet into intact bedrock below any voids or thick clayey seams. Furthermore, it is assumed that the rock socket is developed using coring rather than blasting techniques. The upper 2 feet of clay should be ignored due to the

potential effects of frost action and construction disturbance. To avoid a reduction in lateral and uplift resistance caused by variable subsurface conditions, it is recommended that drawings instruct the contractor to notify the engineer if subsurface conditions significantly different from those encountered in our borings are disclosed during drilled pier installation. Under these circumstances, it may be necessary to adjust the overall length of the piers. To facilitate pier length adjustments that may be necessary because of variable soil and rock conditions, it is recommended that a Geotech engineer representative observe the drilled pier excavations.

A drilled pier foundation should be designed with a minimum shaft diameter of 30 inches to facilitate cleanout, inspection, and possible dewatering of the pier excavation. Temporary casing will be required during the pier excavation to control possible groundwater seepage and support the sides of the excavation in weak soil or weathered rock zones. Care should be taken so that the sides and bottom of the excavations are not disturbed during construction. The bottom of the shaft should be free of soil or loose rocks before reinforcing steel and concrete placement.

A concrete slump of at least 6 inches is recommended to facilitate temporary casing removal. It should be possible to remove the casing from a pier excavation during concrete placement provided that the concrete inside the casing is maintained at a sufficient level to resist any earth and hydrostatic pressures outside the casing during the entire casing removal procedure. It is strongly recommended that the contract for pier excavations or micropile drilling be based on a total linear footage of soil and rock excavation calculated using probable bearing levels. Add or deduct unit prices for pier excavations or micropile drilling should be applied to greater or lesser amounts of total drilling per pier or pile rather than calculated on an individual pier or pile basis.

When shafts are used in groups, the lateral capacities of the shafts in the second, third, and subsequent rows of the group should be reduced compared to the capacity of a single, independent shaft. Guidance for applying p-multiplier factors to the p values in the p-y curves for each row of pier foundations within a pier group is illustrated in figure 4.

Where the Front row will be Pm is 0.8; Second row; Pm is 0.4, Third and subsequent row and Pm is 0.3. For a single row of shafts supporting a laterally loaded grade beam, group action for lateral resistance of shafts should be considered when spacing is less than three shaft diameters (measured center-to-center). However, spacing closer than 3D (where D is the diameter of the shaft) is not recommended, due to the potential for the installation of a new shaft disturbing an adjacent installed shaft, likely resulting in axial capacity reduction.
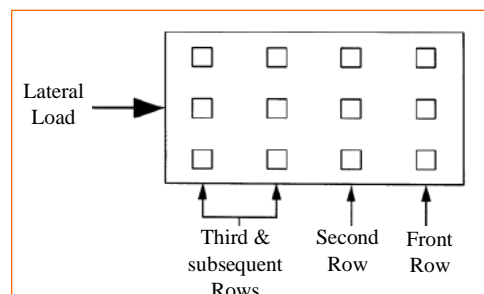
Figure 4. shafts used in groups

Where the Front row will be Pm is 0.8; Second row; Pm is 0.4,Third and subsequent row and Pm is 0.3. For a single row of shafts supporting a laterally loaded grade beam, group action for lateral resistance of shafts should be considered when spacing is less than three shaft diameters (measured center-to-center). However, spacing closer than 3D (where D is the diameter of the shaft) is not recommended, due to the potential for the installation of a new shaft disturbing an adjacent installed shaft, likely resulting in axial capacity reduction.

Regarding drilled shaft construction considerations, to prevent the collapse of the sidewalls and/or to control groundwater seepage, the use of temporary steel casing and/or slurry drilling procedures may be required for constructing the drilled shaft foundations. The drilled shaft installation process should be performed under the direction of the Geotechnical Engineer. The Geotechnical Engineer should document the shaft installation process, including soil/rock and groundwater conditions encountered, consistency with expected conditions, and details of the installed shaft. A concrete slump of at least 6 inches is recommended to facilitate temporary casing removal. It should be possible to remove the casing from a pier excavation during concrete placement provided that the concrete inside the casing is maintained at a sufficient level to resist any earth and hydrostatic pressures outside the casing during the entire casing removal procedure. Care should be taken not to disturb the sides and bottom of the excavation during construction. The bottom of the shaft excavation should be free of loose material before concrete placement. Concrete should be placed as soon as possible after the foundation excavation is completed to reduce potential disturbance of the bearing surface.

Aggregate piers, also known as vibro stone columns or vibro-replacement, are used to improve the load-bearing capacity of weak soils. They are particularly effective in granular soils and have been widely used in constructing embankments, industrial structures, and residential buildings (Mitchell & Huber, 2014). The design of aggregate piers involves determining the optimal spacing, diameter, and depth of the piers to achieve the desired soil improvement. The installation process increases the

density and strength of the surrounding soil, leading to improved load distribution and reduced settlement (Greenwood, 2004). Design methodologies often rely on empirical data and field testing to validate assumptions. Construction of aggregate piers involves drilling a hole into the ground, followed by the introduction of aggregate material. The aggregate is then compacted using a vibrating probe, which helps to densify the soil and form a stiff column. This process may be repeated in lifts to ensure thorough compaction and soil improvement (Kempfert & Gebreselassie, 2006).

Based on our evaluation of the soil conditions encountered at the site and our experience on other similar projects, it is believed that aggregate piers (stone columns) offer an economical alternative to undercut/replacement and deep foundation options. To provide initial guidance, it is recommended that the structural engineer consult with one or more specialty contractors for further details. Additional information can be found in the U.S. Department of Transportation Federal Highway Administration, Publication No. FHWA-SA-98-086, Demonstration Project 116. General comments concerning this approach are provided in the subsequent paragraphs.

Aggregate piers are constructed by drilling a hole, removing a volume of soil, and then building a bottom bulb of clean, well-graded crushed aggregate while vertically pre-stressing and pre-straining subsoils underlying the bottom bulb. The aggregate pier shaft is built on top of the bottom bulb, using open-graded base course stone placed in thin lifts. The rammed aggregate pier elements are a proprietary subgrade reinforcing system and should be designed and constructed by an installer licensed by the ground improvement foundation company. The design parameters should be verified by a full-scale modulus test (similar to a pile load test) performed in the field. The Geotechnical Consultant should be retained to monitor the modulus test and subsequent production rammed aggregate pier installations.

The installer should provide detailed design calculations sealed by a professional engineer licensed in the State of Tennessee. The design calculations should demonstrate that the ground improvement method is estimated to control long-term settlements to less than 1-inch total and ½-inch differential, or a more stringent requirement if determined by the structural engineer. After the implementation of the above-mentioned ground improvement program and planned grading as discussed herein, the proposed building could be designed to rest on shallow footings overlying stone column modified subgrade. Shallow footings may be preliminarily designed for an allowable bearing pressure of 5,000 psf. This value should be confirmed by the stone column contractor/designer. The stone column specialty contractor should coordinate ground modification work including

spacing of stone columns with the structural engineer to achieve the required bearing pressure and facilitate the spacing of control joints in the structure. Considering the apparent karst activity at the site, considerations should be given to the use of cement-treated aggregate for stone column construction to minimize surface water migration into the ground and mitigate karst risk.

The proposed building columns and walls could be designed to rest on shallow foundations after subgrade remediation via stone columns as discussed herein. Based on our evaluation of the soil conditions encountered and our experience with other similar projects, it is believed that stone columns offer an economical alternative to deep foundations. Ground improvement options may include aggregate piers using vibro-replacement techniques or rammed aggregate piers extending to suitable natural subgrade. It is recommended that this report and the appendices be provided to the ground improvement contractors/designers for pricing and subsequent design.

Stone columns are similar to aggregate piers but are typically used in cohesive soils to reduce settlement and increase load-bearing capacity. They are effective in improving ground conditions for a variety of structures, including roadways, railways, and industrial facilities (Baumann & Bauer, 1974). The design of stone columns involves assessing soil conditions and load requirements to determine the appropriate column spacing, diameter, and depth. Stone columns increase the shear strength of the soil and accelerate consolidation by providing drainage paths for pore water (Priebe, 1995). Design approaches often incorporate both analytical methods and field testing to ensure accuracy.

Stone columns are constructed using a vibratory probe to displace soil and introduce coarse aggregate material. The probe compacts the aggregate as it is inserted, forming a column that enhances the strength and stiffness of the surrounding soil. This method is particularly effective in reducing liquefaction potential in seismic regions (Barksdale & Bachus, 1983). When selecting and designing deep foundation systems, engineers must consider a variety of factors, including soil conditions, load requirements, environmental impact, and cost. Proper site investigation and soil testing are crucial for determining the most suitable foundation type and design parameters. Advanced modeling techniques and field testing can enhance the reliability and performance of these systems (Das, 2010). Quality control during construction is vital for the successful implementation of deep foundations. This includes monitoring drilling and installation processes, ensuring the correct placement of materials, and conducting post-construction testing to verify performance. Techniques such as load testing, cross-hole sonic logging, and pile integrity testing are commonly used

to assess the quality of installed foundations (FHWA, 2006).

Conventional stone columns are constructed using a vibro-replacement or vibro-displacement method. A similar approach, consisting of rammed aggregate piers or Geopier® elements, involves removing a volume of soil and then building a bottom bulb of clean stone or aggregate. The Geopier shaft is built on top of the bottom bulb, using well-graded highway base course stone placed in thin lifts (12-inches compacted thickness). The lifts are compacted by a repeated ramming action that also stresses the soil laterally. Our preliminary design consideration indicates the rammed aggregate pier elements will be capable of supporting a net allowable bearing pressure of 5,000 psf. The recommended allowable bearing pressure is the pressure in excess of the minimum surrounding overburden pressure at the footing base elevation. This bearing pressure should be considered preliminary and should be confirmed by a stone column specialty contractor. An allowable passive resistance of 750 psf will be appropriate below the upper 2 feet of the soil profile. Passive resistance in the upper 2 feet of the soil profile should be neglected.

Current design methods are relatively empirical and based on field evaluations of a select number of projects. The foundation systems are proprietary and would be designed and installed by a specialty contractor. The installer should provide detailed design calculations sealed by a professional engineer licensed in the State of Tennessee. It is also recommended that specialty contractors should be contacted and given an opportunity to perform settlement analyses and confirm that settlements will be within the client's tolerable limits. The design calculations should demonstrate that stone column soil reinforcement will control long-term settlements to desired tolerable levels. The geotechnical engineer should be retained to monitor the field instrumentation and a contractor-executed load test program to evaluate the performance of the stone column design.

Drilled piers, also known as drilled shafts or caissons, are cylindrical foundation elements that transfer building loads to deeper, more stable soil or rock layers. They are typically used in large-scale infrastructure projects such as bridges, high-rise buildings, and industrial facilities where high load-bearing capacity and stability are required (Brown et al., 2010). The design of drilled piers involves careful consideration of soil properties, load requirements, and environmental factors. Key design parameters include the diameter and depth of the pier, the type of reinforcing steel used, and the concrete mix. Load-bearing capacity is typically determined through a combination of soil testing and empirical formulas (O'Neill & Reese, 1999). Construction of drilled piers involves drilling a cylindrical hole into the ground, placing a steel reinforcement cage,

and then filling the hole with concrete. The use of temporary casing or drilling fluid may be necessary to support the excavation and prevent collapse in unstable soils (Reese & Van Impe, 2001). Quality control is critical during construction to ensure the integrity and performance of the piers.

Recent advancements in deep foundation technology include the use of high-performance materials, automated installation techniques, and improved monitoring systems. Innovations such as self-compacting concrete, real-time monitoring of installation parameters, and the integration of geotechnical data into building information modeling (BIM) are enhancing the efficiency and reliability of deep foundation systems (Ng et al., 2018).

4. Conclusions

In conclusion, this review paper has comprehensively explored various types of foundations crucial to civil engineering practice: shallow foundations, floor slabs, and deep foundations such as drilled piers, micropiles, aggregate piers, and stone columns. By examining definitions, design methodologies, and construction recommendations for each type, this study has highlighted their respective advantages, challenges, and suitable applications in diverse geotechnical contexts. Shallow foundations, including isolated footings and raft foundations, remain fundamental for structures where soil bearing capacity is sufficient near the surface. They offer cost-effective solutions for buildings and structures with moderate loads. Floor slabs, essential for residential and industrial constructions, require careful consideration of load distribution and material properties to ensure long-term performance and durability. Conversely, deep foundations like drilled piers, micropiles, aggregate piers, and stone columns are indispensable for transferring heavy structural loads to deeper, more competent soil or rock layers. Their design intricacies involve geotechnical analysis, structural compatibility, and construction techniques tailored to specific ground conditions. By synthesizing current knowledge and practices, this review contributes valuable insights into the complex interplay between foundation types, design principles, and construction methodologies. It underscores the importance of informed decision-making in selecting and implementing appropriate foundation systems to ensure the safety, stability, and longevity of civil engineering projects in varying environmental and geological settings. Future research should continue to refine and innovate these foundational technologies in response to evolving engineering challenges and sustainability imperatives.

Acknowledgments

Conflict of interest

The authors declare that they have no conflict of interest.

References

[1] Brauns, J. "Initial bearing capacity of stone columns and sand piles." Int. Symp. on Soil Reinforcing and Stabilizing Techniques in Engineering Practice. Vol. 1. 1978.

[2] Yahiaoui, Asma, Saida Dorbani, and Lilya Yahiaoui. "Machine learning techniques to predict the fundamental period of infilled reinforced concrete frame buildings." Structures. Vol. 54. Elsevier, 2023. https://doi.org/10.1016/j.istruc.2023.05.052

[3] Black, Jonathon, Vinayagamoothy Sivakumar, and J. D. McKinley. "Performance of clay samples reinforced with vertical granular columns." Canadian geotechnical journal 44.1 (2007): 89-95. https://doi.org/10.1139/t06-081

[4] Abu-Farsakh, M. Y., Hossein Alimohammadi, and Louay N. Mohammad. "Finite element analysis to evaluate the benefits of geosynthetic reinforcement in flexible pavements over weak subgrade for low volume traffic roads." Geosynth Int (2020). https://annualmeeting.mytrb.org/OnlineProgramArchive/Details/12 333

[5] Alimohammadi, Hossein, and Behrooz Izadi Babokani. "Finite element electrodynamics modeling of a layered piezoelectric composite shell with different materials by using numerical software." ISSS Journal of Micro and Smart Systems 9.1 (2020): 79-88. https://doi.org/10.1007/s41683-020-00052-3

[6] Alimohammadi, Hossein. "A framework for evaluation of existing pavement conditions and selection of feasible maintenance/rehabilitation alternatives; a case study in some routes of Livingston Parish in the state of Louisiana." SN Applied Sciences 2.2 (2020): 289. https://doi.org/10.1007/s42452-020-1999-6

[7] Zheng, Guangfan, et al. "Effectiveness of geosynthetics in the construction of roadways: a full-scale field studies review." IFCEE 2021 (2021): 223-232. https://doi.org/10.1061/9780784483411.022

[8] Alimohammadi, Hossein, et al. "Performance evaluation of geosynthetic reinforced flexible pavement: a review of full-scale field studies." International Journal of Pavement Research and Technology 14 (2021): 30-42. https://doi.org/10.1007/s42947-020-0019-y

[9] Alimohammadi, Hossein. Effectiveness of Geogrids in Roadway Construction: Determine a Granular Equivalent (GE) Factor. Diss. Iowa State University, 2021.

[10] Alimohammadi, Hossein, et al. "Field and simulated rutting behavior of hot mix and warm mix asphalt overlays." Construction and Building Materials 265 (2020): 120366. https://doi.org/10.1016/j.conbuildmat.2020.120366

[11] Baumann, V., and G. E. A. Bauer. "The performance of foundations on various soils stabilized by the vibro-compaction method." Canadian Geotechnical Journal 11.4 (1974): 509-530. https://doi.org/10.1139/t74-056

[12] Alimohammadi, Hossein, and Jamal Tahat. "A case study experimental pile load testing (PLT) for evaluation of driven pile behaviors." Arabian Journal of Geosciences 15.9 (2022): 884. https://doi.org/10.1007/s12517-022-10176-5

[13] Alimohammadi, Hossein, and Jamal N. Tahat. "A case study pile load testing (PLT) to evaluate driven pile behaviors." Indian Geotechnical Journal 52.4 (2022): 959-968. https://doi.org/10.1007/s40098-022-00613-3

[14] Alimohammadi, Hossein, Mohsen Amirmojahedi, and Jamal N. Tahat. "A case history of application of deep compaction method with comparison to different ground improvement techniques." Transportation Infrastructure Geotechnology 10.4 (2023): 543-568. https://doi.org/10.1007/s40515-022-00229-3

[15] Satvati, S., et al. "Evaluation the Effects of Geosynthetic Reinforcement on Bearing Capacity of Shallow Foundations in Soil Slopes." 101st Transp. Res. Board Annu. Meet (2022). https://annualmeeting.mytrb.org/OnlineProgram/Details/17240

[16] Alimohammdi, Hossein, et al. Effectiveness of Geotextiles/Geogrids in Roadway Construction; Determine a Granular Equivalent (GE) Factor. No. MN 2021-26. Minnesota. Department of Transportation, 2021. https://www.dot.state.mn.us/research/reports/2021/202126.pdf

[17] Alimohammadi, Hossein. "A State-of-the-art Large-scale Laboratory Approach to Evaluating the Effectiveness of Geogrid Reinforcement in Flexible Pavements." (2021).

[18] Alimohammadi, Hossein, et al. "Finite element viscoelastic simulations of rutting behavior of hot mix and warm mix asphalt overlay on flexible pavements." International Journal of Pavement Research and Technology 14 (2021): 708-719. https://doi.org/10.1007/s42947-020-0057-5

[19] Alimohammadi, Hossein, et al. "Rutting performance evaluation of hot mix asphalt and warm mix asphalt mixtures by using dynamic modulus, hamburg wheel tracking tests, and viscoelastic finite element simulations." International Conference on Transportation and Development 2020. Reston, VA: American Society of Civil Engineers, 2020. https://doi.org/10.1061/9780784483183.009

[20] Zheng, Junxing, Hantao He, and Hossein Alimohammadi. "Three-dimensional Wadell roundness for particle angularity characterization of granular soils." Acta Geotechnica 16 (2021): 133-149. https://doi.org/10.1007/s11440-020-01004-9

[21] Alimohammadi, Hossein, Keyvan Yashmi Dastjerdi, and Mohammadali Loftollahi Yaghin. "The study of progressive collapse in dual systems." Civil and Environmental Engineering 16.1 (2020): 79-85. https://doi.org/10.2478/cee-2020-0009

[22] Alimohammadi, H., et al. "Performance Evaluation of Hot Mix and Warm Mix Asphalt Overlay Layers Based on Field Measurements and Finite Element Viscoelastic Simulations." Transp. Res. Board Conf. 99th Annu. Meet. 2020. https://annualmeeting.mytrb.org/OnlineProgramArchive/Details/13 743

[23] Alimohammadi, Hossein, Amin Hesaminejad, and M. Lotfollahi Yaghin. "Effects of different parameters on inelastic buckling behavior of composite concrete-filled steel tubes." Int. Res. J. Eng. Technol 6.12 (2019): 603-608.

[24] Alimohammadi, Hossein, Mostafa Dalvi Esfahani, and Mohammadali Lotfollahi Yaghin. "Effects of openings on the seismic behavior and performance level of concrete shear walls." International Journal of Engineering and Applied Sciences 6.10 (2019): 34-39.

[25] Alimohammadi, Hossein, and B. Izadi Babokani. "Finite element analysis of a Piezoelectric layered plate with different materials." Int. J. Eng. Appl. Sci 6.7 (2019).

[26] Alimohammadi, Hossein, and Mohammadali Lotfollahi Yaghin. "Study on the effect of the concentric brace and lightweight shear steel wall on seismic behavior of lightweight steel structures." STUD 203 (2019): 0-3.

[27] Alimohammadi, Hossein, and Murad Abu-Farsakh. Finite element parametric study on rutting performance of geosynthetic reinforced flexible pavements. No. 19-05396. 2019. https://trid.trb.org/View/1572248

[28] Alimohammadi, Hossein, and Ashfaq A. Memon. "Case Study of Mechanically Stabilized Earth (MSE) Retaining Wall Failure in the State of Tennessee; Recommendations for Future Design and Constructions." Journal of Civil Engineering Researchers 5.1 (2023): 52-65. https://doi.org/10.61186/JCER.5.1.52

[29] Alimohammadi, H., et al. "A full-scale field approach for evaluating the geogrid reinforcement effectiveness in flexible pavement." 22nd Int. Conf. Soil Mech. Geotech. Eng. 2022.

[30] Alimohammadi, H., and J. Tahat. "A State-of-The-Art Evaluation of Driven Pile Behaviors Using Pile Load Testing (PLT)." 101st Transp. Res. Board Annu. Meet (2022).

[31] Alimohammadi, Hossein. Effectiveness of Geogrids in Roadway Construction: Determine a Granular Equivalent (GE) Factor. Diss. Iowa State University, 2021.

[32] Alimohammadi, Hossein. Rutting behavior of laboratory, field, and finite element simulated hot mix and warm mix asphalt overlays. MS thesis. Iowa State University, 2021.

[33] Alimohammadi, H., and M. Abu-Farsakh. "Evaluating Geosynthetic Reinforcement Benefits of Flexible Pavement." 8th Annual Graduate Student Research Conference. 2019.

[34] H. Alimohammadi and A. Memon "Failure Analysis and Recommendations For Improving Mechanically Stabilized Earth (MSE) Retaining Wall Design and Construction: A Case Study from Tennessee, USA" Transportation Research Board 103rd Annual Meeting, TRBAM-24-00338, 2024.

[35] Alimohammadi, Hossein, and Ashfaq A. Memon. "A Case Study of Failure Analysis of an MSE Retaining Wall in Tennessee: Lessons Learned and Recommendations for Reconstruction." (2023).

[36] Alimohammadi, Hossein, and Ashfaq A. Memon. "Forensic Investigation of Slope Stability Issues and Design Practices: A Case Study in Nashville, Tennessee." (2023).

[37] H. Alimohammadi and J. Tahat "Evaluation of Driven Pile Using Pile Load Testing: A Case Study in the State of Ohio" Geo-Congress 2024 conference, 2024.

[38] H. Alimohammadi and J. Tahat "Evaluating Driven Pile Behaviors Through Case Study Experimental Pile Load Testing (PLT)" 48th Annual Conference on Deep Foundations, 2023

[39] Satvati, Sajjad, et al. "Bearing capacity of shallow footings reinforced with braid and geogrid adjacent to soil slope." International Journal of Geosynthetics and Ground Engineering 6 (2020): 1-12. https://doi.org/10.1007/s40891-020-00226-x

[40] Alimohammadi, H., et al. "Evaluating the Rutting Performance of Hot Mix Asphalt and Warm Mix Asphalt Mixtures by Using Viscoelastic Finite Element Simulations." Int. Conf. Transp. Dev. 2020. https://doi.org/10.1061/9780784483183.009

[41] Alimohammadi, Hossein, et al. "Evaluation of geogrid reinforcement of flexible pavement performance: A review of large-scale laboratory studies." Transportation Geotechnics 27 (2021): 100471. https://doi.org/10.1016/j.trgeo.2020.100471

[42] Alimohammadi, Hossein, and Behrooz Izadi Babokani. "Finite element electrodynamics modeling of a layered piezoelectric composite shell with different materials by using numerical software." ISSS Journal of Micro and Smart Systems 9.1 (2020): 79-88. https://doi.org/10.1007/s41683-020-00052-3

[43] H. Alimohammadi, M. D. Esfahani, "Investigating the Opening Effect of Constant Cross-Section and Various Forms of Seismic Behavior and Performance levels in Concrete Shear Walls" First international conference on civil engineering architecture and stable urban development, 2015.

[44] H. Alimohammadi, and M. Lotfollahi Yaghin "Evaluation of seismic properties of light weight concentric brace on seismic behavior of light weight steel structures" National Conference in applied civil engineering and new advances, 2014.

[45] H. Alimohammadi, and M. Lotfollahi Yaghin "Evaluation of seismic properties of lightweight steel frames coated with lightweight steel shear wall" First international conference on urban development based on new technologies and 4th national conference on urban development, 2014

[46] Alimohammadi, Hossein, and Ashfaq Memon. "Comprehensive Sinkhole Mitigation: A Case Study and Application of Compaction Grouting in Karstic Environments in in the State of Tennessee, USA." Journal of Civil Engineering Researchers 6.2 (2024): 1-16. https://doi.org/10.61186/JCER.6.2.1

[47] Alimohammadi, Hossein, and Ashfaq A. Memon. "Mitigation of A Sinkhole in Nashville, Tennessee: A Case Study with Compaction Grouting Approach."

[48] H. Alimohammadi and A. Memon "Failure Analysis and Recommendations For Improving Mechanically Stabilized Earth (MSE) Retaining Wall Design and Construction : A Case Study from Tennessee, USA" Transportation Research Board 103rd Annual Meeting, 2024

[49] Alimohammadi, Hossein, and Ashfaq A. Memon. "Case Study of Mechanically Stabilized Earth (MSE) Retaining Wall Failure in the State of Tennessee; Recommendations for Future Design and Constructions." Journal of Civil Engineering Researchers 5.1 (2023): 52-65. https://doi.org/10.61186/JCER.5.1.52

[50] Ambily, A. P., and Shailesh R. Gandhi. "Behavior of stone columns based on experimental and FEM analysis." Journal of geotechnical and geoenvironmental engineering 133.4 (2007): 405-415. https://doi.org/10.1061/(ASCE)1090-0241(2007)133:4(405)

[51] Andreou, Panagiotis, et al. "Experimental study on sand and gravel columns in clay." Proceedings of the Institution of Civil Engineers-Ground Improvement 161.4 (2008): 189-198. https://doi.org/10.1680/grim.2008.161.4.189

[52] Barksdale, Richard D., Robert Charles Bachus, and R. D. Barksdale. Design and construction of stone columns. US Department of Transportation, Federal Highway Administration, 1983.

Examination of the Value of Domestic Component Levels and the Weight of Company Benefits in High-Rise Building Projects

Talitha Nursyifa Octavia, [ID][a] I Nyoman Dita Pahang Putra, [ID][a,*]

[a] *Departement of Civil Engineering, Universitas Pembangunan Nasional "Veteran" Jawa Timur, Indonesia*

ABSTRACT

In a construction project, various project management activities assist in achieving project goals in planning, procurement, implementation, and control. In the construction sector, the Ministry of Public Works and Public Housing (PUPR) has mandated that at least 30-85% of products used should be domestic, as measured by the Domestic Component Level (TKDN), and the maximum value for the Company Benefit Weight (BMP) should be 15%. When combined, the TKDN and BMP values should be at least 40%. This regulation aims to reduce product imports and boost the purchase of domestic products, which can significantly improve the national economy if consistently implemented. This study employs a quantitative analysis method using data such as material specifications, material/tool prices, worker wages, Work Unit Price Analysis (AHSP), and Cost Budget Plans (RAB). The calculation shows that the total value for the project is 81.85%, comprising 73.381% for TKDN and 8.43% for BMP. Therefore, it can be confirmed that the construction project of ITS Tower 2 Building in Surabaya complies with the Presidential Regulation of the Republic of Indonesia Number 12 of 2021 mandates meeting the minimum threshold of 40%.

1. Introduction

A construction project involves undertaking tasks to transform an initial concept into a tangible structure or infrastructure. To achieve the project's objectives, various resources are utilized, including labor, construction machinery, both permanent and temporary materials, supplies and facilities, financial resources, technology or methods, and time [1]. The phases of a construction project encompass planning, procurement, execution, and monitoring, which together form an interconnected framework known as project management [2]. The presence of project management in construction projects aids in accurately and efficiently determining project costs, quality, and execution time [3]. Moreover, in the book "Construction Project Management," Clough et al. state that construction management goes beyond merely overseeing the construction and managing a company; it involves coordinating all the components within it [4].

In project management, particularly in Indonesia, specific elements serve as a guideline for incorporating

---

* Corresponding author. Tel.: +628123260260; e-mail: putra_indp.ts@upnjatim.ac.id.

domestic products into construction projects, including both goods and services [5]. Utilizing domestic products is anticipated to decrease the need for importing goods or services, as the current use of local products in the construction industry remains quite limited [6]. The current situation shows that many foreign products and investments entering developing countries are subject to a policy known as Local Content Requirements (LCR), which is designed to safeguard the domestic industry [7]. In Indonesia, the policy can be assessed in terms of value by determining the Domestic Component Level (TKDN), as outlined in Presidential Regulation Number 12 of 2021 concerning Government Procurement of Goods/Services article 66, clause 2 specifies that the requirement to use domestic products applies to goods and services where the TKDN value, combined with the minimum Company Benefit Weight (BMP), must be at least 40% [8]. Among the two assessment indicators, each has a specified minimum value. For the TKDN value, it must adhere to the decision outlined in Ministry of Public Works and Public Housing Regulation No. 602/KPTS/M/2023, which sets the minimum TKDN value for construction services in the Cipta Karya sector at 30-85% [9]. For the BMP value, the guidelines outlined in the Regulation of the Minister of Industry of the Republic of Indonesia Number 30/M-IND/PER/6/2006 specify that the maximum allowable Company Benefit Weight (BMP) is 15%. This BMP value is based on four indicators, including aspects such as business empowerment [10].

To support the calculation of TKDN values, it is essential to use secondary data, such as technical specifications, to minimize unnecessary waste and avoid rework caused by material standard failures and irregular work. This helps prevent confusion between contract creators, unit prices of materials, and wages. The Work Unit Price Analysis (AHSP) is employed to accurately forecast construction costs by summing the unit prices of materials, tools, and labor. Additionally, The Cost Budget Plan (RAB) serves as a guideline for financial planning and management, aiding in decision-making, performance monitoring, and work schedule oversight [11-13].

Therefore, to enhance the use of domestic products in Indonesia, it is hoped that this will foster national pride, enable the production of goods with quality on par with international standards, and achieve competitive pricing compared to foreign products [14]. In this endeavor, it is anticipated that The government will take a primary role in advancing and disseminating information about the use of Domestic Products (PDN) [15]

2. Research Objectives

To determine the TKDN value and assess the BMP value for the Tower 2 Building Construction project at Institut Teknologi Sepuluh Nopember Surabaya, the focus will be on the main building structure work, ranging from the foundation to the roof floor, excluding architectural work and Mechanical, Electrical, and Plumbing (MEP) systems

3. Data Analysis

The data analysis section outlines the steps the author will undertake in this study after acquiring both primary and secondary data from the implementing contractor, PT. Wijaya Karya (Persero) Tbk. The following describes the process for analyzing the data:

a.   Identify the Domestic Component Level (TKDN) Value on each Component

Identify the TKDN value for each component, including materials, work tools, and labor for specific tasks. To determine these values, consult the official website provided by the Ministry of Industry of the Republic of Indonesia at https://tkdn.kemenperin.go.id/. If certain items are not listed on the site, assume their TKDN value is 0%. Additionally, analyze the Work Unit Price (HSP) to assess its impact on TKDN costs.

b.   Analyzing the Price of Work Units (HSP) as a Determinant of TKDN Costs

Work Unit Price Analysis (HSP) is needed in the data calculation process; to find out the unit price of each job based on TKDN, the first step is to determine the amount of price of materials, tools, and labor obtained from the multiplication between the unit price and the coefficient. The second step, after the price amount is obtained, then enter the TKDN value of each item from material components, tools, and labor. For the final step, Additionally, multiply the price of each item by its TKDN value to determine the unit price of the work according to TKDN standards. After that, the sum of each price according to the contract and the amount of price based on the TKDN value is carried out.

c.   Recapitulation of TKDN Values in Structural Work

The process of recapitulating the TKDN value in structural work requires Cost Budget Plan (RAB) data as a reference for work sub-items in determining the amount of price according to the contract and the amount of price based on the TKDN value and the number of TKDN value weights. The sub-items of structural work to be reviewed consist of:

- Earthworks
- Foundation work
- 1st to 11th floor work

- Roofing floor work
- Staircase structure work from the 1st floor to the roof floor

d. Identification of the Value of Company Benefit Weights (BMP) in Construction Services

Under the Minister of Industry of the Republic of Indonesia Number 16 of 2011, Company Benefit Weight (BMP) is awarded to companies based on several criteria. This involves providing support to micro and small businesses, including small cooperatives, through partnerships, as well as emphasizing occupational health & safety and environmental management certificates; promoting environmental sustainability; and providing after-sales service facilities.

e. Calculation of the Company's Benefit Weight Value (BMP)

The calculation of the BMP value also adheres to the Regulation issued by the Minister of Industry of the Republic of Indonesia Number 16 of 2011. BMP is computed by multiplying the accumulated weight of the determining factors by the maximum weight, with the total value not exceeding 15%.

f. Results of Combining TKDN Values with BMP

In the final step, the TKDN and BMP values will be combined to determine the extent to which domestic products are utilized in construction services

4. Result and Discussion

4.1. Determination of the Domestic Component Level (TKDN) Value

Under Government Regulation of the Republic of Indonesia No. 29 of 2018, Article 61 Paragraphs 1 and 2, domestic products (DN) must have a minimum TKDN value of 25%. To calculate the Domestic Component Level (TKDN), it is essential to consider project resources, including materials, tools, and labor.

a. *Calculation of Domestic Component Level (TKDN) of Materials*

To calculate the TKDN value for materials, the initial step is to identify the materials used in the structural work of the ITS Tower 2 Construction project in Surabaya, based on the project's technical specifications. These specifications also provide information about the brands used, which helps determine the TKDN value listed on the official website of the Ministry of Industry of the Republic of Indonesia, https://tkdn.kemenperin.go.id/ .

Table 1.

Calculation Example of Domestic Component Level (TKDN) of Materials

Materials	Brand	TKDN (%)
Meranti Formwork Wood	local	100,00%
Dolken Wood, 8-10 cm	local	100,00%
12 mm thick plywood (Phenolic Film)	Source of Graha Sejahtera	82,53%
Semen PC 40 Kg	Semen Gresik	84,41%
Spun pile with a diameter of 60 cm and K-600 grade	Wika Beton	71,47%
Spun pile with a diameter of 30 cm and K-600 grade	Wika Beton	71,47%
Sand Tide	Local	100,00%
Ready Mix Concrete K-400	Merak Jaya	94,20%
Ready Mix Concrete K-350		94,20%

Table 2.

Calculation Example of Domestic Component Level (TKDN) of Work Tools

Work Tools	Made (LN/DN)	Owned (LN/DN)	TKDN (%)	Unit
Rent a stress pile tool	LN	DN	75%	H
3-ton forklift rental - min. 8 hours	LN	DN	75%	H
Crane rental 30 tons - min. 8 hours	LN	DN	75%	H
Hydraulic piling rental - min. 8 hours (including mob/de)	LN	DN	75%	H
Concrete pump rental - min. 3 hours	LN	DN	75%	H
Welding equipment rental	LN	DN	75%	H
Compressor rental	LN	DN	75%	H
Welding set rental (min. 5 hours, etc.)	LN	DN	75%	H
Cost a dump truck 5-ton	LN	DN	75%	D

An example of this calculation is illustrated in Table 1.

Table 1 shows that the materials used have a variable TKDN value, including a spun pile with a diameter of 60 cm K-600 with the brand Wijaya Karya Beton, which has a TKDN value of 71.47%. Meanwhile, meranti formwork wood has a TKDN value of 100% because the material comes from nature.

b. *Calculation of Domestic Component Level (TKDN) of Work Tools*

The calculation of the TKDN value for work tools is explained through various categories as detailed in the Regulation issued by the Minister of Industry of the Republic of Indonesia Number 16 of 2011. Specifically:

- Tools manufactured in Indonesia (DN) and owned by DN companies are valued at 100% TKDN.
- Tools produced in Indonesia (DN) but owned by foreign (LN) companies are assigned a TKDN value of 75%.
- For tools made in Indonesia (DN) and owned by joint ventures between foreign (LN) and domestic (DN) companies, the TKDN value is 75% plus (25% multiplied by the percentage of DN ownership).
- Tools made abroad (LN) and owned by domestic (DN) companies have a TKDN value of 75%.
- Tools manufactured abroad (LN) and owned by foreign (LN) companies are valued at 0% TKDN.

Table 2 shows that nearly all the tools used in the work are imported but owned by domestic companies, giving them a TKDN value of 75 percent. However, some tools are manufactured domestically and held by domestic companies, resulting in a TKDN value of 100%.

c. *Calculation of Domestic Component Level (TKDN) of Labor*

When calculating the TKDN value for labor, it is evaluated according to their nationalities. In line with the Regulation issued by the Minister of Industry of the Republic of Indonesia Number 16 of 2011, Indonesian workers are assigned a TKDN value of 100%, while foreign workers are given a value of 0%. An example of this calculation is provided in Table 3.

Table 3.

Calculation Example of Domestic Component Level (TKDN) of Labor

Labor	Citizenship (WNI/WNA)	TKDN (%)
Mandor	WNI	100%
Head masonry	WNI	100%
Blacksmith's head	WNI	100%
Blacksmith's head	WNI	100%
Chief painter	WNI	100%
Head Carpenter	WNI	100%

Table 4.

Calculation of Work Unit Price Analysis (AHSP) Based on Domestic Component Level (TKDN) Value

Description	Cow.	Sat.	Unit Price	Total Price (IDR)	TKDN Value (%)	Total KDN Price (IDR)
a	b	c	d	e = b x d	f	g = e x f
1m3 Concrete Work K - 175 (Ready Mix)						
Tenaga:						
Mandor	0,1000	Day	Rp 100.000	Rp 10.000	100,00%	Rp 10.000
Head Masonry	0,0250	Oh	Rp 90.000	Rp 2.250	100,00%	Rp 2.250
Masonry	0,2500	Oh	Rp 82.000	Rp 20.500	100,00%	Rp 20.500
Unskilled Worker / Laborer	1,0000	Oh	Rp 72.500	Rp 72.500	100,00%	Rp 72.500
			Sum:	Rp 105.250	Number of KDN:	Rp 105.250
Material:						
Ready Mix Concrete K-175	1,0200	m3	Rp 580.000	Rp 591.600	94,20%	Rp 557.287
			Sum:	Rp 591.600	Number of KDN:	Rp 557.287
Equipment:						
Rental of concrete pump – minimum 3 hours	0,1200	Hour	Rp 1.685.000	Rp 202.200	75,00%	Rp 151.650
			Sum:	Rp 202.200	Number of KDN:	Rp 151.650
			Total Price:	Rp 899.050	KDN Price:	Rp 814.187

Table 5.
Calculation Example of The Cost Budget Plan (RAB) Based on The Value of TKDN

No.	Work Items	Unit	Volume	Unit Price (IDR)	Total Price (IDR)	KDN Unit Price (IDR)	Total KDN Price (IDR)
a	b	c	d	e	f = d x e	g	h = d x g
II.3.	1st FLOOR						
1	Concrete Plate Ground Floor, fc' = 24.90 Mpa, tbl=15 cm						
	Working Floor Rebate fc'=14.53 Mpa, tbl=5 cm	m3	60,654	Rp 899.050	Rp 54.531.203	Rp 814.187	Rp 49.383.914
	Ready Mix Concrete fc' = 24.90 Mpa, K-300	m3	200,22	Rp 970.450	Rp 194.303.499	Rp 881.446	Rp 176.483.118
	Ready Mix Concrete fc' = 33.20 Mpa, K-400	m3	181,96	Rp 1.016.350	Rp 184.937.841	Rp 924.684	Rp 168.258.007
	Reinforcement	Kg	28684	Rp 12.958	Rp 371.697.531	Rp 6.148	Rp 176.345.650
2	Concrete Plate Ground floor, fc' = 24.90 Mpa, tbl=20 cm						
	Working Floor Rebate fc'=14.53 Mpa, tbl=5 cm	m3	16,398	Rp 899.050	Rp 14.742.397	Rp 814.187	Rp 13.350.838
	Ready Mix Concrete fc' = 24.90 Mpa, K-300	m3	52,77	Rp 970.450	Rp 51.210.647	Rp 881.446	Rp 46.513.905
	Ready Mix Concrete fc' = 33.20 Mpa, K-400	m3	65,591	Rp 1.016.350	Rp 66.663.413	Rp 924.684	Rp 60.650.935
	Reinforcement	Kg	6409,3	Rp 12.958	Rp 83.052.694	Rp 6.148	Rp 39.402.956
3	Concrete Plate Ramp Ground floor, fc' = 24.90 Mpa, tbl=10 cm						
	Brick collage pair	m2	11,16	Rp 117.661	Rp 1.313.091	Rp 117.661	Rp 1.313.091
	Sand	m3	4,3952	Rp 263.182	Rp 1.156.738	Rp 240.432	Rp 1.056.747
	Ready Mix Concrete fc' = 24.90 Mpa, K-300	m3	-	Rp 970.450	Rp -	Rp 881.446	Rp -
	Ready Mix Concrete fc' = 33.20 Mpa, K-400	m3	8,7904	Rp 1.016.350	Rp 8.934.123	Rp 924.684	Rp 8.128.340
	Reinforcement	Kg	1282,9	Rp 12.958	Rp 16.624.141	Rp 6.148	Rp 7.887.044
	Bekisting plat	m2	87,904	Rp 455.022	Rp 39.998.254	Rp 438.699	Rp 38.563.367
3	Concrete Elevator Wall, fc' = 33.20 Mpa, tbl=15 cm						
	Ready Mix Concrete fc' = 33.20 Mpa, K-400	m3	16,472	Rp 1.016.350	Rp 16.740.809	Rp 924.684	Rp 15.230.929
	Reinforcement	Kg	4057,5	Rp 12.958	Rp 52.577.455	Rp 6.148	Rp 24.944.490
	Formwork dining	m2	219,62	Rp 716.656	Rp 157.391.991	Rp 637.307	Rp 139.965.330

Continued on the next page

Table 5.
Calculation Example of The Cost Budget Plan (RAB) Based on The Value of TKDN

No.	Work Items	Unit	Volume	Unit Price (IDR)	Total Price (IDR)	KDN Unit Price (IDR)	Total KDN Price (IDR)
4	Reinforced Concrete Wall (Shearwall), fc' = 33.20 Mpa, tbl=25 cm						
	Ready Mix Concrete fc' = 33.20 Mpa, K-400	m3	49,345	Rp 1.016.350	Rp 50.151.791	Rp 924.684	Rp 45.628.522
	Reinforcement	Kg	7387,6	Rp 12.958	Rp 95.729.875	Rp 6.148	Rp 45.417.431
	Formwork dining	m2	394,76	Rp 716.656	Rp 282.907.123	Rp 637.307	Rp 251.583.251
5	Concrete Columns						
-	K1 90x150 cm						
	Ready Mix Concrete fc' = 33.20 Mpa, K-400	m3	129,09	Rp 1.016.350	Rp 131.197.572	Rp 924.684	Rp 119.364.658
	Reinforcement	Kg	33020	Rp 12.958	Rp 427.873.602	Rp 6.148	Rp 202.997.443
	Column formwork	m2	458,98	Rp 553.723	Rp 254.145.415	Rp 537.399	Rp 246.653.393
-	K2 80x110 cm						
	Ready Mix Concrete fc' = 33.20 Mpa, K-400	m3	36,062	Rp 1.016.350	Rp 36.652.020	Rp 924.684	Rp 33.346.317
	Reinforcement	Kg	11892	Rp 12.958	Rp 154.093.764	Rp 6.148	Rp 73.107.198
	Column formwork	m2	155,72	Rp 553.723	Rp 86.227.909	Rp 537.399	Rp 83.685.973
-	K3 70x90 cm						
	Ready Mix Concrete with a compressive strength of 33.20 MPa, K-400	m3	43,029	Rp 1.016.350	Rp 43.732.524	Rp 924.684	Rp 39.788.219
	Reinforcement	Kg	9970,5	Rp 12.958	Rp 129.199.866	Rp 6.148	Rp 61.296.706
	Column formwork	m2	218,56	Rp 553.723	Rp 121.021.626	Rp 537.399	Rp 117.453.997
-	K4 40x50 cm						
	Ready Mix Concrete with a compressive strength of 33.20 MPa, K-400	m3	25,184	Rp 1.016.350	Rp 25.595.758	Rp 924.684	Rp 23.287.237
	Reinforcement	Kg	7199,9	Rp 12.958	Rp 93.297.180	Rp 6.148	Rp 44.263.280
	Column formwork	m2	226,66	Rp 553.723	Rp 125.504.565	Rp 537.399	Rp 121.804.782
-	K5 50x50 cm						
	Ready Mix Concrete with a compressive strength of 33.20 MPa, K-400	m3	8,5375	Rp 1.016.350	Rp 8.677.088	Rp 924.684	Rp 7.894.488
	Reinforcement	Kg	2991,5	Rp 12.958	Rp 38.764.213	Rp 6.148	Rp 18.391.030
	Column formwork	m2	68,3	Rp 553.723	Rp 37.819.258	Rp 537.399	Rp 36.704.374
-	K6 70x40 cm						

Table 5.
Calculation Example of The Cost Budget Plan (RAB) Based on The Value of TKDN

No.	Work Items	Unit	Volume	Unit Price (IDR)		Total Price (IDR)		KDN Unit Price (IDR)		Total KDN Price (IDR)	
	Ready Mix Concrete with a compressive strength of 33.20 MPa, K-400	m3	15,299	Rp	1.016.350	Rp	15.549.342	Rp	924.684	Rp	14.146.922
	Reinforcement	Kg	6870,2	Rp	12.958	Rp	89.024.556	Rp	6.148	Rp	42.236.205
	Column formwork	m2	120,21	Rp	553.723	Rp	66.561.894	Rp	537.399	Rp	64.599.698
6	Concrete Blocks										
-	Balok Separator 20x30 cm										
	Ready Mix Concrete with a compressive strength of 24.90 MPa, K-300	m3	1,44	Rp	970.450	Rp	1.397.448	Rp	881.446	Rp	1.269.282
	Ready Mix Concrete with a compressive strength of 33.20 MPa, K-400	m3	2,28	Rp	1.016.350	Rp	2.317.278	Rp	924.684	Rp	2.108.279
	Reinforcement	Kg	413,61	Rp	12.958	Rp	5.359.679	Rp	6.148	Rp	2.542.810
	Beam formwork	m2	11,4	Rp	575.723	Rp	6.563.238	Rp	559.399	Rp	6.377.152
7	Steel Column										
	WF Frame 300.150.6,5.9	Kg	1378,7	Rp	30.851	Rp	42.532.749	Rp	14.602	Rp	20.130.750
	Iron Meni Painting	m2	45,12	Rp	34.431	Rp	1.553.513	Rp	25.398	Rp	1.145.952
	Full Plate, tbl=16mm	Kg	71,691	Rp	29.461	Rp	2.112.079	Rp	15.175	Rp	1.087.932
	Plat Rip/stiffener, tbl=10mm	Kg	114,43	Rp	29.461	Rp	3.371.203	Rp	20.238	Rp	2.315.788
	Exactly. armature Ø 16, length 40 cm	bh	32	Rp	69.890	Rp	2.236.480	Rp	46.435	Rp	1.485.917
8	Steel Beam										
	WF Frame 250.125.6.9	Kg	480,73	Rp	30.851	Rp	14.830.828	Rp	14.602	Rp	7.019.431
	Iron Meni Painting	m2	12,19	Rp	34.431	Rp	419.710	Rp	25.398	Rp	309.600
	Connector Plate, tbl=10mm	Kg	9,81	Rp	29.461	Rp	289.012	Rp	20.238	Rp	198.532
	Full Plate, tbl=16mm	Kg	5,65	Rp	29.461	Rp	166.455	Rp	15.175	Rp	85.741
	Plat Rip/stiffener, tbl=10mm	Kg	18,84	Rp	29.461	Rp	555.045	Rp	20.238	Rp	381.279
	Exactly. armature Ø 16, length 40 cm	Pcs	18	Rp	69.890	Rp	1.258.020	Rp	46.435	Rp	835.828
	Mur Builds Ø14	Pcs	24	Rp	17.710	Rp	425.040	Rp	11.465	Rp	275.171
9	Practical column 10x10 cm, fc'=14.53 Mpa	m1	215	Rp	75.268	Rp	16.182.586	Rp	51.707	Rp	11.117.080
10	Beam 10x15 cm, fc'=14.53 Mpa	m1	33,81	Rp	94.319	Rp	3.188.920	Rp	69.845	Rp	2.361.447
11	Concrete Table Plate 10cm thick										

Table 5.
Calculation Example of The Cost Budget Plan (RAB) Based on The Value of TKDN

No.	Work Items	Unit	Volume	Unit Price (IDR)	Total Price (IDR)	KDN Unit Price (IDR)	Total KDN Price (IDR)
	Ready Mix Concrete fc' = 14.53 Mpa, K-175	m3	0,17	Rp 899.050	Rp 152.839	Rp 814.187	Rp 138.412
	Reinforcement	Kg	17,78	Rp 12.958	Rp 230.396	Rp 6.148	Rp 109.307
	Plate formwork	m2	1,7	Rp 455.022	Rp 773.537	Rp 438.699	Rp 745.788
				Total Fee:	Rp3.735.518.823	KDN Fee:	Rp2.723.171.265

Table 3 shows that the workers in the ITS Tower 2 Building Construction project in Surabaya have a TKDN value of 100% because they have a workforce that is entirely Indonesian citizens or from within the country.

4.2. Analysis of Work Unit Pricing (AHSP) Based on the Domestic Component Level (TKDN) Value

In calculating the Work Unit Price Analysis (AHSP), It's important to take into account elements like materials, labor, and work tools. These components have unit prices determined by documents from the implementing contractor and are associated with the TKDN values outlined in the previous section. An example of this calculation is shown in Table 4.

4.3. Calculation of The Cost Budget Plan (RAB) Based on The Value of TKDN

The RAB calculation is conducted following the AHSP calculation. This process involves multiplying the unit price of each task by its corresponding volume. An example of the RAB calculation is provided in Table 5.

4.4. Calculation of the Cost Budget Plan (RAB) According to TKDN Values

The recapitulation is derived from summing the costs of each task related to the main building structure work, as detailed in Table 6.

Table 6.
Calculation of The Cost Budget Plan (RAB) Based on The Value of TKDN

NO	WORK ITEMS	TOTAL FEE (IDR)	TOTAL KDN FEE (IDR)	TKDN VALUE (%)
a	b	c	d	e = d/c
1	Earthworks	Rp 239.546.767	Rp 237.140.317	98,995%
2	Foundation Work	Rp 11.487.408.097	Rp 7.617.294.802	66,310%
3	Ground Floor	Rp 3.735.518.823	Rp 2.723.171.265	72,899%
4	Second Floor	Rp 4.377.157.389	Rp 3.243.016.213	74,090%
5	Third Floor	Rp 3.524.576.254	Rp 2.613.958.969	74,164%
6	Fourth Floor	Rp 3.309.922.404	Rp 2.445.818.446	73,894%
7	Fifth Floor	Rp 2.848.307.620	Rp 2.165.497.377	76,028%
8	Sixth Floor	Rp 2.857.104.151	Rp 2.171.370.045	75,999%
9	Seventh Floor	Rp 2.857.104.151	Rp 2.175.728.136	76,152%
10	Eighth Floor	Rp 2.857.104.151	Rp 2.175.728.136	76,152%
11	Ninth Floor	Rp 2.652.074.662	Rp 1.989.398.726	75,013%
12	Tenth Floor	Rp 2.699.124.290	Rp 2.026.258.456	75,071%

Table 6.
Calculation of The Cost Budget Plan (RAB) Based on The Value of TKDN

NO	WORK ITEMS	TOTAL FEE (IDR)	TOTAL KDN FEE (IDR)	TKDN VALUE (%)
13	Eleventh Floor	Rp 3.223.131.244	Rp 2.431.229.001	75,431%
14	Roofing Floor	Rp 4.344.676.876	Rp 3.422.288.158	78,770%
15	Str. Work. Stairs 1 To 2nd Floor	Rp 140.051.114	Rp 90.672.113	64,742%
16	Str. Work. Stairs 2nd To 3rd Floor	Rp 78.634.821	Rp 58.401.696	74,270%
17	Str. Work. Stairs From 3rd To 4th Floor	Rp 63.198.654	Rp 46.937.514	74,270%
18	Str. Work. Stairs 4th Floor To Fifth Floor	Rp 61.363.362	Rp 45.696.530	74,469%
19	Str. Work. 5th Floor To 6th Floor Stairs	Rp 61.363.362	Rp 45.696.530	74,469%
20	Str. Work. Stairs 6th Floor To 7th Floor	Rp 61.363.362	Rp 45.696.530	74,469%
21	Str. Work. 7th Floor To Eighth Floor Stairs	Rp 61.363.362	Rp 45.696.530	74,469%
22	Str. Work. Stairs From 8th Floor To 9th Floor	Rp 61.363.362	Rp 45.696.530	74,469%
23	Str. Work. Stairs 9th Floor To 10th Floor	Rp 61.363.362	Rp 45.696.530	74,469%
24	Str. Work. Stairs 10th Floor To 11th Floor	Rp 61.363.362	Rp 45.696.530	74,469%
25	Str. Work. Stairs To Roof 11	Rp 100.303.926	Rp 75.638.651	75,409%
	TOTAL	Rp 51.824.488.927	Rp 38.029.423.731	73,381%

Table 7.
Recapitulation of the Company's Benefit Weight Value (BMP)

No.	Types of Activities	Weight	BMP Value (%)
1	Empowerment of Small Businesses including Small Cooperatives through Partnerships	28,09%	4,21%
2	Certificate Ownership		
-	Occupational Health and Safety (SMK3/OHSAS 18000)	6%	3%
-	Environmental Management (ISO 14000)	14%	
3	Community Development	8,13%	1,22%
4.	After-sales Service Facilities	0%	0%
	TOTAL	56,22%	8,43%

The results of the calculation from Table 6 that the structural work of the main building of Tower 2 ITS Surabaya has a total construction cost of IDR 51,824,488,927 with a total cost based on the TKDN value

of IDR 38,029,423,731. Meanwhile, for the total construction cost and total cost based on the TKDN value, the percentage of TKDN value for the structure of the ITS Tower 2 Building Surabaya was 73.381%. The percentage of TKDN value is obtained from the following calculation:

% TKDN $\quad$ = (KDN Cost/Total Cost) x 100%
$\quad$ = (IDR 38,029,423,731 / IDR 51,824,488,927) x 100%
$\quad$ = 73,381%

4.5. Summary of the Company's Benefit Weight (BMP) Value

The outcomes of the company's contributions to Environmental Responsibility and Social Responsibility (CSR), based on data collected from interviews with relevant parties, are displayed in Table 7.

From the results of the recapitulation of the BMP value in Table 7, it can be concluded that the total weight obtained from the four factors is 56.22% and the total percentage of BMP value is 8.43% from the following calculations:

Total BMP value (%) = 56.22% x 15% = 8.43%

4.6. Results of the Percentage of TKDN Value and BMP Value in the ITS Tower 2 Building Construction Project Surabaya

In line with Presidential Regulation Number 12 of 2021 concerning Government Procurement of Goods/Services, Article 66, Clause 2 stipulates that the requirement to use domestic products includes goods and services with a Domestic Component Level (TKDN) value combined with a minimum Company Benefit Weight (BMP) value of 40%. For the main building structure of the ITS Tower 2 Construction project in Surabaya, the TKDN value is 73.381% and the BMP value is 8.43%. Thus, the total value, combining TKDN and BMP, is 81.85%. This result indicates that the structural work for the main building of the ITS Surabaya Tower 2 meets the established requirements.

5. Conclusions

Based on the research conducted on the ITS Surabaya Tower 2 Building Construction project, the following conclusions can be drawn:

a. The TKDN value for the main building structure work in the ITS Surabaya Tower 2 project is 73.381%.
b. The BMP value for the implementing contractor in this project is 8.43%.

c. Combining the TKDN value of 73.381% with the BMP value of 8.43% results in a total value of 81.85%.

References

[1] Sucita, I. Ketut, and Agung Budi Broto. "identifikasi dan penanganan risiko K3 pada proyek konstruksi gedung." Jurnal Poli-Teknologi 10.1 (2011). https://doi.org/https://doi.org/10.32722/pt.v10i1.433

[2] Siswanto, A. B., and Salim, M. A. Manajemen Proyek. Semarang, CV. Pilar Nusantara, 2019.

[3] Husen, A. Manajemen Proyek. Yogyakarta, CV. Andi Offset, 2009

[4] Clough, R. H., Sears, G. A., Sears, S. K. Construction Project Management. Hoboken, Jhon Wiley & Sons, Inc., 2000.

[5] Khakim, Dwi Lutfil, and I. Nyoman Dita Pahang Putra. "Analysis of Domestic Component Level (TKDN) and Company Benefit Weight (BMP) in Construction Projects." International Journal of Mechanical, Electrical and Civil Engineering 1.3 (2024): 23-37. https://doi.org/10.61132/ijmecie.v1i3.19

[6] Ningtyas, Diah Kurniawati, and I. Nyoman Dita Pahang Putra. "Analysis of the Calculation Value of Domestik Component Level (TKDN) on high-rise building projects." Jurnal VORTEKS 5.1 (2024): 341-348. https://doi.org/10.54123/vorteks.v5i1.347

[7] Puspitawati, Dewi Fitri. "Analisis Yuridis Kebijakan Tingkat Komponen Dalam Negeri (Tkdn) Dalam Bidang Farmasi Pada Perspektif Regulasi World Trade Organization (Wto)." JISIP (Jurnal Ilmu Sosial dan Pendidikan) 7.3 (2023): 2688-2694. https://doi.org/10.58258/jisip.v7i1.5403

[8] Presiden Republik Indonesia. Peraturan Presiden (Perpres) Nomor 12 Tahun 2021 tentang Perubahan atas Peraturan Presiden Nomor 16 Tahun 2018 tentang Pengadaan Barang/Jasa Pemerintah, 2021 Retrived from https://peraturan.bpk.go.id/Details/161828/perpres-no-12-tahun-2021

[9] Menteri Pekerjaan Umum dan Perumahan Rakyat. Keputusan Kementrian Pekerjaan Umum dan Pekerjaan Perumahan Rakyat No. 602/KPTS/M/2023 tentang Batas Minimum Nilai Tingkat Komponen Dalam Negeri Jasa Konstruksi, 2023 Retrieved from https://bp2jksulsel.info/assets/front/foto_pengumuman/35cf030e5ba9ceda4ba5a7d91cbb9363.pdf

[10] [10] Menteri Perindustrian Republik Indonesia. Peraturan Menteri Perindustrian Republik Indonesia Nomor 30/M-IND/PER/6/2006 Tahun 2006 tentang Pedoman Penggunaan Produksi Dalam Negeri, 2006 Retrieved from https://www.mkri.id/index.php?page=web.PeraturanPIH&id=6&pages=84&menu=6&status=1

[11] Lam, Patrick TI, Mohan M. Kumaraswamy, and S. Thomas Ng. "The use of construction specifications in Singapore." Construction Management and Economics 22.10 (2004): 1067-1079. https://doi.org/https://doi.org/10.1080/0144619042000213265

[12] Kalbuadi, Fakhri, and Bambang Endro Yuwono. "STUDY OF WORK UNIT PRICE PERMEN PUPR NUMBER 28 OF 2016 WITH PERMEN PUPR NUMBER 1 YEAR 2022 IN JU 1 RIVER EXCAVATION WORK." ADI Journal on Recent Innovation 5.1 (2023): 93-99. https://doi.org/10.34306/ajri.v5i1.991

[13] Sihombing, Denny Jean Cross. "Development of construction project cost budget application using rapid application development method." Jurnal Mantik 7.3 (2023): 1685-1696. https://doi.org/10.35335/mantik.v7i3.4207

[14] Zulmawan, W. "Efektivitas Aturan Penggunaan Produk dalam Negeri pada Pengadaan Barang/Jasa Pemerintah." Unes Law Review, 6.1 (2023), 2152-2167. https://doi.org/10.31933/unesrev.v6i1

[15] Purwanto, Edy Dwi, Harsoyo Harsoyo, and Aris Toening Winarni. "Analisis Implementasi Peningkatan Penggunaan Produk Dalam Negeri (P3DN) Pada Sektor Kesehatan Dalam E-Procurement Secara E-Catalog Guna Mendorong Utilisasi Produk Dalam Negeri Dan Mewujudkan Indonesia Yang Mandiri." Jurnal Media Administrasi 6.2 (2021): 56-80. https://doi.org/10.56444/jma.v6i2.472

Evaluation of the Impact of Driving Techniques on the Subsoil Stability of Bridge E2 in Manta, Ecuador

Mohammadfarid Alvansazyazdi, [ID] [a,b,c*] Jhonny Patricio Flores Jarrin, [ID] [c] Marcelo Fabian Oleas Escalante, [ID] [c] Mahdi Feizbahr, [ID] [d] Rodriguez Andrade Yuri Mauricio, [ID] [c] Luis Miguel Leon Torres, [ID] [b,e] Dora Paulina Gaibor Llanos, [ID] [b] Sergio David Saltos Mancheno, [ID] [b] Alexis Sergio Villalba Jacome, [ID] [b] Jimenez Merchan Carmita Guadalupe, [ID] [c]

ᵃ Institute of Science and Concrete Technology, ICITECH, Universitat Politècnica de València, Spain

ᵇ Faculty of Engineering and Applied Sciences, Civil Engineering Department, Central University of Ecuador, Av. Universitaria, Quito 170521, Ecuador

ᶜ Faculty of Engineering, Industrial and Architecture, School of Civil Engineering, Laica Eloy Alfaro de Manabi University, Manta, Ecuador

ᵈ School of Civil Engineering, Engineering Campus, University Sains Malaysia, Nibong Tebal , Penang, Malaysia

ᵉ Benito Juarez University, 36th Street Nte. 1609, Christopher Columbus, 72330 Heroic Puebla de Zaragoza, Pue., Mexic

ABSTRACT

This study explored the subsurface dynamics related to pile driving for the foundation of the E2 Bridge in Manta, Ecuador, using advanced geotechnical modeling. The objective was to evaluate the impact of various driving techniques on the mechanical properties of the soil, focusing on the stress distribution and the resulting deformations. The methodology included simulation analysis to compare different driving techniques and adjust them according to the specific soil characteristics at the construction site. The results revealed that by adapting the driving techniques to the local soil conditions, a 25% improvement in subsoil stability was achieved. The conclusions highlight the importance of customizing civil engineering practices according to the geotechnical specificities of each project. The adaptation of driving techniques is proposed as a practical and feasible measure to optimize construction processes, ensuring a more efficient and safer building. Furthermore, the study offers fundamental perspectives for the standardization of driving techniques in different geological contexts, contributing significantly to the improvement of foundation methodologies used in civil engineering.

1. Introduction

The evaluation of the structural integrity of bridges under the influence of seismic loads constitutes a vital field of research within civil engineering. This study highlights the need to consider soil- structure interaction (SSI) and erosion effects on pile foundations, building on previous research such as Kazakov et al. [1]. Specifically, this work

* Corresponding author. Tel.: +593987026212; e-mail: faridalvan@uce.edu.c.

focuses on Bridge E2 in Manta, Ecuador, a case where erosion and SSI have significantly compromised its structural integrity, highlighting the need for improved construction methods. This approach not only seeks to improve the seismic resilience of existing structures, but also to guide the design of new infrastructure adapted to local geotechnical complexities [2-4].

Recent studies, such as Naik and Hegde 5], have shown that significant erosion around piles can drastically alter the stiffness and strength of foundations, directly impacting structural stability during seismic events. In addition, variability in soil mechanical properties, such as density and shear strength, is crucial in the dynamics of SSI under seismic loads, which can lead to unpredictable structural response, as indicated by Gharad and Sonparote [6]. Mowafy et al. [7] identified the depth of erosion as a critical factor in the behavior of pile foundations under seismic conditions. In this context, the application of advanced distributed plasticity models in piles, as suggested by Malek et al. [8], is presented as a promising approach to achieve more accurate predictions of the seismic response of structures affected by erosion.

The present research extends previous studies on the effect of SSI on the seismic behavior of bridges with pile foundations, such as that of Liang et al. [9], by adopting advanced computational methods to address the complex soil-structure interaction dynamics, referencing Cao et al. (2021) [10]. Proper seismic risk assessment and implementation of mitigation strategies for bridges exposed to severe erosion and seismicity conditions require a comprehensive approach, as highlighted by Mohanty et al. [11], which considers both the current condition of the foundation and the soil characteristics themselves.

The analytical approach of this study, which benefits from recent advances in seismic analysis of bridges, incorporates performance-based assessments that comprehensively consider both scour risk and SSI, as detailed in Zhang et al. [12]. In addition, the importance of implementing design and rehabilitation strategies aimed at increasing the seismic resilience of bridges whose foundations have been affected by erosive processes is emphasized, as suggested by He et al. [13]. The central purpose of this research is to develop an analytical and design framework that improves the understanding and management of seismic risks in erosion-affected bridges by providing design and rehabilitation strategies that strengthen seismic resilience in challenging geotechnical contexts.

2. Materials and Methods

2.1. Background

The Manta-Manaos Multipurpose Project is of great relevance for national development. Its execution involved strategic planning by the government, supported by studies of the Ministry of Transportation and Public Works (MTOP). Among these studies, the Manta-San Plácido-Quevedo Highway in its preliminary phase and the access to the Port of Manta in its final phase stand out, as shown in Figure 1.

The earthquake of April 16, with a magnitude of 7.8 on the Richter scale, led the government to prioritize works in the affected areas, including the expansion of the Manta-Colisa Road. This effort seeks to reactivate the province of Manabí, improving connectivity through the port of Manta, where works are also being developed to optimize its services.

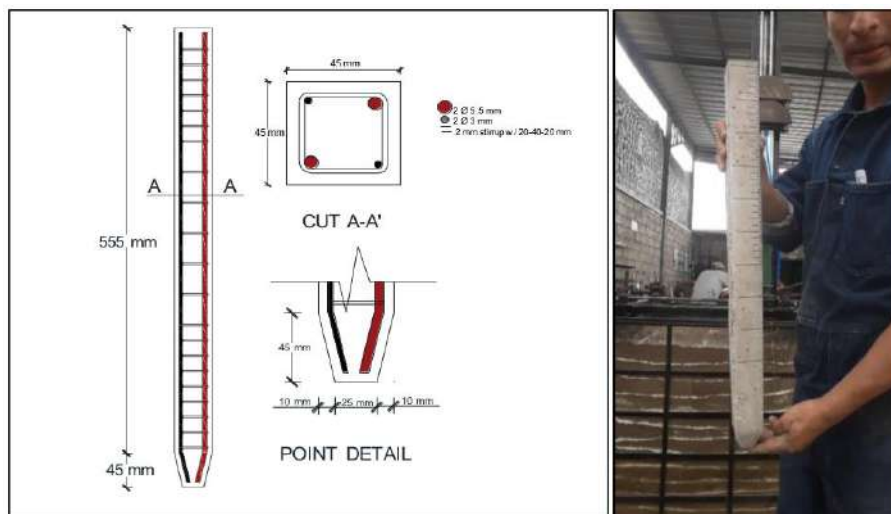Figure 1. Port of Manta - Colisa Project.

Figure 2. Dimensions of the mini-pile

The project includes the widening of the road from the port of Manta to Colisa (Jaramijo) to 6 lanes and the construction of 9 road interchanges (bridges). These improvements are crucial for the economic development and post-earthquake recovery of the region, facilitating transportation and trade.

2.2. Equipment Design

The design of the scale model of the equipment was based on the collection of information and visual analysis of the pile driving process at the E-2 bridge. The scales used were 1:10 in depth and 1:20 in plan, selected to ensure the resistance of the scale pile to impact without damage, with a minimum area of 1,600 mm². The choice of scale facilitates handling and maintains adequate visual perception. The scale model, made of carbon steel, stainless steel, acrylic and anti-corrosion paint, will be donated to the soils laboratory for practice and future research on pile driving. Pile P-2 of Bridge E-2 was selected for simulation in the scale model because of its representativeness in the foundation.

2.3. Mini piles

Geometry and mechanical strength were considered in the design of the mini-piles. The geometry was established according to previously defined scales. To ensure the mechanical resistance, tests were carried out with mortar, strong enough to withstand the driving in the limited area of the mini-pile. Pile P-2 of bridge E-2 was taken as a reference, whose piles are 12.00 m deep and 45 cm x 45 cm in cross-sectional area. Depending on the scale, the mini-piles were designed with 60 cm depth and 45 mm x 45 mm in cross-sectional area, with a modification at the

pile footing to 25 mm x 25 mm in cross-sectional area. To manufacture the mini-piles, a metal mold made of a black iron pipe (50 mm x 3 mm) modified with cuts and welds to facilitate demolding was used as shown in Figure 2.

The mini-piles, modeled according to the geometric properties established in section 2.2.1, were manufactured using a mold and different mortar mixtures. The mechanical properties were determined by compression tests in a universal machine, using mortar samples with different proportions of cement, sand, additives and water/cement ratio (w/c).

Initially, three types of piles were manufactured: PL-1 (mortar), PL-2 (longitudinally reinforced mortar) and PL-3 (confined reinforced mortar). These were subjected to impact resistance tests with a 3.8 kg sledgehammer to evaluate their behavior under impact stresses. Subsequently, the mechanical properties of the mortar were improved by adding nano silica and reducing the w/c ratio to increase strength, as can be observed, their characteristics in Table 1.

Table 1.

Characteristics of elaborated mini piles

Code	Dosage	Reinforcement
PL-1	M-1	It does not have
PL-2	Concrete 210 kg/cm^2	It does not have
PL-3	M-1	2 rods of 8 mm
PL-4	MP-4	2 5 mm corrugated rods
		2 wire of 2.6 mm
		2.6 mm wire stirrups

2.3.1. Mini pile driving procedure

The location of the mini-piles was based on the information from the foundation of pile P-2 on bridge E-2. Rows of three mini-piles were driven, repeating the process until six mini-piles were completed. The driving method

used was similar to that used for the E4 bridge foundation. The location of each mini-pile was staked out, and hand auger borings were drilled to a depth of 150 mm.

2.3.2. Penetration test of mini piles

The mini-pile driving test consists of counting the number of blows and measuring the penetration caused by the impact of a hammer. Tests were performed with four different masses (M-1 of 0.58 kg, M-2 of 1.34 kg, M-3 of 2.40 kg and M-4 of 3.80 kg) after driving the mini- piles to a depth of 450 mm. The number of blows and penetration per blow were recorded. To perform the test, an additional cap and extension was used on the mini-pile due to the limited span of the driving hammer. The cap includes a handle and a ruler to measure penetration, and the extension consists of a tube with two metal plates of the same cross-section as the mini-pile.

3. Results

The comprehensive analysis carried out in this study revealed that the pile driving technique employed has a significant impact on the subsurface stability and structural integrity of the foundations. It was found that adapting the driving technique to the specific soil conditions can significantly mitigate settlement, optimizing the efficiency of the construction process and improving overall structural safety. This critical relationship is clearly demonstrated in Table 2, which presents a comparison of the settlements recorded with different driving techniques. The results show a substantial improvement in the stability of the subsoil when the driving techniques are properly adjusted to the characteristics of the ground. This strategic adaptation not only reduces the risk of structural failure, but also contributes to the durability and reliability of the infrastructure under seismic conditions.

Table 2.

Penetration of Mini Piles as a Function of Mass Applied

Pile Identification	Penetration (mm)			
	with 0.58 kg	with 1.34 kg	with 2.40 kg	with 3.80 kg
P-1	20.4	9.3	12.6	20.1
P-2	5.4	6.4	9.3	21.8
P-3	6.3	6.7	7.3	14.3
P-4	8.8	6.0	5.2	12.8
P-5	6.2	4.5	4.3	13.9
P-6	11.7	4.4	6.7	10.0
Average	9.8	6.2	7.5	15.5

The average penetration shown in this table was calculated by removing the extreme values (the largest and smallest) for each mass series. This procedure is based on a robust data analysis methodology designed to minimize the impact of anomalies in the result set. This technique ensures that the averages more closely reflect typical penetration conditions, providing a more accurate and representative measure of overall subsurface behavior under different driving techniques.

The efficiency of the driving process was evaluated by examining the relationship between pile penetration depth and the number of blows required to achieve it. These findings are crucial for establishing optimal parameters to maximize driving efficiency while ensuring the integrity of the subsoil.

Figure 3 illustrates this correlation, highlighting how variations in the number of blows influence the penetration depth achieved. This graphical representation is fundamental to understand the importance of adjusting the driving intensity to the specific mechanical characteristics of the soil, to minimize the risk of structural damage.

3.1. Characterization of the Mechanical Strength of the Mortar

The choice of the appropriate mortar for pile construction is essential, since this material must resist not only the intense forces applied during the driving process but also the constant loads throughout the bridge's service life. The research highlighted significant differences in mechanical strength that can be attributed to variations in mortar composition.

Tables 3 to 6 present a comprehensive comparative analysis of the strength of various mortar mixes, including modifications with nano silica additions and variations in the water/cement ratio. The data obtained are crucial in determining the mortar mixes that best meet the specific strength and durability requirements needed for the piles, thus ensuring maximum efficiency and structural safety under adverse operational and loading conditions
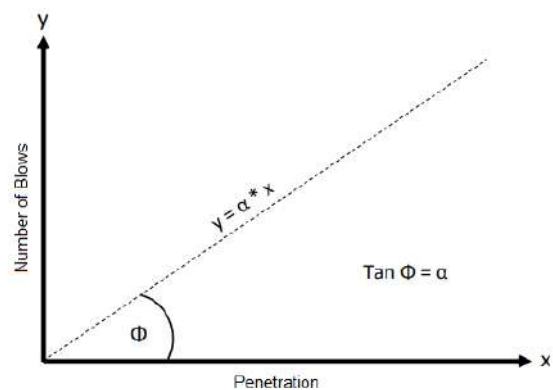

Figure 3. Curve of number of blows vs. penetration

Table 4.

 Results of specimen mortar with Nano Silica.

Code	Material	Dosage (gr)	Specimen Dimensions (mm)	Compressive Strength (Kg/cm^2)
			a = b = c	7 days
MS-1	Cement	1499,09	46	79,046
	Rio Sand	415,63		
	Homogenized Sand	429,69		
	Water	179,17		
	Nano Silica	11,33		
MS-2	Cement	1487,76	46	114,35
	Rio Sand	415,63		
	Homogenized Sand	429,69		
	Water	179,17		
	Nano Silica	22,66		
MS-3	Cement	1465,1	46	106,639
	River sand	415,63		
	Homogenized Sand	429,69		
	Water	179,17		
	Nano Silica	45,31		

Table 5.

Results of mortar specimen with nano silica plus super plasticizer

Code	Material	Dosage (gr)	Specimen Dimensions (mm)	Compressive Strength (Kg/cm^2)		
			a = b = c	7 days	14 days	28 days
MP-1	Cement	1477,5	46	159,972	174,682	207,928
	Sand	1535,78				
	Water	900				
	Nano Silica	22,5				
	Plasticizer	7,5				
MP-2	Cement	1477,5	46	119,983	145,53	149,233
	Sand	1535,78				
	Water	900				
	Nano Silica	22,5				
	Plasticizer	7,5				
MP-3	Cement	1477,5	36	128,851	151,936	172,739
	Sand	1535,78				
	Water	900				
	Nano Silica	22,5				
	Plasticizer	7,5				

Table 6.

Results of mortar specimen with w/c reduction

Code	Material	Dosage (gr)	Specimen Dimensions (mm)	Compressive Strength (Kg/cm^2)		
			a = b = c	7 days	14 days	28 days
MP-4	Cement	1477,5	46	239,579	379,427	343,442
	Sand	1535,78				
	Water	450				
	Nano Silica	22,5				
	Plasticizer	22,5				
MP-5	Cement	1477,5	46	406,422	423,175	518.826
	Sand	1535,78				
	Water	450				
	Nano Silica	22,5				
	Plasticizer	22,5				
MP-6	Cement	1477,5	46	227,509	243,632	239,95
	Sand	1535,78				
	Water	450				
	Nano Silica	22,5				
	Plasticizer	22,5				

4. Discussion

The research highlights how careful selection and adaptation of driving techniques to the specific geotechnical characteristics of the site contribute significantly to the stability of pile foundations. This observation is supported by the data presented in Table 1, where improvements in stability are correlated with modifications in driving techniques. The underlying theory, based on soil dynamics and material mechanics, suggests that proper calibration of the number of blows, as detailed in Figure 1, is crucial to optimize pile penetration and avoid damage due to oversaturation or material fatigue.

This meticulous adjustment ensures that the force applied during driving is ideal for the soil conditions, an aspect that aligns with the theories of loading and energy transfer in granular media. In addition, optimizing the driving force helps to maximize the efficiency of the process and minimize the risks of compromising the structural integrity of the piles. This approach is supported by recent studies addressing the interaction between driving techniques and soil physical properties, highlighting the importance of an adaptive design based on local site conditions.

On the other hand, Tables 2 to 5 illustrate how optimized mortar mixes not only improve the mechanical strength of piles but also extend their service life. Relevant literature in materials science suggests that tailoring construction material specifications to specific geotechnical and environmental conditions can offer significant benefits in terms of durability and structural functionality. This approach ensures that piles not only meet current loading and durability requirements but are also prepared to adequately respond to future demands and changing environmental conditions.

The discussion is also enriched with references to sustainable design practices and emerging technologies that could be integrated into the development of more advanced materials and construction techniques. The implementation of these innovations in the design of pile foundations may represent a significant step forward in civil engineering, promoting the adaptability and resilience of infrastructure in the face of future challenges.

In conclusion, this research not only validates existing techniques but also proposes innovative adaptations that could be crucial for the evolution of civil engineering practices regarding pile installation and structural integrity management under various geotechnical and environmental conditions.

5. Conclusions

This study has confirmed that adapting driving techniques to the specific characteristics of the subsoil contributes significantly to reducing settlements and improving the stability of pile foundations. As shown in Table 1, flexibility in the driving process is essential to adapt construction practices to variations in subsurface conditions, thus optimizing the effectiveness of pile installation. This approach allows not only to preserve the structural integrity of the foundations but also to increase efficiency and safety during bridge construction.

The correct relationship between the number of blows and the depth of penetration is key to ensuring the efficiency of the driving process. Figure 1 provides a crucial frame of reference for fine-tuning the driving technique to maximize effectiveness without compromising the integrity of the subsoil or pile material. This fine-tuning is essential to optimize energy transfer during driving and to avoid excesses that can lead to overload damage or material fatigue, thus ensuring an efficient and durable pile installation.

The structural integrity of piles depends to a large extent on the composition of the mortar used. Tables 2 to 5 highlight the importance of choosing mortar mixes that not only meet basic structural requirements, but also provide optimum performance under extreme loading conditions. These results highlight the urgency of developing new mortar composites that can improve structural response under different environmental and loading conditions. This innovative approach to mortar selection is crucial to extend the service life of piles and ensure the safety and durability of the overall infrastructure.

Based on the findings of this study, it is advisable to implement detailed protocols for geotechnical evaluation prior to pile driving, and to promote experimentation with innovative mortar mixes. These measures are designed to improve the durability and effectiveness of piles under dynamic loads. Adopting these practices will not only optimize mortar characteristics to better withstand extreme conditions, but also ensure that the interaction between the soil and the structure is properly evaluated and managed, thus minimizing risks and maximizing structural stability.

References

[1] Kazakov, K., L. Mihova, and D. Partov. "Constitutive models for FE analysis of pile founded buried arch bridge." IOP Conference Series: Materials Science and Engineering. Vol. 951. No. 1. IOP Publishing, 2020. http://doi.org/10.1088/1757-899X/951/1/012004

[2] Akbari, Ali, Mohammad Nikookar, and Mahdi Feizbahr. "Reviewing Performance of Piled Raft and Pile Group Foundations under the Earthquake Loads." Research in Civil and Environmental Engineering 1.5 (2013): 287-299.

[3] Alvansazyazdi, Mohammadfarid, et al. "Nano-silica in Holcim general use cement mortars: A comparative study with traditional and prefabricated mortars." Advances in Concrete Construction 17.3 (2024): 135. https://doi.org/10.12989/acc.2024.17.3.135

[4] Feizbahr, Mahdi, et al. "Review on various types and failures of fibre reinforcement polymer." Middle-East Journal of Scientific Research 13.10 (2013): 1312-1318.

[5] Naik, Uddhav U., and Ganesh Hegde. "Simulation Analysis of Bridge's Deck Dynamic Response subjected to Vehicular Load considering Road Roughness." Solid State Technology 63.5 (2020): 6321-6331.

[6] Gharad, Anand M., and Ranjan S. Sonparote. "Influence of soil-structure interaction on the dynamic response of continuous and integral bridge subjected to moving loads." International Journal of Rail Transportation 8.3 (2020): 285-306. https://doi.org/10.1080/23248378.2019.1632753

[7] Mowafy, Yousry Mohamed, Ahmed Rushdy Towfeek, and Ahmed Kamal Mohamed. "Numerical study on piles performance in sand slope stability under variable conditions." Journal of Al-Azhar University Engineering Sector 14.50 (2019): 29-35.

[8] Malek, Muhamad Aziman Abdul, et al. "Experimental study of impact loading effect on bridge substructures including piles." Structures. Vol. 31. Elsevier, 2021. https://doi.org/10.1016/j.istruc.2021.02.010

[9] Liang, Feng, et al. "Nonlinear forced vibration of spinning pipes conveying fluid under lateral harmonic excitation." International Journal of Applied Mechanics 13.09 (2021): 2150098. https://doi.org/10.1142/S1758825121500988

[10] Cao, Ran, Anil Kumar Agrawal, and Sherif El-Tawil. "Overheight impact on bridges: A computational case study of the Skagit River bridge collapse." Engineering Structures 237 (2021): 112215. https://doi.org/10.1016/j.engstruct.2021.112215

[11] Mohanty, Piyush, et al. "A shake table investigation of dynamic behavior of pile supported bridges in liquefiable soil deposits." Earthquake Engineering and Engineering Vibration 20 (2021): 1-24. https://doi.org/10.1007/s11803-021-2002-2

[12] Zhang, Xiyin, et al. "Experimental study of frozen soil effect on seismic behavior of bridge pile foundations in cold regions." Structures. Vol. 32. Elsevier, 2021. https://doi.org/10.1016/j.istruc.2021.03.119

[13] He, Lian-Gui, et al. "Seismic assessments for scoured bridges with pile foundations." Engineering Structures 211 (2020): 110454. https://doi.org/10.1016/j.engstruct.2020.110454

Experimental Evaluation of The Impact Resistance of Alkali-Activated Slag Concrete Under High Temperature

Mohammadhossein Mansourghanaei, [iD] a,*

ª Ph.D. in Civil Engineering, Department of Civil Engineering, Chalous Branch, Islamic Azad University, Chalous, Iran

ABSTRACT

In recent years, the use of activated alkaline slag concretes (AASC), has had a wide perspective in civil engineering science due to its many environmental benefits (due to the reduction of the emission of CO2 gas in the air) and high resistance to impact loads. is in this article, a mixed design of ordinary portland cement concrete (OPCC) containing 500 kg/m3 of portland cement as a control concrete and a mixed design of AASC containing granulated blast furnace slag (GBFS) was made, and the impact resistance of the concrete was tested under the weight-drop impact test (WDIT). It was evaluated at temperatures of 21, 300 and 600 ℃ at the age of 90 days. The obtained results indicate that the increase in temperature has caused a drop in the results of the WDIT, so that in OPCC, the energy absorbed and the flexibility index of concrete samples at a temperature of 600 ℃ drop by 76.92% and it obtained 86.95% improvement compared to 21 ℃ temperature, while in active alkali concrete, these figures brought 66.66 and 14.28% drop in results, respectively. In this regard, the number of impacts required for the occurrence of initial cracks and failure in the concrete sample had a downward trend with increasing temperature. In this experimental research, AASC showed superior results compared to OPCC. The results obtained from the analysis of the images of the scanning electron microscope (SEM) on the concrete samples overlapped with the other tests of this research.

1. Introduction

In line with the development of national security and passive defense in the field of civil engineering infrastructure, many laboratory works have been done to produce structural concrete in strategic and sensitive centers of the country [1-3]. The strength of the reinforced concrete structures of these centers plays an important role in reducing destruction and human injuries caused by the enemy's defense operations. Improving the strength of concrete can be achieved through the type of materials used in its mixture [4-10].

Ordinary cement production has always brought environmental concerns due to the consumption of mineral resources, fossil fuels, and the production and emission of poisonous carbon dioxide gas. Research has shown that cement factories are responsible for the release of about 5% of the total carbon dioxide entering the earth's atmosphere

---

* Corresponding author. Tel.: +989121712070; e-mail: Mhm.Ghanaei@iauc.ac.ir.

[11]. In order to solve these problems, alkali active concrete which does not use cement was proposed by the researchers. In the production process of this type of concrete, aluminosilicate materials and active alkali solution replace ordinary cement, the final product of this combination is the production of a large volume of hydrated gels with high adhesion and filling characteristics in the matrix of activated alkali cement. Alkaline cements are a group of active alkali materials, materials that show superior engineering properties compared to Portland cement [12]. On the other hand, the amount of carbon dioxide produced in the production process of alkali-active materials is much lower than the production process of ordinary cement [13].

According to yerde's theory, the fireproof property of concrete is perhaps the most important point in the safety of structures, and this is the property that fully reveals the advantages of concrete in this field, therefore, in concrete structures, protection against Rupture against excessive heat is provided at the same time [14]. The results of the research conducted on the effect of heat on AASC showed that there are no significant changes in the mechanical properties of concrete under the temperature of 27 to 100 °C, a decrease of up to 40% in the mechanical properties of concrete, after applying A temperature of 350 °C occurs in the early stages, and it has also been reported that the exit of water from the chemical bonding space in hydrated calcium silicate (C-S-H) leads to the failure of concrete at a temperature of more than 450 °C [15]. In general, it is believed that activated alkalis perform better than OPCCs in facing fire due to their ceramic characteristics [16-18]. The resistance of AASC when exposed to heat depends on the chemical composition of the concrete constituents, as well as the temperature and the way it is processed [19].

Impact resistance can be investigated by several types of tests, including explosion test, projectile impact test, pendulum impact test, and WDIT. Impact loads are divided into two groups of impact with low speed and impact with high speed according to the impact speed. One of the advantages of carrying out impact test is to determine the failure energy of the samples, the failure energy is one of the most important indicators of the science of fracture mechanics. High fracture energy is a sign of resistance of samples against crack propagation. Researches have shown that, in concrete exposed to impact, microcracks extend ahead of the crack tip and create the area of the fracture process that originates from local strain [14]. If the degree of compaction in the microstructure of concrete is high, the propagation of microcracks against impact loads is delayed. Superior impact resistance of weight-drop type in activated alkali concrete compared to OPCC has been reported in many researches [20-22]. In line with the application of high heat to concrete samples, with the increase of temperature and consequently the increase of

cracks on the surface of the sample, the concrete becomes crystalline or hollow and becomes very fragile against impact [23]. The objectives and innovation in this laboratory research through the production of alkali-active concrete can be summarized as follows:

1. The mechanical and microstructural properties of alkali activated concrete are improved compared to OPCC.
2. Helping to reduce the volume of toxic carbon dioxide gas emissions compared to OPCC production, according to the report provided by other researchers in this regard.
3. Helping to maintain the health of the environment by using (in the composition of activated alkali concrete) slags accumulated in iron smelting factories, known as environmentally harmful substances.
4. Maintaining and reducing the consumption of mineral resources that are used as the main materials during the process of making ordinary cement.
5. Maintaining and reducing the consumption of fossil fuels that are used as fuel in conventional cement factories.

2. Materials

In this laboratory research, type 2 Portland cement produced by Gilan Sabz Cement Industries (Diylman) with a density of 3250 kg/m3 and a specific surface area of 3000-3200 cm2/g, produced under the ISIRI 389 standard, was used. The slag of the metallurgical furnace, a product of Isfahan iron smelting factory, with a density of 2750 kg/m3, a specific surface area of 2200 cm2/g, and an apparent density of 960 kg/m3 was used according to the ASTM C989/C989M standard, the chemical characteristics of this product in Table 1 shows. The water used for the preparation of lime water and the construction of the mixture plan in the upcoming research is drinking water of Lahijan city, this water has a pH in the range of 5.6 to 5.7 and a density of 1000 kg/m3. According to clauses 9-10-4-2 and 9-10-4-3 of the fourth edition of Iran's National Building Regulations, water that is drinkable, has no specific taste and smell, and is clean and smooth can be used without testing. used in concrete, unless previous records indicate that this water is unsuitable for concrete. Consumable aggregate is synthetic and based on the requirements of ASTM C33 standard, prepared from sand factories in Lahijan city, some characteristics of the aggregate are shown in Table 2. Research has shown that fresh activated alkali concrete has a weaker performance due to the high viscosity in the activated alkali solution compared to concrete containing fresh normal portland

cement. To solve this problem, a superplasticizer based on polycarboxylate is often used due to Strong bonds between calcium with positive charge and polycarboxylate with negative charge is the best option [24]. In this regard, the 4th generation superplasticizer based on normal polycarboxylate, a product of Durocham Middle East company, was used based on the characteristics of Table 3.

The activated alkali solution used in this research is a combination of sodium silicate and sodium hydroxide solution with a weight ratio of 2.5, which was used with a combined density of 1483 kg/m3. Some of the characteristics of the activated alkali solution used in this research are in Table 4 is shown.

Table 1.

Chemical Characteristics of GBFS (%)

CaO	SiO$_2$	Al$_2$O$_3$	Fe$_2$O$_3$	MgO	SO$_3$	Na$_2$O	K$_2$O	Tio$_2$	MnO	L.O.I
36.72	35.5	9.17	7.49	6.24	0.12	1.21	0.92	2.49	0.18	0.02

Table 2.

Characteristics of Aggregates

Concrete Materials	Water Absorption (%)	Density (kg/m^3)	Modulus of Softness (mm)	Maximum Diameter (mm)	Minimum Diameter
Fine Aggregates	2.9	2650	2.85	4.75	75(µm)
Coarse Aggregates	2.2	2750	5.7	19	4.75(mm)

Table 3.

Characteristics of Normal Polycarboxylate Superplasticizer

Flash Point	Chlorine Ion Content	pH	Standard	Density (kg/m^3)	Color	Physical State
Does Not Have	Does Not Have	About 7	ASTM C494	1100	Brown	Liquid

Table 4.

Characteristics of Active Alkali Solution

Molecular Formula	The weight (molar) ratio of silicate to water	The weight (molar) ratio of silicate to sodium	Molar Mass (gr/mol)	Melting Temperature (C)	Modulus of Elasticity (p)	Density (kg/m^3)	Molarity (mol/m^3)	Color
NaOH	-	-	39.99	318	3.3	2130	12	White
Na$_2$SiO$_3$	47	2.4	122.06	1088	-	2400	12	White

Table 5.

Specifications of Concrete Mix Design

Type Concrete	SuperplaSticizer	FA[1]	CA[2]	Water	GBFS	Cement	Quantity	density concrete mix (kg/m^3)	Curing conditions After mold removal	Ratio W/C
OPCC	7	765	1000	225	0	500	kg/m^3	2497	In the Water	45%
	0.0028	30.63	40.04	9.01	0	20.02	%			
AASC	7	726.63	1000	225	500	0	kg/m^3	2494.63	Heat + Dry Environment	45%
	0.0028	30.57	40.08	9.19	20.04	0	%			

- In AASC, the W/C ratio means the ratio of activated alkali solution to the slag of the used GBFS.

1- FA = **Fine Aggregates**

2- CA = **Coarse Aggregates**

3. Mix Design

There is no separate standard for the design of alkali-active concrete mix, therefore, according to some laboratory researches [25], the alkali-active concrete mix plan has been prepared and adjusted according to the standard of preparation normal concrete under the recommendation of the ACI 211.1-89 committee. The concrete mix plan in this laboratory research is shown in Table 5.

4. Construction and Curing

At first, according to the mixture plan in Table 5, the consumable materials were weighed and then the dry materials including cement (or GBFS) and aggregate were poured into the circulating electric mixer and the mixing process lasted for 1.5 minutes. ended Next, wetter materials including water (or active alkali solution) were added to the mixture and the combination of materials continued for another 2.5 minutes. Then, the fresh concrete

mixture was poured into pre-oiled and foiled metal molds in three stages. In this direction, in order to apply compaction, 25 impact were given to the concrete mixture in each stage by a special rod. At the end, the molds containing concrete samples were stored in a dry environment under a temperature of 21 °C. After this time passed, the samples were molded and the OPCC samples were stored and processed in lime water at a temperature of 21 °C until the time of the test. AASC samples were subjected to heat treatment at 60 °C after molding for 48 hours in the oven to improve the strength of this type of concrete. After this time, the concrete samples They were removed from the oven and stored and processed in a dry environment under a temperature of 21 °C until the time of the test. In line with heat treatment in activated alkali concrete, research has shown that samples of activated alkali concrete subjected to heat treatment at temperatures of 50-70 °C have greater strength than samples at temperatures of 20 °C [14].

5. Standard and Method of Conducting Tests

Impact resistance test of the weight-drop type at the age of 90 days according to ACI 544-2R standard on concrete disc samples with dimensions of 35.6 x 15 cm at temperatures of 21, 300 and 600 °C was done. This test is in the field of examining the mechanical properties of concrete and is a good criterion for measuring the resistance of structures exposed to impact loads. According to the standard mentioned in this test, the weight of the hammer is 4.54 kg, the height of the fall of the weight is 45.7 cm, and the diameter of the metal ball is 6.35 cm. To perform the test, after the curing age and during the determined thermal process, the disc samples were placed inside the impact device just under the weight drop in such a way that the metal ball is placed exactly in the center of the sample, then the number of impacts which is registered for the occurrence of the first crack (N1) and the final rupture (N2) by a counter installed in the upper part of the device. The fracture energy for the occurrence of the first crack (E1) and final rupture (E2) was calculated in terms of joules through equation 1. In this regard, N is the number of impacts to create a crack, W is the weight of the hammer, and H is the height of the fall of the weight. Before performing the high temperature tests in the WDIT, which was performed at the age of 90 days, according to the ISO834 standard, the concrete samples were placed in the oven at 300 and 600 °C for 1 hour. Then, the samples were left in the furnace for another 1 hour so as not to be affected by temperature shock. After the samples were taken out of the furnace, the samples were kept at room temperature for 24 hours to reach the temperature equilibrium. The use of this standard has been reported in other researches about

tests under high heat in concrete [26]. SEM analysis was performed at the age of 90 days in concrete under 21 °C by SEM with FEI Quanta 200 model. Next, the microstructure was examined.

$$E_n = N \times W \times H \tag{1}$$

6. Results and Analysis of Tests

6.1. The Results and Analysis of the Impact Resistance Test

The results of impact test of falling weight in concrete are shown based on figures 1, 2 and 3. According to these results, it can be seen that the increase in temperature caused a drop in the results in the WDIT, so that in OPCC, the energy absorbed and the flexibility index of concrete samples under the temperature of 600 °C 76.92% decrease and 86.95% improvement compared to the temperature of 21 °C, respectively, while in activated alkali concrete, these figures are 66.66% and 14.28%, respectively. accompanied the number of impacts required to cause initial cracks in concrete samples decreased with increasing temperature. So that in OPCC, the maximum (10 impact) and minimum (2 impact) number of impacts for the occurrence of initial cracks were obtained at 21 and 600 °C. For AASC, the maximum (14 impact) and minimum (6 impacts) number of impacts for the occurrence of primary cracks were obtained at 300 and 600 °C. The number of impacts required for the appearance of the final crack in the concrete sample had a downward trend with increasing temperature. So that in OPCC, the maximum (23 impact) and minimum (5 impact) number of impacts for the occurrence of initial cracks were obtained at 21 and 600 °C. For AASC, the maximum (12 impact) and minimum (9 impact) number of impacts for the occurrence of initial cracks were obtained at 300 and 600 °C. Alkali active concrete showed superior results compared to OPCC. This issue is due to the presence of aluminosilicate materials and the better pozzolanic activity of GBFS compared to Portland cement in the concrete composition, which leads to the production of a higher volume of hydrated gels such as hydrated calcium silicate (C-S-H) in the composition of activated alkali concrete. has been These gels improve compaction and strength in concrete by filling holes, pores and creating bonds in the interfacial transfer zones (ITZ) between paste and aggregate. The results of the SEM analysis on the concrete samples from this research overlapped with other tests of this research.

6.2. SEM Results and Analysis

In this research, the images obtained from the SEM imaging test at a scale of 10 micrometers are displayed in
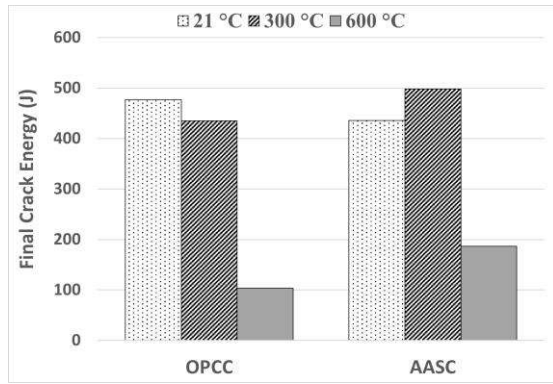
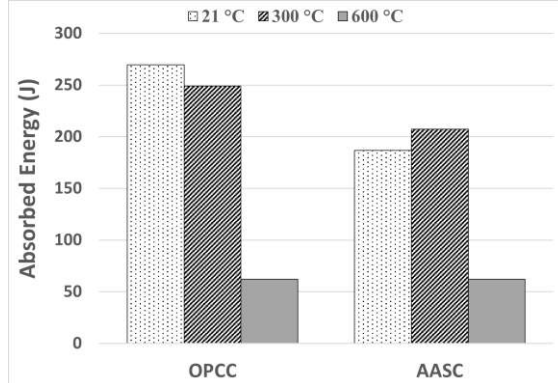Fig. 1. The Energy Resulting from the Occurrence of the Final Crack
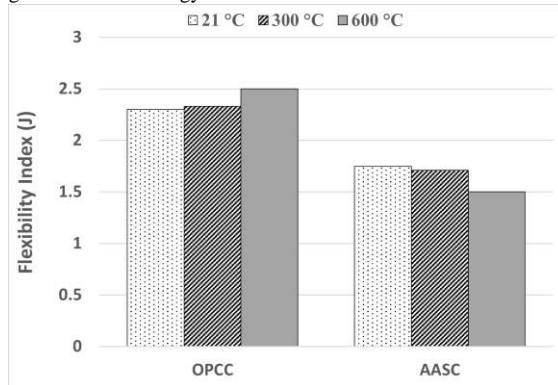

Fig. 2. Absorbed Energy

Fig. 3. Flexibility Index

Figure 4. In these images, the microstructure of concrete in mixed designs can be summarized in three basic phases:

1. The first phase includes hydration and geopolymerization products, including hydrated gels that are mainly dark in color in the pictures, these gels, after forming and in combination with other concrete components, are the main factor in strengthening the microstructure of concrete through the filling of pores and cavities, as well as the improvement of bonding in the ITZ and interlayer zones (in hydrated gels) are known.

2. The second phase includes unreacted crystals that are formed as a result of impurities in raw materials or unreacted particles in the process of hydration and geopolymerization, and they are mostly white in the pictures.

3. The third phase includes the bonding of cement paste with aggregates in the interfacial transition area, as well as the bonding of interlayers in the structure of hydrated gels.

In the images of activated alkali concrete, no tree structure can be seen that shows weakness in the microstructure of the concrete sample. In OPCC containing portland cement, more pores, holes and the volume of clinker grains of unhydrated cement are seen than in the sample of activated alkali concrete. The presence of dark colored areas in the images indicates the completion of a large part of the geopolymerization process and the production of hydrated gels. The white masses in the images of this design can be attributed to the alkaline active-forming crystals that did not participate in the geopolymerization process, and the very small points in the microstructure of activated alkali concrete can be attributed to unhydrated GBFS particles. attributed the microcracks in the picture can be considered as active alkali concrete samples due to heat treatment at 60 °C. In OPCC, in the bulk part of Portland cement paste, ions such as calcium, sulfate, hydroxide and aluminate, which are formed through aerobic (dissolution) into calcium silicate and calcium aluminate, combine together and form a gel. They give ettringite (C-A-S-H) and calcium hydroxide ($Ca(OH)_2$), in the sense that ettringite is created as a result of the reaction of calcium aluminate with calcium sulfate, and with the progress in the hydration stage, weak C-S-H crystals and the second generation of crystals that formed from calcium hydroxide ($Ca(OH)_2$) and ettringite gel (C-A-S-H), they start to fill the empty spaces in the ettringite and portlandite network, and with this operation, the density, hardness, and resistance of the ITZ concrete increases [14]. The researches of others have shown that in activated alkali concrete, the pozzolanic reaction by converting CH to C-S-H condenses and homogenizes the microstructures [27]. The results of SEM analysis in this laboratory research are in full overlap and harmony with the results of other tests in this article.

7. Conclusions

In this laboratory study, the production of AASC and its comparison with OPCC was investigated, following the impact resistance test of the weight-drop type. The analysis of SEM images was also done in order to evaluate the microstructure and verify the results of other tests. The results obtained in this research are presented as follows:
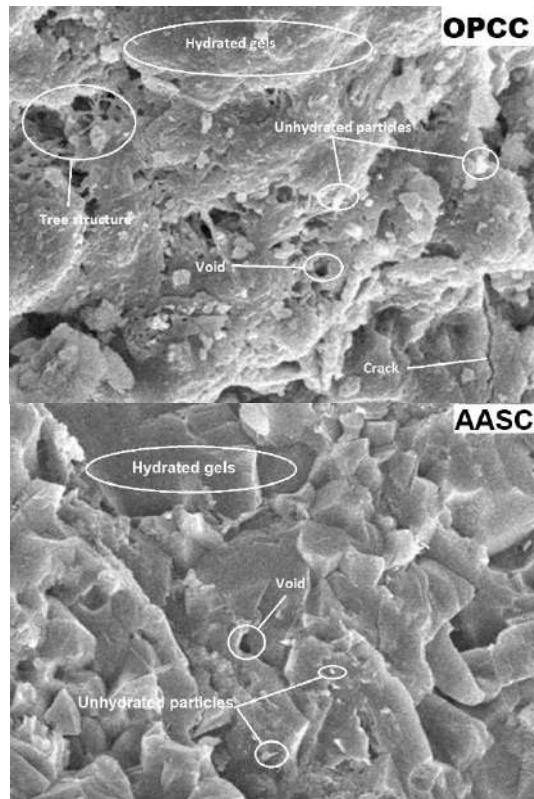
Fig. 4. Results of SEM Analysis

1. Increasing the temperature caused a decrease in the results of the WDIT, so that in OPCC, the energy absorbed and the flexibility index of the concrete samples at a temperature of 600 ℃ decreased by 76.92% and 86.95%, respectively. obtained the percentage of improvement compared to the temperature of 21 ℃, while in active alkali concrete, these figures were 66.66 and 14.28%, respectively, and the results decreased.

2. The number of impacts required to cause the initial crack in the concrete sample decreased with the increase in temperature. So that in OPCC, the maximum (10 impact) and minimum (2 impact) number of impacts for the occurrence of initial cracks were obtained at 21 and 600 ℃. For AASC, the maximum (14 impact) and minimum (6 impact) number of impacts for the occurrence of initial cracks were obtained at temperatures of 300 and 600 ℃.

3. The number of impacts required for the appearance of the final crack in the concrete sample had a downward trend with increasing temperature. So that in OPCC, the maximum (23 impact) and minimum (5 impact) number of impacts for the occurrence of initial cracks were

obtained at 21 and 600 ℃. For AASC, the maximum (12 impact) and minimum (9 impact) number of impacts for the occurrence of initial cracks were obtained at 300 and 600 ℃.

4. In the impact resistance test of the weight-drop type, AASC showed superior results compared to OPCC. This issue is due to the better activity of GBFS compared to Portland cement in the concrete composition, which has led to the production of a higher volume of hydrated gels in the concrete composition. These gels improve the density and strength of concrete by filling holes and voids.

5. The results of the SEM analysis on concrete samples were in overlap and coordination with other tests of this research.

References

[1] Mansourghanaei, Mohammadhossein. "Experimental Study of Impact Strength in Ordinary Concrete under High Temperature, Along with Validation by SEM and XRD." Passive Defense 14.1 (2023): 1-10.

[2] Mansourghanaei, Mohammadhossein, Morteza Biklaryan, and Alireza Mardookhpour. "Investigation of the Impact Resistance, Microstructure and Weight Loss in Fibrous Pozzolanic Concrete Containing Fibers, Under High Temperatures." Passive Defense Quarterly 13.3 (2022): 11-23.

[3] Mansourghanaei, Mohammadhossein, Morteza Biklaryan, and Alireza Mardookhpour. "Comparing the Impact Strength of Alkali Activated Concrete and Normal Concrete Under High Heat Based on XRD and SEM Tests." Passive Defense 13.1 (2022): 47-56.

[4] Mansourghanaei, Mohammadhossein, Morteza Biklaryan, and Alireza Mardookhpour. "Experimental study of the effects of adding silica nanoparticles on the durability of geopolymer concrete." Australian Journal of Civil Engineering 22.1 (2024): 81-93. https://doi.org/10.1080/14488353.2022.2120247

[5] Mansourghanaei, Mohammadhossein, Morteza Biklaryan, and Alireza Mardookhpour. "Experimental study of properties of green concrete based on geopolymer materials under high temperature." Civil Engineering Infrastructures Journal 56.2 (2023): 365-379. https://doi.org/10.22059/ceij.2022.345402.1856

[6] Mansourghanaei, Mohammadhossein, and Morteza Biklaryan. "Experimental evaluation of compressive, tensile strength and impact test in blast furnace slag based geopolymer concrete, under high temperature." Journal of Civil Engineering Researchers 4.2 (2022): 12-21. https://doi.org/10.52547/JCER.4.2.12

[7] Mansourghanaei, Mohammadhossein, and Morteza Biklaryan. "Experimental study of compressive strength, permeability and impact testing in geopolymer concrete based on Blast furnace slag." Journal of Civil Engineering Researchers 4.3 (2022): 31-39. https://doi.org/10.52547/JCER.4.3.31

[8] Mansourghanaei, Mohammadhossein, Morteza Biklaryan, and Alireza Mardookhpour. "Experimental Study of Mechanical Properties of Geopolymer Concrete as Green Concrete with a Sustainable Development Approach in the Construction Industry, Under High Temperature." Journal of Civil Engineering Researchers 4.4 (2022): 1-11. https://doi.org/10.61186/JCER.4.4.1

[9] Mansourghanaei, Mohammadhossein. "Evaluation of mechanical properties of reinforced concrete based on non-destructive test of ultrasonic waves, Under high heat." NDT Technology 2.9 (2022): 52-62. https://doi.org/10.30494/jndt.2022.333675.1085

[10] Mansourghanaei, Mohammadhossein. "Laboratory study of mechanical properties of ordinary concrete under high heat consumption in hydraulic structures, along with validation by SEM and XRD tests." Iranian Dam and Hydroelectric Powerplant 9.3 (2022): 11-23. http://journal.hydropower.org.ir/article-1-483-en.html

[11] Nosrati, A., et al. "Portland cement structure and its major oxides and fineness." Smart Structures and Systems, An International Journal 22.4 (2018): 425-432.

[12] Allahverdi, A. L. I., Ebrahim Najafi Kani, and Mahshad Yazdanipour. "Effects of blast-furnace slag on natural pozzolan-based geopolymer cement." Ceramics-Silikáty 55.1 (2011): 68-78.

[13] Neupane, Kamal, Des Chalmers, and Paul Kidd. "High-strength geopolymer concrete-properties, advantages and challenges." Advances in Materials 7.2 (2018): 15-25.

[14] Mehta, Povindar K., and Paulo Monteiro. "Concrete: microstructure, properties, and materials." McGraw-Hill Publishing (2014).

[15] Siddique, Rafat, and Deepinder Kaur. "Properties of concrete containing ground granulated blast furnace slag (GGBFS) at elevated temperatures." Journal of Advanced Research 3.1 (2012): 45-51. https://doi.org/10.1016/j.jare.2011.03.004

[16] Bakharev, Tatiana. "Thermal behaviour of geopolymers prepared using class F fly ash and elevated temperature curing." Cement and concrete Research 36.6 (2006): 1134-1147. https://doi.org/10.1016/j.cemconres.2006.03.022

[17] Mane, Shweta, and H. Jadhav. "Investigation of geopolymer mortar and concrete under high temperature." Magnesium 1.5 (2012): 384-390.

[18] Comrie, Douglas C., and Waltraud M. Kriven. "Composite cold ceramic geopolymer in a refractory application." Ceramic Transactions 153 (2003): 211-225.

[19] Türkmen, İbrahim, et al. "Fire resistance of geopolymer concrete produced from Ferrochrome slag by alkali activation method." 2013 International Conference on Renewable Energy Research and Applications (ICRERA). IEEE, 2013.

[20] Alberti, Marcos G., Alejandro Enfedaque, and Jaime C. Gálvez. "Improving the reinforcement of polyolefin fiber reinforced concrete for infrastructure applications." Fibers 3.4 (2015): 504-522. https://doi.org/10.3390/fib3040504

[21] Olivito, Renato Sante, and F. A. Zuccarello. "An experimental study on the tensile strength of steel fiber reinforced concrete." Composites Part B: Engineering 41.3 (2010): 246-255. https://doi.org/10.1016/j.compositesb.2009.12.003

[22] Islam, Azizul, et al. "Influence of steel fibers on the mechanical properties and impact resistance of lightweight geopolymer concrete." Construction and Building Materials 152 (2017): 964-977. https://doi.org/10.1016/j.conbuildmat.2017.06.092

[23] Gholhaki, Madjid, and Ghasem Pachideh. ". Assessing Effect of Temperature Rise on the Concrete Containing Recycled Metal Spring and Its Comparison with Ordinary Fibres." Journal of Structural and Construction Engineering 6.2 (2019): 141-156. https://dx.doi.org/10.22065/jsce.2018.93911.1278

[24] Pilehvar, Shima, et al. "Physical and mechanical properties of fly ash and slag geopolymer concrete containing different types of micro-encapsulated phase change materials." Construction and Building Materials 173 (2018): 28-39. https://doi.org/10.1016/j.conbuildmat.2018.04.016

[25] Deb, Partha Sarathi, Pradip Nath, and Prabir Kumar Sarker. "Drying shrinkage of slag blended fly ash geopolymer concrete cured at room temperature." Procedia Engineering 125 (2015): 594-600. https://doi.org/10.1016/j.proeng.2015.11.066

[26] Kong, Daniel LY, and Jay G. Sanjayan. "Effect of elevated temperatures on geopolymer paste, mortar and concrete." Cement and concrete research 40.2 (2010): 334-339. https://doi.org/10.1016/j.cemconres.2009.10.017

[27] Du, Hongjian, Suhuan Du, and Xuemei Liu. "Durability performances of concrete with nano-silica." Construction and building materials 73 (2014): 705-712. https://doi.org/10.1016/j.conbuildmat.2014.10.014

Author Guidelines EditEdit Author Guidelines

GENERAL GUIDELINES FOR AUTHORS

Journal of civil engineering researches invites unsolicited contributions of several forms: articles, reviews and discussion articles, translations, and fora. Contributions should fall within the broad scope of the journal, as outlined in the statement of scope and focus. Contributors should present their material in a form that is accessible to a general anthropological readership. We especially invite contributions that engage with debates from previously published articles in the journal.

Submissions are double-blind peer-reviewed in accordance with our policy. Submissions will be immediately acknowledged but due to the review process, acceptance may take up to three months. Submissions should be submitted via our website submission form (see links above for registration and login). Once you login, make sure your user profile has "author" selected, then click "new submission" and follow the instructions carefully to submit your article. If problems arise, first check the FAQ and Troubleshooting guide posted below. If you are still experiencing difficulty, articles can be submitted to the editors as email attachments.

Each article should be accompanied by a title page that includes: all authors' names, institutional affiliations, address, telephone numbers and e-mail address. Papers should be no longer than 10,000 words (inclusive of abstract 100-150 words, footnotes, bibliography and notes on contributors), unless permission for a longer submission has been granted in advance by the Editors. Each article must include a 100 words "note on contributor(s)" together will full institutional address details, including email address. We request that you submit this material (title page and notes on the contributors) as "supplementary files" rather than in the article itself, which will need to be blinded for peer-review.

We are unable to pay for permissions to publish pieces whose copyright is not held by the author. Authors should secure rights before submitting translations, illustrations or long quotes. The views expressed in all articles are those of the authors and not necessarily those of the journal or its editors. After acceptance, authors and Special Issue guest editors whose institutions have an Open Access library fund must commit to apply to assist in article production costs. Proof of application will be requested. Though publication is not usually contingent on the availability of funding, the Journal is generally under no obligation to publish a work if funding which can be destined to support open access is not made available.

 Word template and guidelines

Our tailored Word template and guidelines will help you format and structure your article, with useful general advice and Word tips.

(La)TeX template and guidelines

We welcome submissions of (La)TeX files. If you have used any .bib files when creating your article, please include these with your submission so that we can generate the reference list and citations in the journal-specific style

Artwork guidelines

Illustrations, pictures and graphs, should be supplied with the highest quality and in an electronic format that helps us to publish your article in the best way possible. Please follow the guidelines below to enable us to prepare your artwork for the printed issue as well as the online version.

Format: TIFF, JPEG: Common format for pictures (containing no text or graphs).

EPS: Preferred format for graphs and line art (retains quality when enlarging/zooming in).

Placement: Figures/charts and tables created in MS Word should be included in the main text rather than at the end of the document.

Figures and other files created outside Word (i.e. Excel, PowerPoint, JPG, TIFF, EPS, and PDF) should be submitted separately. Please add a placeholder note in the running text (i.e. "[insert Figure 1.]")

Resolution: Rasterized based files (i.e. with .tiff or .jpeg extension) require a resolution of at least 300 dpi (dots per inch). Line art should be supplied with a minimum resolution of 800 dpi.

Colour: Please note that images supplied in colour will be published in colour online and black and white in print (unless otherwise arranged). Therefore, it is important that you supply images that are comprehensible in black and white as well (i.e. by using colour with a distinctive pattern or dotted lines). The captions should reflect this by not using words indicating colour.

Dimension: Check that the artworks supplied match or exceed the dimensions of the journal. Images cannot be scaled up after origination

Fonts: The lettering used in the artwork should not vary too much in size and type (usually sans serif font as a default).

Authors services:

For reformatting your manuscript to fit the requirement of the Journal of Civil Engineering Researchers and/or English language editing please send an email to the following address:

researchers.services@gmail.com

Noted: There is a fixed charge for these mentioned services that is a function of the manuscript length. The amount of this charge will be notified through a reply email.

FAQ AND TROUBLESHOOTING FOR AUTHORS

I cannot log in to the system. How do I acquire a new user name and password?

If you cannot remember your username, please write an email to (journals.researchers@gmail.com), who will locate your username and notify you. If you know your username, but cannot remember your password, please click the "Login" link on the left-hand menu at homepage. Below the fields for entering your username and password, you will notice a link that asks "Forgot your password?"; click that link and then enter your email adddress to reset your password. You will be sent an automated message with a temporary password and instructions for how to create a new password. TIP: If you do not receive the automated email in your inbox, please check your SPAM or Junk Mail folder. For any other issues, please contact our Managing Editor,Kamyar Bagherinejad (admin@journals-researchers.com).

How do I locate the online submission form and fill it out?

First you need to register or login (see above). Once you are logged in, make sure the "roles" section of your profile has "Author" selected. Once you assign yourself the role of "Author," save your profile and then click the "New Submission" link on your user home page.

Once you arrive at the submission form page, please read the instructions carefully filling out all necessary information. Unless specified otherwise by the editors, the journal section to be selected for your submission should be "Artlcles." Proceed to the remaining sections, checking all boxes of the submission preparation checklist, and checking the box in the copyright notice section (thus agreeing to journals-researchers's copyright terms). Once the first page is completed, click "Save and Continue." The next page allows you to upload your submission. Use the form to choose your file from your computer. Make sure you click "Upload." The page will refresh and you may then click "Save and Continue." You will then proceed to a page for entering the metadata for your article. Please fill out all required fields and any further information you can provide. Click "Save and Continue." The next page allows you to upload supplementary files (images, audiovisual materials, etc.). These are not required, but if you wish to provide supplementary materials, please upload them here (do no forget to click "Upload." Then click "Save and Continue." This brings you to the final page of the submission form. Please click "Finish Submission" in order to close the

submission process. You wil then be notified by email that your article has been successfully submitted. TIP: If you do not receive the automated email in your inbox, please check your SPAM or Junk Mail folder. For any other issues, please contact our Managing Editor, Kamyar Bagherinejad (admin@journals-researchers.com).

Why am I not receiving any email notifications from HAU?

Unfortunately, some automated messages from Open Journal Systems arrive in users' Spam (or Junk Mail) folders. First, check those folders to see if the message was filtered into there. You may also change the settings of your email by editing your preferences to accept all mail from [jcer] and related journals-researchers.com email accounts.

I am trying to upload a revised article following an initial round of peer-review, but I cannot locate where to upload the article. Where do I submit a revised article?

Follow the login process outlined above and when you successfully login you will see on your user home page a link next to "Author" for "active" articles in our system (usually it is only one article, but if you have mulitple submissions currently in our system, the number could be higher. Click the "Active" link and you will be led to a page that lists your authored articles currently in our system. Click the link under the column labeled "Status" and this will take you to a page showing the current review status of your article. At the very bottom of the screen, you will see an upload form under the heading "Editor decision." Here you may upload your revised article. An automated email will be sent to the editors and you may also notify them directly via email. You may then logout.

I successfully submitted an article; how long will it take for the editors to respond to me with a decision.

For all articles that are recommended for peer-review, the editors of JCER strive to notify authors of a decision within 4-6 weeks. You may contact JCER's Managing Editor, Kamyar Bagherinejad (admin@journals-researchers.com). if you have any questions relating to the review process and its duration.

For all other inquiries, please contact: Kamyar Bagherinejad (Managing Editor)

Privacy Statement

The names and email addresses entered in this journal site will be used exclusively for the stated purposes of this journal and will not be made available for any other purpose or to any other party.

Articles

Section default policy

Make a new submission to the Articles section.

Copyright Notice EditEdit Copyright Notice

Privacy Statement EditEdit Privacy Statement

The names and email addresses entered in this journal site will be used exclusively for the stated purposes of this journal and will not be made available for any other purpose or to any other party.

Scholars Pavilion

Scholars Pavilion or **Scholars Chartagi** is a monument donated by the Islamic Republic of Iran to the United Nations Office at Vienna. The monument architecture is claimed by the Islamic Republic News Agency of Iran to be a combination of Islamic and Achaemenid architecture, although the latter clearly predominates in the decorative features, with Persian columns and other features from Persepolis and other remains from the Achaemenid dynasty. The Chahartaq pavilion form runs through the architecture of Persia from pre-Islamic times to the present.

Statues of four famous Persian medieval scholars, Omar Khayyam, Al-Biruni, Muhammad ibn Zakariya al-Razi and Ibn-Sina are inside the pavilion. This monument donated in June 2009 in occasion of Iran's peaceful developments in science.

J-Researchers